THEORETICAL STUDIES OF MAGNETIZED PLASMA TURBULENCE:
ION-CYCLOTRON TURBULENCE, AND SHEAR FLOW TURBULENCE
AND ITS APPLICATIONS TO TOKAMAK EDGE PHENOMENA

Tzihong Chiueh
Institute for Fusion Studies
The University of Texas at Austin
Austin, Texas 78712

May 1985

THEORETICAL STUDIES OF MAGNETIZED PLASMA TURBULENCE:

ION-CYCLOTRON TURBULENCE, AND SHEAR FLOW TURBULENCE

AND ITS APPLICATIONS TO TOKAMAK EDGE PHENOMENA

APPROVED BY SUPERVISORY COMMITTEE:

DEDICATION

To my parents,

Chiueh Wu Yu Jane and Chiueh King Mu,

for their total dedication and

support to their sons.

THEORETICAL STUDIES OF MAGNETIZED PLASMA TURBULENCE:

ION-CYCLOTRON TURBULENCE, AND SHEAR FLOW TURBULENCE

AND ITS APPLICATIONS TO TOKAMAK EDGE PHENOMENA

by

TZIHONG CHIUEH, B.S., M.S.

DISSERTATION

Presented to the Faculty of the Graduate School of

The University of Texas at Austin

in Partial Fulfillment

of the Requirements

for the Degree of

DOCTOR OF PHILOSOPHY

THE UNIVERSITY OF TEXAS AT AUSTIN

August 1985

patience in the preparation of the manuscripts of this re-
search, and to Mr. T. Valdez for the preparation of the
figures in Chapter IV.

Finally, I would like to express my deep grati-
tude to Dr. Patrick H. Diamond for his never-failing pa-
tience as an educator as well as for the inspiration of
his ingenuity and incisive attitude as a researcher.

The University of Texas at Austin

May 15, 1985

TABLE OF CONTENTS

LIST OF FIGURES

C H A P T E R   I

INTRODUCTION

This thesis is devoted to two major studies:
high-frequency turbulence and low-frequency turbulence in
magnetized plasmas. In the case of high-frequency turbu-
lence, we concentrate on ion-cyclotron turbulence (Chap-
ters II and III) where emphasis is placed on the examina-
tion of the dynamics of phase-space density granula-
tions[10,11] (clumps) in weak collective dissipation regimes.
Nonlinear instabilities of the granulations (which occur
below linear threshold), the necessary condition for sta-
tionary turbulence, and anomalous transport which depends
sensitively on the presence of clumps are also themes of
this study.

For low-frequency turbulence, we address on
(electrostatic) MHD[22] shear flow turbulence in the presence
of a stabilizing sheared magnetic field. In the limit of
vanishing magnetic shear, the plasma behaves as an incom-
pressible fluid. In this limit, we study two types of
free shear flow turbulence (Chapter IV) characterized by
the mean flow profiles: mixing-layer flows where turbulence

evolution is largely governed by large-scale wave fluctuations,[26] and wake or jet flows where turbulence contains mostly small-scale nonwave fluctuations.[29] Finally, we extend this analysis to turbulence observed in the tokamak edge (Chapter V). At the edge region, a large radial D.C. electric field is observed.[45,46] The resulting radially varying poloidal flow can locally drive turbulence. We place our emphasis on the origin of turbulence and the non-linear mechanisms for saturation of instabilities.

This research on several problems related to high-frequency and low-frequency turbulence of magnetized plasmas is motivated by a number of laboratory experiments, space observations, computer simulations, as well as our intention to extend the existing plasma turbulence theory of clumps to more realistic situations. In Chapters II and III, we study the two-point theory (clump theory) of current-driven ion-cyclotron turbulence, where incoherent (nonwave) fluctuations, usually neglected in conventional theories, and wave fluctuations both participate in determining the evolution of the turbulence. The reason for our interest in this subject is twofold. First, an elegant plasma turbulence theory[10] of the nonwave fluctuations has been recently developed in the context of one-dimensional

Vlasov plasmas. There, nonwave fluctuations were shown to evolve in a way different from that of wave fluctuations. In conventional wave theories, dielectric functions are the primary concern, and the nonwave fluctuations are ignored because they are incoherent with electric field fluctuations, and thus not directly related to dielectric response. Hence, this new theory challenges the notion that waves are the sole building blocks of plasma turbulence. In view of the simple model of a one-dimensional plasma adapted in previous work on this theory, we are motivated to extend it to a realistic three-dimensional magnetized plasma.

Second, several laboratory[1,2,3] and space experiments[4,5] have observed large-amplitude ion-cyclotron frequency fluctuations, and the anomalous transport commonly associated with them. In particular, a great deal of attention[4] is recently focused on the causes of potential drop along auroral field lines, which is of central importance for understanding the formation of auroral arcs. It has been speculated[6] that ion-cyclotron turbulence, excited by a field-aligned current, may be responsible for the potential drop via enhanced resistivity. We are motivated to pursue the clump theory of ion-cyclotron turbulence because the space plasmas are collisionless and thus provide

a suitable environment for clumps. Also, the timescale of quasi-linear relaxation is longer than that of nonlinear wave-particle interactions, thus implying that quasi-linear relaxation may not occur. Furthermore, in the presence of replenishing electrons streaming into the active region, the application of quasi-linear theory to this problem may be questionable. Hence, the clump theory is more appropriate for the study of turbulence and anomalous transport in space.

In the case of low-frequency turbulence of magnetized plasmas, our studies are stimulated by many reasons both directly and indirectly. The study in Chapter V is in an attempt to explain the change of turbulence characteristics observed[45] in the tokamak edge. An E X B poloidal flow is caused by a large-scale D.C. radial electric field (probably created by some mechanism related to plasma interaction with wall or limiters) is observed. The turbulence is isotropic near the inflection point of the poloidal flow in comparison to anisotropic spectra observed in nearby regions. Independently, flow visualizations constructed from experimental data[47] of probe array suggest the presence of vortex-like motion in this region.

Therefore, a new mechanism, which was not noticed previously, for driving turbulence near the edge region

may exist, and be relevant to tokamak confinement. We are thus motivated to study this problem.

When magnetic shear is negligible, the incompressible electrostatic MHD equations are equivalent to the two-dimensional incompressible Navier-Stokes equation; thus plasmas behave in a way similar to that of two-dimensional incompressible fluids. Fluid turbulence is interesting by itself, primarily because it is easier to conduct well-controlled experiments; and hence better understanding can be gained, providing clues for any theoretical treatment. In Chapter IV, we are thus motivated to study several interesting questions raised by experiments.

Though we have divided the thesis into studies on high-frequency turbulence and low-frequency turbulence of magnetized plasmas, it actually contains three relatively independent works. The discussion of each of them is self-contained. In view of the large amount of background information needed to introduce our studies, we provide the necessary introductory discussions at the beginning of the appropriate section for each work (Chapters II, IV, and V) and will not repeat them here. In the remainder of this chapter we will give a brief summary of each individual research.

In Chapters II and III, we address the two-point theory of current-driven ion-cyclotron turbulence. The necessary analytical tools for later discussion are developed in Chapter II. The structures of the Vlasov equation are considerably complicated by the cross-field acceleration and guiding-center drift of charged particles. Here, we first construct a renormalization scheme for the one-point Vlasov equation in the guiding-center coordinate, from which a renormalized dielectric function is subsequently obtained. In this one-point renomalization scheme, nonlinear terms are approximated by non-Markovian diffusion in the parallel velocity, perpendicular velocity, phase angle, and guiding center space. In the limit of Markovian approximation, the nonlinear diffusion can then be reduced to that obtained by Dum and Dupree,[7] treating charged particles as the stochastically accelerated ones in a magnetic field.

We also construct an evolution equation for the two-point, one-time correlation function. Our efforts are primarily focused on approximating the triplet correlation, and deriving the source of small-scale fluctuations. The triplet can be expressed as relative diffusion of the correlation function in (the corresponding) phase-space; the

diffusion coefficients vanish at zero phase-space separation. The source can be expressed as a Fokker-Planck type equation. This Fokker-Planck relaxation of the average particle distribution is mainly due to interactions between particles of different species. This is because like-species interactions can only lead to relaxation of temperature anisotropy, a much slower process.

In Chapter III, we solve the two-point, one-time correlation equation for ions and electrons. The steady state solutions have logarithmic singularities, reflecting the strong small-scale correlation of phase-space density fluctuations. In particular, we derive a necessary condition for stationary current-driven ion-cyclotron turbulence. In the ion-cyclotron regime, waves, when emitted by the clumps (macroparticles), are weakly damped. Hence, the nature of turbulence consists of a mixture of waves and clumps. This necessary condition is a Vlasov analogue to the fluctuation-dissipation theorem of the test-particle model. Furthermore, the expression for this necessary condition is generally valid for other types of wave-clump turbulence. Using the analogy with the test-particle model, it is easy to understand that when the source, arising from relaxation of the average distribution function,

overdrives the system, the fluctuations can grow. Non-linear instabilities of current-driven ion-cyclotron turbulence of this kind are examined, and growth rates are obtained.

We also search for the parameter regimes where clump effects are important. Intuitively, it is clear that these regimes must be those where collective dissipation is relatively strong, since clumps result from wave-particle interactions. One of the important regimes is that perpendicular ion temperature T_i is larger than parallel electron temperature T_e. Anomalous transport in this regime can significantly deviate from those obtained by conventional quasi-linear wave theories. Finally, as an important result of this study, which can immediately be examined by experiments, perpendicular ion heating is the principal sink for extracting the current energy in current-driven ion-cyclotron turbulence. This is in contrast to the prediction of quasi-linear wave theories, which is that parallel electron heating is the major energy sink.

In a two-dimensional incompressible magnetized plasma (or fluid), free shear flow turbulences that evolve from an initially prescribed mean flow profile will develop

and approach favorable states. Experiments show that two
qualitatively different favorable states occur for turbu-
lence in the presence of two different types of mean flows.
The first type of turbulence contains mostly large-scale
fluctuations, and is associated with the mixing-layer type
of shear flow. Mean flows of this type contain infinite
amounts of energy, which is due to the infinitely large
volume occupied by the flow of different velocities across
the shear layer. Hence, the large-scale wave fluctuations
can always draw energy from the mean flow to sustain them-
selves. It is also observed[26,27] that the shear layer
grows linearly in time, whereas the mean flow profile can
remain in approximately its original shape during the
course of expansion. In Chapter IV, we study this type of
turbulence, adapting two experiment-consistent assumptions
that the mean flow evolves self-similarly, while its
lengthscale varies in time, and that the large-scale un-
stable wave fluctuations grow with nonlinear growth rates,
where nonlinear modifications are due to turbulent scram-
bling by other large-scale modes. Since wave fluctuations
are unstable and dominate turbulence, we can safely ignore
the nonwave fluctuations and use the quasi-linear theory
to describe turbulence evolution. In this study, we show

that the mean flow indeed expands linearly in time and the expansion rate is consistent with that measured by Aref et al. and Brown et al.

The second type of turbulence consists primarily of small-scale fluctuations and is associated with shear flow such as jets or wakes. For this type of flow, mean flow velocities on sides of a shear layer are the same; hence, it has only a finite amount of free energy stored in the layer. Though the large-scale wave fluctuations can initially be excited, they can no longer be sustained. Thus, small-scale fluctuations are of central attention for this type of turbulence.

With intermediate values of Reynolds numbers ($R_e \approx 300$), experiments[29] show that two-dimensional large-scale (and less regular) vortex streets can intermittently reappear from a turbulent state. In our opinion, two points are inferred from this observation. First, the turbulence is two-dimensional. In three-dimensional turbulence, vortex stretching and folding are the principal processes for creating small-scale fluctuations. It is difficult to understand why after being stretched and entangled, the three-dimensional vortex tubes should reorganize themselves into a regular two-dimensional pattern.

However, if the turbulence (or small-scale fluctuations) are two-dimensional, then this kind of reformation is much more likely. Second, the reformation of large-scale vortex streets is a result of nonlinear spatial rearrangement of small vortices as opposed to the formation of large vortices in mixing-layer turbulence, which is a linear wave excitation process. This is true because the flow has already become turbulent and thus the evolution must be in a nonlinear phase.

With Reynolds number, $R_e = 300$, we probably can assume the flow is approximately invicid. For our study of two-dimensional invicid turbulence, this experiment provides us a basis for comparison.

Theoretically, the mathematical structure of a two-dimensional shear flow is similar to that of a one-dimensional Vlasov plasma. Thus, small-scale nonwave structures (vorticity clumps) can be expected to exist. The similarity stems from the following observations:

(A) $\dfrac{d\rho}{dt} = 0$, conservation of vorticity.

$\dfrac{df}{dt} = 0$, conservation of phase-space density.

(B) Locally, coordinates can be expressed as

$$V_E(x) \approx \left. \frac{dV_E}{dx} \right|_{x=0} \cdot x$$, local coordinate in the inhomogeneous direction.

v , velocity in phase space.

y , coordinate in the translationally invariant direction.

z , position in phase space, translationally invariant.

(C) The Fourier components in the invariant direction,

$$\phi_k(x) = \int dx' \nabla^{-2}(x,x') \rho_k(x')$$

, relation between the stream functions ϕ_k and vorticity ρ_k.

$$\phi_k = \int dv \left[\frac{4\pi n_o q}{k^2} \right] f_k(v)$$, Poisson's equation

where ∇^{-2} is an inverse Laplacian.

(D) For two nearby points in both cases, their relative trajectories are determined by the relative "forces." At small separation the relative "forces" are small, and hence lead to preservation of their structural integrity for a long time. With this observation, we attempt to pursue a vorticity clump theory of two-dimensional shear flows.

We show that the dominant contribution of triplet correlation, in the two-point equation of vorticity, is the relative diffusion of vorticity correlation. Most importantly, we show that the source of vorticity correlation, which arises from relaxation of the mean vorticity, is positive definite. That is, turbulence can not only rearrange the mean vorticity creating small-scale granulations, but it is also able to sustain them. In a single-species one-dimensional Vlasov plasma, the source, by marked contrast, vanishes due to the conservation laws of energy and momentum during elastic collisions. However, vortex collisions are inelastic; hence the constraint of Vlasov plasmas fails and thus the source survives.

Finally, we are able to obtain the stationary vorticity correlation function, and thus the vorticity wavenumber spectrum. The latter is anisotropic because of the shearing of the mean flow. In the limit of high wavenumbers, the spectrum is separable as a product of a function of the magnitude of wavenumbers $|k|$ and a function of the direction of wavenumbers (k_x/k_y). The function that depends on the magnitude of wavenumbers obeys the power law, $|k|^{-1}$, which coincides with that obtained by using a Komogoroff-type enstrophy cascade argument. The angular

dependence of the wavenumber spectrum is primarily because the small-scale vortices are still large enough to experience the shearing due to the mean flow; whereas the $|\underset{\sim}{k}|$ dependence of the spectrum is because the small-scale vortices are so small that a statistical equilibrium is established. Thus the creation of vortices (incoherent source) balances the destruction (turbulent scrambling) and leads to a self-similar vorticity cascade.

In Chapter V, we are concerned about turbulence observed in the tokamak edge, particularly about the effects of an observed D.C. electric field on turbulence. We begin with examining its effects on density-gradient-driven turbulence by extending the previous study of Terry and Diamond.[49] We find that the electric field induced poloidal flow can Doppler-shift the electron diamagnetic drift frequency ω_{*e}, yielding the observed fluctuation frequency which reverses its sign across the shear layer. We also find that the shear flow gradient modifies (reduces) the radial correlation length of density fluctuations Around the region of the greatest radial gradient of the poloidal flow, modifications of the radial correlation length become so large that the poloidal shear flow should be regarded as the dominant free energy source. Here,

instabilities associated with the inflection of the shear
flow velocity occur. The unstable modes do not have singu-
lar points; thus their radial and poloidal length-scales
are comparable. Hence, the turbulence spectrum is iso-
tropic in contrast to the anisotropic turbulence spectra of
other regions, where the singular-layer solution of resis-
tive instabilities arise. The presence of magnetic shear
tends to suppress the instabilities, but does not complete-
ly stabilize all modes (especially long wavelength modes).
Linear instabilities for different magnetic shear strength
arise due to insufficient overlap between the (shear flow)
driving region and the resistive dissipation region.

        In the nonlinear phase, this study departs from
that of free shear flow turbulence discussed in Chapter
IV. In this study magnetic shear, which provides an energy
sink available to nonlinearly stabilize the unstable modes
is included. Also tokamak edge turbulence has a fixed
mean flow profile (probably due to limiters), while in the
previous case, the flows are free to relax.

        Two possible nonlinear saturation mechanisms are
proposed. When magnetic shear is weak and the width of
the resistive layer is much greater than that of the shear
flow layer, saturation of unstable modes relies on en-
strophy cascade which transfers energy from the high-k

unstable to the low-k stable modes. When magnetic shear is moderate or strong, the width of the resistive layer comparable to that of the shear flow layer, saturation can be achieved via nonlinear mode broadening. By this, the modes extend into the dissipation region and effectively transfer energy from the localized source to the sink, thus suppressing the instabilities.

We are able to determine the correlation lengths and time of turbulence self-consistently. Using these, the scalings of the saturated electric field, density, and magnetic field fluctuations of each process are obtained. For parameters of the TEXT tokamak, the saturation mechanism is dominated by the nonlinear broadening of mode widths. Our results are consistent with the observations.

CHAPTER   II

TWO-POINT THEORY OF CURRENT-DRIVEN
ION-CYCLOTRON TURBULENCE (A)

This chapter and Chapter III address the two-point (clump) theory of ion-cyclotron turbulence driven by a relative drift between ions and electrons. In this chapter, we first present background information needed to introduce this study, and then develop the necessary analytical tools, to be used in the next chapter.

2.1   Introduction

Strong current-driven ion-cyclotron waves have been identified in several experiments[1,2,3] and in satellite[4,5] data. Possible consequences, such as anomalous transport, ion heating, and anomalous resistivity have been the principal foci of attention. There is also increasing theoretical interest in anomalous transport[3,6] due to ion-cyclotron turbulence, which may be related to the formation of auroral arcs and ion-conic distributions along auroral field lines.

Traditionally, anomalous transport has been studied using quasi-linear theory.[3] However, this theory is unsatisfactory for the following three reasons:

First, there remains, in the transport coefficients, a fluctuation spectrum $\langle E^2 \rangle_{\underset{\sim}{k}}$ which is frequently left undetermined or treated in an ad hoc way.

Second, its relevant time scale is that for evolution of the resonant part of the distribution function, which is usually longer than that for nonlinear interaction (this point will be discussed further in Section 3.1).

Third, the processes for average distribution function relaxation include only quasi-linear diffusion resulting from wave fluctuations. However, due to incoherent fluctuations, the processes for relaxation of the average distribution function also include a drag force, which counterbalances the D.C. electric field set up by the D.C. current. Hence, with the diffusion due to waves alone, the quasi-linear theory is inadequate for description of a steady state. Clearly, for time scales of interest, one needs a more complete nonlinear theory to describe plasma turbulence. In the past the conventional nonlinear theories[7,8] (which assume a broad

fluctuation spectrum--this assumption is adopted here also) usually employed a stochastically-accelerated-particle-orbit calculation[9] to account for enhanced collective dissipation due to nonlinearity. These theories include only wave fluctuations and can only describe the initial phase of turbulence with linearly excited waves. As soon as these self-consistent waves are damped out by the nonlinear interactions, the theories fail. In particular, incoherent fluctuations were not taken into account at all, and thus the finite frequency line-width observed in turbulent plasmas cannot be explained with these theories.

Recently, a new plasma turbulence theory (clump theory) has been developed and applied to a one-dimensional model problem,[11,12] which has also been studied using particle simulations.[13] This one-dimensional study focused on a physical situation dominated by incoherent ballistic fluctuations, rather than waves. The particle simulations that support the conclusions of the theoretical work used a low ion to electron mass ratio of $M_i/m_e = 4$. In this case, the electron and ion distribution functions overlap in velocity space, yielding very effective collisionless momentum exchange between particles and

ballistic fluctuations. However, this situation is not at all universal. Indeed, plasma turbulence is usually associated with collective resonances, hence the most general treatment should contain both wave and nonwave fluctuations. In view of these considerations of relevance, we are motivated to study phase space turbulence in a three-dimensional, magnetized plasma which can support collective oscillations.

In this case, incoherent nonwave fluctuations (clumps) arise from the imperfect mixing of a Vlasov plasma. Particle-orbit stochasticity due to wave-particle interactions generates small-scale phase space density granulations that ballistically propagate at the resonant velocites, $v = \omega - n\omega_{ci}/k_{\parallel}$. By way of contrast, the wave fluctuations are generated from a coupling between the gradient of the average distribution function and the electric field, and hence are intrinsically coherent with the fluctuating electric field. By satisfying the requirement that the dielectric function vanishes ($\epsilon_{k,\omega} = 0$), wave-like phase space density fluctuations and the fluctuating electric field can self-consistently exist. Nonlinear modifications to the wave fluctuations do nothing more than introduce nonlinear collective dissipation into

the dielectric functions $\epsilon_{\underline{k},\omega}$, which modifies wave stability. Each type of fluctuation has a different character. The wave fluctuations of a given wavenumber k, satisfying the dispersion relation, appear to be periodic in time; the nonwave fluctuations, $\omega - n\omega_c = k_\parallel v_\parallel$, appear as macroparticles which propagate ballistically and are shielded by the short-range electric field.

The mechanism whereby these ballistic structures arise can be easily understood. The turbulent electric field rearranges the average particle distribution by scattering chunks of particles off their original locations in phase space, thus creating spatially-varying and complicated structures. At the same time, the tidal forces produced by the resulting turbulent electric field tend to tear the chunk of particles apart. However, if the size of a clump is small enough so that every particle in it feels the same tidal force, this clump can retain its structural integrity for a time long compared to the average correlation time of the system. Decay processes such as this will be offset by the continuous generation of clumps due to relaxation of the average particle distribution. The competing processes discussed above are described by an evolution equation of the two-point,

one-time phase space density correlation function $\langle\delta f(1,t)\delta f(2,t)\rangle$, which has the form,

$$\left[\frac{\partial}{\partial t} + \underset{\sim}{v}\cdot\frac{\partial}{\partial\underset{\sim}{X}} - \frac{\partial}{\partial\underset{\sim}{q}}\cdot\underset{\approx}{D}(-)\cdot\frac{\partial}{\partial\underset{\sim}{q}}\right]\langle\delta f(1,t)\delta f(2,t)\rangle$$

$$= S(1,2) \simeq - \frac{\partial}{\partial t}(\langle f(1)\rangle\langle f(2)\rangle) \qquad (2:1\text{-}1)$$

where $\underset{\sim}{q}$ is the appropriate relative coordinate of phase space, and $\underset{\approx}{D}(-)$ is a relative diffusion coefficient, which vanishes at $\underset{\sim}{q} = 0$ where two points in phase space feel the same tidal forces. In the limit $\underset{\sim}{q} = 0$, the correlation function is secularly driven by the source, which evolves quasi-stationarily. At steady state, $t \to \infty$, a singular correlation function yields. The driving force, in Eq. (2:1-1) is related to relaxation of the average particle distribution due to turbulent scattering by both the wave and nonwave fluctuations.

It can be shown that clump fluctuations can be excited from thermal noise at a lower threshold free energy than that required for the wave fluctuations. This leads to the interesting paradox that in the limit of vanishing fluctuation amplitude, one would expect linear and nonlinear stability boundaries to coincide, yet in

fact the nonlinear theory here yields a lower value of
threshold free energy. This paradox can be resolved if
one realizes that different time scales are appropriate to
each case. The linear analysis of a nonlinear partial
differential equation is valid for a finite time, after
which transition to nonlinear evolution occurs. In a
Vlasov plasma, the linear theory is valid up to a time τ,
there $\tau < \tau_c$ and τ_c is the amplitude-dependent wave-
particle decorrelation time. In a linearly stable plasma,
nonlinear instability can occur if the free energy ex-
ceeds the threshold value. In this case, the thermal
level of fluctuations will determine the size of τ_c, and
the clump fluctuations then grow on this time scale.

Furthermore, when linear waves are weakly damped
in plasmas, wave fluctuations can be emitted by the macro-
particles (in analogy to those emitted by the discrete
particles in the test-particle model) and can coexist
with clump fluctuations in plasma turbulence. Because of
this relationship between the wave and clump fluctuations,
competition between formation and decay of the clump fluc-
tuations can now be viewed as competition between emis-
sion and dissipation of waves. This can be understood
as follows.

Schematically, Eq. (2:1-1) can be expressed as

$$(\gamma_\omega + \frac{1}{\tau_{cl}})<\delta f \delta f>_\omega = <S>_\omega \qquad (2:1\text{-}2)$$

where γ_ω and τ_{cl} are the growth rate and life-time of clump fluctuations, respectively. Note that the source is proportional to the fluctuation spectrum, hence we let $<S>_\omega = (R_\omega/\tau_{cl})<\delta f \delta f>_\omega$, where R_ω is an operator, which includes the effect whereby $\hat{f}$ (incoherent fluctuation) is shielded by the plasma response function $\epsilon_{k,\omega}$. We can further express R_ω as $\sum_{k} \overline{R}_{k,\omega}/|\epsilon_{k,\omega}|^2$, where $\overline{R}_{k,\omega}$ is another operator proportional to the seed electric field fluctuations of macroparticles. Thus Eq. (2:1-2) yields

$$(\gamma_\omega \tau_{cl} + 1) \cong \sum_{k} \frac{\overline{R}_{k,\omega}}{|\epsilon_{k,\omega}|^2} \qquad (2:1\text{-}3)$$

$$\gamma_\omega \cong \frac{1}{\tau_{cl}} \left\{ \left[\overline{R}_{k,\omega}/(Im\epsilon_{k,\omega}) \left[\frac{\partial Re\ \epsilon_{k,\omega}}{\partial k} \right] \right] \Big|_{k=k_\omega} - 1 \right\} \qquad (2:1\text{-}4)$$

where the spectral k-sum is mainly determined by the pole contribution, $Re\epsilon_{k,\omega} = 0$, at the collective resonances. The steady state, $\gamma_\omega = 0$, is determined by the collective dissipation $Im\epsilon$ and the generation of waves by clump emission $\overline{R}$. By contrast, in the previous analysis of the

clump-dominant regime, the shielding factor $1/|\epsilon|^2$ is not close to collective resonance, hence the process whereby nonlinear evolution was regulated by a finite collective dissipation (Imϵ) was not considered. Consequently, in stationary turbulence of the wave-clump regime, waves must be oversaturated; this finite collective dissipation can explain the finite frequency linewidth observed in stationary turbulence. Indeed, in general, waves should be viewed as broadened collective resonances. Progress[14, 15] in this direction has also been made in other areas of plasma turbulence; in particular, in the clump theory[14] of drift-wave turbulence.

Turbulence in a magnetized plasma can exhibit different types of strongly correlated small-scale granulations in phase space. In the case of low-frequency turbulence in a magnetized plasma, such as drift-wave turbulence, perpendicular dynamics are due to the spatial wandering of guiding centers because of random $E \times B_o$ convection. Perpendicular scattering in velocity space is small, since that requires the time scale of the fluctuating electric field to be comparable to the cyclotron frequency. The perpendicular spatial extent of clumps is limited by the average length scale of the tidal force,

which is the spectrum-averaged perpendicular wavelength $(\overline{k}_\perp)^{-1}$. In velocity space, the perpendicular scale of the clump can extend up to a thermal velocity v_t. In contrast, for high-frequency turbulence in a magnetized plasma, the gyro-motion of particles can resonate with the turbulent field and thus lead to perpendicular scattering in velocity space. Furthermore, the perpendicular length scale, $(\overline{k}_\perp)^{-1}$, of the turbulent field is smaller than the gyro-radius (usually $\overline{k}_\perp \rho \gtrsim 1$ in high frequency problems); the former then not only determines the perpendicular correlation length of the clump fluctuations, but also limits their sizes to be within $v_t(\overline{k}_\perp \rho)^{-1}$, (where $\overline{k}_\perp \rho > 1$) in the perpendicular velocity direction.

In ion-cyclotron turbulence, the electric field is almost perpendicular to the magnetic field $(\overline{k}_\perp \gg \overline{k}_\parallel)$. The ion perpendicular diffusion dominates parallel diffusion, and the latter can thus be ignored for the time scale of interest. On the other hand, the electrons are strongly magnetized $(\overline{k}_\perp \rho_e \ll 1)$ and are thus tied to the magnetic field lines. Their dynamics are essentially one-dimensional. These observations allow us to depict the clump structure more precisely. The electron clump appears in position space as a long, thin $(\overline{k}_\perp \gg \overline{k}_\parallel)$,

cigar-shaped group of electrons travelling at a speed $v_\parallel \approx n\omega_{ci}/k_\parallel$; the ion clump, on the other hand, appears as a tether-rod with tether length ρ_i gyrating about the guiding center, if $\bar{k}_\perp \rho_i > 1$, and as a cigar if $\bar{k}_\perp \rho_i < 1$, propagating at a ballistic velocity $\gamma_\parallel \cong \omega - n\omega_{ci}/k_\parallel$. Both cigar and rod have radii $(\bar{k}_\perp)^{-1}$ and lengths $(\bar{k}_\parallel)^{-1}$ (Fig. 3.1). Quantitatively, the phase space density correlation functions of both species are described by the equations,

$$\left\{\frac{\partial}{\partial t} + \underset{\sim}{v} \cdot \frac{\partial}{\partial \underset{\sim}{X}} - \frac{\partial}{\partial \underset{\sim}{q}_\perp} \cdot \underset{\sim}{D}_\perp(-) \cdot \frac{\partial}{\partial \underset{\sim}{q}_\perp}\right\}^i \langle \delta f(1,t)\delta f(2,t)\rangle^i$$

$$= \langle S\rangle^i \qquad\qquad (2:1\text{-}5)$$

and

$$\left[\frac{\partial}{\partial t} + v_{\parallel} \frac{\partial}{\partial Z} - \frac{\partial}{\partial \bar{v}_\parallel} \cdot D_\parallel(-) \cdot \frac{\partial}{\partial v_\parallel}\right]^e \langle \delta f(1,t)\delta f(2,t)\rangle^e$$

$$= \langle S\rangle^e, \qquad\qquad (2:1\text{-}6)$$

for ion-cyclotron turbulence. At steady state, Eqs. (2:1-5) and (2:1-6) can be solved, yielding

$$\langle \delta f(1)\delta f(2)\rangle^i = \tau_{c1}^i(\underset{\sim}{X}, \underset{\sim}{v})\langle S(1,1)\rangle^i \qquad (2:1\text{-}7)$$

$$\langle \delta f(1)\delta f(2)\rangle^e \approx \tau^e_{cl}(\underline{X}_-,\underline{v}_-)\langle S(1,1)\rangle^e \qquad (2:1-8)$$

where

$$\tau^i_{cl} = -\tau_i\left[\ln\frac{3}{4}\left[\overline{k}^2_\perp X^2_{\perp-} + \frac{\overline{k}^2_\perp X^2_{\perp-}}{2\omega^2_{ci}} + \overline{k}^2_\parallel(Z^2_\parallel + 2v_{\parallel-}Z_-\tau_i\right.\right.$$

$$\left.\left. + 2v^2_{\parallel-}\tau^2_i)\right]\right]^i \qquad (2:1-9)$$

$$\tau^e_{cl} = -\tau_e\left[\ln\frac{1}{3}\left[\frac{\overline{k}^2_\perp X^2_{\perp-}}{2} + \overline{k}^2_\parallel(Z^2_- + 2v_{\parallel-}Z_-\tau_e + 2v^2_{\parallel-}\tau^2_e)\right]\right]^e$$

$$(2:1-10)$$

and τ_i, τ_e are the particle-decorrelation times for ions
and electrons, respectively. Eqs. (2:1-7), (2:1-8),
(2:1-9) and (2:1-10) illustrate the strong correlation
of the charged particles at small separations in phase
space. It should be noted that, in Eq. (2:1-9) the term
$\overline{k}^2_\perp v^2_{\perp-}/2\omega^2_{ci}$ can be expressed as $\overline{k}^2_\perp\rho^2_i(v_{\perp-}/v_{ti})^2/2$, indicat-
ing that, as discussed previously, the ion clump size in
the perpendicular velocity space depends on the value of
$\overline{k}_\perp\rho_i$ as compared with unity. On the other hand, in the
parallel velocity space, both ion and electron clumps
have short-range correlation. As a result, in velocity
space the ion clump appears as a gyrating tether-disc
perpendicular to the magnetic field, with the disc radius

$v_{ti}(\overline{k}_\perp \rho_i)^{-1}$ and tether length v_{ti} if $\overline{k}_\perp \rho_i > 1$, and as a thin disc of radius v_{ti} if $\overline{k}_\perp \rho_i < 1$; the thickness of either disc is $(\overline{k}_\parallel \tau_i)^{-1}$. In contrast, the electron clump, in velocity space, appears as a thin disc of radius v_{te} and thickness $(\overline{k}_\parallel \tau_e)^{-1}$ (Fig. 3-1).

A relevant quantity worthy of examination is the velocity-integrated clump amplitude $<\delta n^2>$, which not only is important for determination of nonlinear instability, but also indicates the probability of observing the clumps experimentally. In ion-cyclotron turbulence, this global clump amplitude is much smaller than that for electron clumps. This is because ion finite-Larmor-radius effects sizably reduce the perpendicular velocity correlation length and thus the ion clump amplitude. As a result, electron clumps are more likely to be observed, and play a more significant role in the phase space dynamics.

When temperatures of both species are approximately equal ($T^i \approx T^e$), current-driven ion-cyclotron waves are weakly damped because the parallel phase velocity $\omega_k/k_\parallel$ can adjust so that there are long wavelength modes that avoid ion Landau-damping. Turbulence, therefore, consists of a mixture of waves and clumps. It is shown

that because of small ion dissipation, the clump modifications to the threhold current for instability are, not significant for an isotropic average ion distribution function. However, if the perpendicular ion temperation $T_\perp^i$ is greater than the electron temperature T^e, the clump effects will be more significant. This is because[16] when $T_\perp^i \approx T^e = T_\parallel^i$ the collective resonance frequency ω_k approaches ion cyclotron harmonic frequencies $n\omega_{ci}$ and enhances ion dissipation. In fact, this state can be reached from an initially isotropic ion distribution function by persistent wave-ion interaction and heating, so long as the current is sufficiently maintained. In the limit of very large perpendicular ion temperature, $T_\perp^i \gg T^e \sim T_\parallel^i$, waves are heavily damped, and thus the nonlocal, collective characters of turbulence are absent. Clumps, shielded by the short-range (Debye length) response, alone determine the evolution of the turbulence.

In this study (Chapters II and III), we investigate the nonlinear theory of current-driven ion-cyclotron turbulence. In particular, the relevant regime of turbulence, where the clumps and waves coexist, is studied. Here we summarize the principal results of this research:

(1) Renormalized one-point and two-point equations describing magnetized Vlasov turbulence have been derived. Since particle motions evolve on two different time scales, the renormalized two-point equation describes the slow, relative motion; the renormalized one-point equation describes the rapid cyclotron motion and yields a renormalized dielectric function.

(2) Shapes of ion and electron clumps have been predicted. The electron clump appears cigar-shaped aligned along the magnetic field in position space, and appears as a thin disc perpendicular to the magnetic field in velocity space. The ion clump, when $\bar{k}_\perp \rho_i > 1$, appears as a gyrating tether-rod about the guiding center in position space and a gyrating tether-disc in velocity space; when $\bar{k}_\perp \rho_i < 1$, the ion clump appears cigar-shaped aligned along the magnetic field in position space, and appears as a thin disc perpendicular to the magnetic field in velocity space (Fig. 3-1).

(3) The clump amplitude of ions is much less than that of electrons because of ion finite-Larmor radius effects.

(4) When $T_\perp^i \geq T_\parallel^i \sim T^e$, ion-cyclotron turbulence is of the wave-clump type. When $T_\perp^i \gg T_\parallel^i \sim T^e$, transition

to the clump-dominant type of turbulence occurs. This transition takes place approximately when $(m_e/M_i)^{1/2} T_\perp^i / T^e \geq 0.1$, where waves are heavily damped.

(5) A necessary condition for the maintenance of stationary ion-cyclotron turbulence is given in Eq. (3:1-16), and is a Vlasov-theory analogue to the prediction of the fluctuation-dissipation theorem of the test-particle model. This results from the fact that the collective dissipation must balance incoherent noise emission from macroparticles at steady state. This expression is valid for turbulence of the wave-clump type.

(6) The nonlinear growth rates in different regimes have been obtained, and are given in Eqs. (3:2-7) and (3:2-8). Nonlinear instabilities grow on the time scales of the particle decorrelation times.

(7) The clump modifications to the instability threshold in the wave-clump regime are small (reduction of threshold drift velocity is within 7 percent, Fig. 3-2). However, the modifications to the fluctuation level at saturation and the anomalous resistivity are more significant. Also while the quasi-linear theory predicts that electron parallel heating is larger than, or equal to, ion perpendicular heating for ion-cyclotron turbulence

$(\overline{k}_\perp^2/\overline{k}_\parallel^2 \approx M_i/m_e$, $\overline{k}_\perp^2 \rho_i^2 \geq 1)$, this theory predicts that ion perpendicular heating is the dominant mechanism for extraction of electron-beam energy.

The remainder of this paper is organized as follows: in Section 2.2 we present a method for the renormalization of the Vlasov equation for a magnetized plasma. The nonlinear terms are approximated by a non-Markovian diffusion process in velocity space and guiding-center space. Subsequently, this renormalized equation is used to obtain the nonlinear dielectric function. In Section 2.3 we renormalize the correlation equation. The triplet terms are approximated as diffusion in the relative coordinates of the corresponding phase space. In steady state, the correlation function can be calculated. In doing so, a steady-state condition for maintenance of stationary turbulence is derived. This is discussed in Section 3.1. In Section 3.2, we investigate the clump instability. A mechanism of saturation by collective resonance damping due to nonlinear ion-wave interaction is proposed. The saturation level and anomalous resistivity are estimated in Section 3.3. Conclusions of this study are discussed in Section 3.4.

2.2 One-Point Equation Renormalization

Though the one-point theory cannot fully de-
scribe the nonlinear evolution of a plasma, renormaliza-
tion provides a useful tool for determination of the non-
linear response of the waves. In this section, we con-
sider renormalization for the case of high-frequency tur-
bulence, and will derive the renormalized dielectric func-
tion $\epsilon_{k,\omega}$ and particle propagator G. In a uniformly mag-
netized and spatially homogeneous Vlasov plasma, the
particle phase-space density of either species satisfies
the equation,

$$\left\{\frac{\partial}{\partial t} + \underset{\sim}{v}\cdot\frac{\partial}{\partial X} + \omega_c \underset{\sim}{v}\times\hat{z}\cdot\frac{\partial}{\partial \underset{\sim}{v}} - \frac{q}{M}\frac{\partial \phi}{\partial \underset{\sim}{X}}\cdot\frac{\partial}{\partial \underset{\sim}{v}}\right\}\delta f$$

$$= \frac{q}{M}\frac{\partial \phi}{\partial \underset{\sim}{X}}\cdot\frac{\partial \langle f\rangle}{\partial \underset{\sim}{v}} \ . \tag{2:2-1}$$

Introducing guiding-center coordinates, one
can transform the above equation into

$$\left\{\frac{\partial}{\partial t} + \omega_c \frac{\partial}{\partial \theta} + U\frac{\partial}{\partial Z} + \frac{c}{B}\left[\frac{\partial \phi}{\partial \underset{\sim}{R}_\perp} \times \hat{z}\right]\cdot\frac{\partial}{\partial \underset{\sim}{R}_\perp}\right.$$

$$\left. - \frac{q}{M}\frac{\partial \phi}{\partial \underset{\sim}{R}}\cdot\frac{\partial}{\partial \underset{\sim}{v}}\right\}\delta f = \frac{q}{M}\frac{\partial \phi}{\partial \underset{\sim}{R}}\cdot\frac{\partial \langle f\rangle}{\partial \underset{\sim}{v}} \tag{2:2-2}$$

where

$$R = X - \frac{v \times \hat{z}}{\omega_c} \ , \ V = v$$

$$\frac{\partial}{\partial R} = \frac{\partial}{\partial X} \ , \ \frac{\partial}{\partial V} = \frac{1}{\omega_c} \hat{z} \times \frac{\partial}{\partial R} = \frac{\partial}{\partial X}$$

$$\theta = \cos^{-1}\left[\frac{x \cdot V_\perp}{V}\right]$$

and $k \equiv |k_\perp|$, $\kappa \equiv k_\parallel$, $V \equiv |v_\perp|$, $U \equiv v_\parallel$, $R \equiv |R_\perp|$.

After a spatial-temporal Fourier transformation in guiding-center coordinates, we obtain

$$\left[\omega_c \frac{\partial}{\partial \theta} - i(\omega - \kappa U)\right] f_{k,\omega} + \frac{q}{M} \sum_{\substack{k' \\ \omega'}} \Phi_{k',\omega'}\left\{\frac{kk'}{\omega_c} \sin(\psi_k - \psi_{k'})\right.$$

$$- i \cdot \frac{\partial}{\partial U} - ik'\left[\cos(\theta - \psi_{k'}) \frac{\partial}{\partial V}\right.$$

$$\left.\left.- \frac{\sin(\theta - \psi_{k'})}{V} \frac{\partial}{\partial \theta}\right]\right\} f_{k'',\omega''}$$

$$= \frac{iq}{M} \Phi_{k,\omega}\left[k\cos(\theta - \psi_k) \frac{\partial}{\partial V} + \frac{\partial}{\partial U}\right] <f>, \qquad (2:2-3)$$

where

$$\psi_k \equiv \cos^{-1}\left[\frac{x \cdot k}{k}\right] \ , \ k'' = k - k', \ \omega'' = \omega - \omega'$$

and

$$f_{\underset{\sim}{k},\omega} = \int_0^\infty dt \int_{-\infty}^\infty d^3\underset{\sim}{x}\delta f(\underset{\sim}{x}, \underset{\sim}{v}, t)\exp\left[i\omega t - i\underset{\sim}{k} \cdot \underset{\sim}{x}\right.$$

$$\left. + \frac{ikV}{\omega_c} \sin(\theta - \psi_k)\right]$$

$$\Phi_{\underset{\sim}{k},\omega} = \int_0^\infty dt \int_{-\infty}^\infty d^3\underset{\sim}{x}\phi(x, t)\exp\left[i\omega t - i\underset{\sim}{k} \cdot \underset{\sim}{x}\right.$$

$$\left. + \frac{ikV}{\omega_c} \sin(\theta - \psi_k)\right]$$

the Fourier components of fluctuations in guiding-center coordinates. In addition, we can define the Fourier components of fluctuations in real space coordinates,

$$\delta f_{\underset{\sim}{k},\omega} = f_{\underset{\sim}{k},\omega} \exp\left[-i \frac{kV}{\omega_c} \sin(\theta - \psi_k)\right] ,$$

$$\phi_{\underset{\sim}{k},\omega} = \Phi_{\underset{\sim}{k},\omega} \exp\left[-i \frac{kV}{\omega_c} \sin(\theta - \psi_k)\right] .$$

To renormalize the nonlinearities, we assume that the fluctuating electric field has a broad spectrum, so that the electric field auto-correlation time is shorter than the particle decorrelation time. We then decompose $f_{\underset{\sim}{k},\omega}$ into

$$f_{\underset{\sim}{k},\omega} = f_{\underset{\sim}{k},\omega}^{(1)} + f_{\underset{\sim}{k},\omega}^{(2)}$$

Here, $f_{\underset{\sim}{k},\omega}^{(1)}$ is the phase-incoherent component, which is not correlated with fluctuations of different $\underset{\sim}{k}$ and ω, and $f_{\underset{\sim}{k},\omega}^{(2)}$ is the phase-coherent component, which is driven by a direct beating of $f_{\underset{\sim}{k}'',\omega''}$ and $\Phi_{\underset{\sim}{k}',\omega'}$. In addition, it is useful to notice that Eq. (2:2-3) can be written as

$$[\omega_c \frac{\partial}{\partial\theta} - i(\omega - \kappa U)] f_{\underset{\sim}{k},\omega} + \frac{q}{M} \sideset{}{'}\sum_{\substack{\underset{\sim}{k}'\\\omega'}} \Phi_{\underset{\sim}{k}',\omega'} \left\{ \frac{kk'}{\omega_c} \sin(\psi_k - \psi_{k'}) \right.$$

$$- i\kappa' \frac{\partial}{\partial U} - ik' \left[\cos(\theta - \psi_{k'}) \frac{\partial}{\partial V} \right.$$

$$\left. - \frac{\sin(\theta - \psi_{k'})}{V} \frac{\partial}{\partial\theta} \right] \Big\} f_{\underset{\sim}{k}'',\omega''}$$

$$= \frac{iq}{M} \Phi_{\underset{\sim}{k},\omega} \left[k \cos(\theta - \psi_k) \frac{\partial}{\partial V} + \kappa \frac{\partial}{\partial U} \right] \langle f \rangle$$

$$- \frac{q}{M} \Phi_{\underset{\sim}{k}_\xi,\omega_\xi} \left\{ \frac{kk_\xi}{\omega_c} \sin(\psi_k - \psi_{k_\xi}) - i\kappa \frac{\partial}{\partial U} \right.$$

$$- ik_\xi \left[\cos(\theta - \psi_{k_\xi}) \frac{\partial}{\partial V} \right.$$

$$\left. - \frac{\sin(\theta - \psi_{k_\xi})}{V} \frac{\partial}{\partial\theta} \right] \Big\} f_{\underset{\sim}{k}-\underset{\sim}{k}_\xi,\omega-\omega_\xi} \,, \qquad (2:2-4)$$

Where the summation $\sideset{}{'}\sum_{\substack{\underset{\sim}{k}'\\\omega'}}$ does not include $\underset{\sim}{k}_\xi$ or ω_ξ, dummy variables.

Hence $f_{k,\omega}$ is driven by the linear source and mode beating. Here $f_{k,\omega}^{(1)}$ is driven by the former and $f_{k,\omega}^{(2)}$ by the latter. Upon renormalization, the nonlinear terms on the left side yield the phase-coherent piece of the full nonlinearity. This phase-coherent piece can be written in a form

$$\int C_{k,\omega}(\theta - \theta')f_{k,\omega}(\theta')d\theta' + B_{k,\omega}(\theta)\phi_{k,\omega} ,$$

where $C_{k,\omega}$ and $B_{k,\omega}$ are operators. In order to obtain $C_{k,\omega}(\theta - \theta')$ and $B_{k,\omega}(\theta)$, we will separate $f_{k,\omega}^{(2)}$ from $f_{k,\omega}^{(1)}$ in Eq. (2:2-4). Hence.

$$\left[\omega_c \frac{\partial}{\partial\theta} - i(\omega - \kappa U)\right]f_{k,\omega}^{(1)} + \int C_{k,\omega}(\theta - \theta')f_{k,\omega}^{(1)}(\theta')d\theta'$$

$$= \frac{iq}{M}\Phi_{k,\omega}\left[k\cos(\theta - \psi_k)\frac{\partial}{\partial V} + \kappa\frac{\partial}{\partial U}\right]<f>$$

$$- B_{k,\omega}(\theta)\phi_{k,\omega} \tag{2:2-5}$$

$$\left[\omega_c \frac{\partial}{\partial\theta} - i(\omega - \kappa U)\right]f_{k,\omega}^{(2)} + \int C_{k,\omega}(\theta - \theta')f_{k,\omega}^{(2)}(\theta')d\theta'$$

$$= -\frac{q}{M}\Phi_{k_\xi,\omega_\xi}\left\{\frac{kk_\xi}{\omega_c}\sin(\psi_k - \psi_{k_\xi}) - i\kappa_\xi\frac{\partial}{\partial U}\right. \tag{2:2-6}$$

$$\left. - ik_\xi\left[\cos(\theta - \psi_{k_\xi})\frac{\partial}{\partial V} - \frac{\sin(\theta - \psi_{k_\xi})}{V}\frac{\partial}{\partial\theta}\right]\right\}f_{k-k_\xi,\omega-\omega_\xi}$$

Now, we can define a propagator $G_{\underset{\sim}{k},\omega}(\theta,\theta')$ so that

$$[\omega_c \frac{\partial}{\partial\theta} - i(\omega - \kappa U)]G_{\underset{\sim}{k},\omega}(\theta,\theta') +$$

$$\text{(2:2-7)}$$

$$+ \int d\theta'' \, C_{\underset{\sim}{k},\omega}(\theta - \theta'')G_{\underset{\sim}{k},\omega}(\theta'',\theta') = \omega_c\delta(\theta - \theta')$$

Therefore $f_{\underset{\sim}{k},\omega}^{(2)}$ can be obtained in terms of $G_{\underset{\sim}{k},\omega}$

$$f_{\underset{\sim}{k},\omega}^{(2)}(\theta) = \int d\theta' \, G_{\underset{\sim}{k},\omega}(\theta,\theta') \cdot (-\frac{q}{M})\Phi_{\underset{\sim}{k}\underset{\sim}{\xi},\omega_\xi}\left[\frac{k k_\xi}{\omega_c} \sin(\psi_k - \psi_{k_\xi})\right.$$

$$- i\kappa_\xi \frac{\partial}{\partial U} - ik_\xi\left[\cos(\theta' - \psi_{k_\xi})\frac{\partial}{\partial V}\right.$$

$$\left.\left.- \frac{\sin(\theta' - \psi_{k_\xi})}{V} \frac{\partial}{\partial\theta'}\right]\right] f_{\underset{\sim}{k}-\underset{\sim}{k}_\xi,\omega-\omega_\xi}(\theta') \quad\text{(2:2-8)}$$

Substituting $f_{\underset{\sim}{k}'',\omega''}^{(2)}$ into $f_{\underset{\sim}{k}'',\omega''}^{(2)}$ on the left side of Eq. (2:2-3), we can obtain $C_{\underset{\sim}{k},\omega}(\theta - \theta')$ and $B_{\underset{\sim}{k},\omega}(\theta)$, the cyclotron harmonic component of which can be written as

$$\text{(2:2-9)}$$

$$C_{\underset{\sim}{k},\omega,n} = -\left(\frac{ik}{\omega_c}, \frac{\partial}{\partial U}, \frac{1}{V}\frac{\partial}{\partial V}, \frac{in}{V}\right) \underset{\substack{\underset{\sim}{k}'\\\omega'\\n'}}{\Sigma} \begin{pmatrix} D_{RR} & 0 & 0 & 0 \\ & 0 & & \\ & 0 & & \\ & 0 & & D_{\underset{\sim}{V}\underset{\sim}{V}} \end{pmatrix} \begin{bmatrix} \frac{ik}{\omega_c} \\ \frac{\partial}{\partial U} \\ \frac{\partial}{\partial V} \\ \frac{in}{V} \end{bmatrix}$$

$$B_{\underset{\sim}{k},\omega,n} = \qquad\qquad\qquad\qquad (2\!:\!2\text{-}10)$$

$$-\left(\frac{ik}{\omega_c},\ \frac{\partial}{\partial U},\ \frac{1}{V}\frac{\partial}{\partial V},\ \frac{in}{V}\right)\ \underset{\substack{\underset{\sim}{k}'\\ \omega'\\ n'}}{\Sigma}\ \begin{pmatrix} B_{RR} & 0 & 0 & 0 \\ & 0 & & \\ & 0 & & \\ & 0 & & B_{\underset{\sim}{VV}} \end{pmatrix}\ \begin{pmatrix} \dfrac{ik'}{\omega_c} \\[6pt] \dfrac{\partial}{\partial U} \\[6pt] \dfrac{\partial}{\partial V} \\[6pt] \dfrac{in'}{V} \end{pmatrix}\ \left\langle \phi_{k'},\omega'\,\delta f_{k',\omega'\ n'}\right\rangle$$

where

$$D_{RR} = \frac{q^2}{M^2}\ |\phi_{\underset{\sim}{k}',\omega'}|^2 G_{\underset{\sim}{k}'',\omega'',n''}\ \cdot\ \frac{k'^2}{2}\ J_{n'}^2(x'),$$

$$D_{\underset{\sim}{VV}} = \frac{q^2}{M^2}\ |\phi_{\underset{\sim}{k}',\omega'}|^2 G_{\underset{\sim}{k}'',\omega'',n''}\ \cdot$$

$$\begin{pmatrix} (\kappa' J_{n'}(x'))^2 & \dfrac{n'\omega_c\kappa'}{V}\ J_{n'}^2(x') & \dfrac{-k'\kappa'}{2}\dfrac{dJ_{n'}^2}{dx'} \\[14pt] \dfrac{n'\omega_c\kappa'}{V}\ J_{n'}^2(x') & \left(\dfrac{n'\omega_c}{V}\ J_{n'}(x')\right)^2 & \dfrac{-n'\omega_c k'}{2V}\ \dfrac{dJ_{n'}^2}{dx'} \\[14pt] \dfrac{-k'\kappa'}{2}\ \dfrac{dJ_{n'}^2}{dx'} & \dfrac{-n'\omega_c k'}{2V}\ \dfrac{dJ_{n'}^2}{dx'} & \left(k'\ \dfrac{dJ_{n'}}{dx'}\right)^2 \end{pmatrix}$$

$$B_{RR} = \frac{q^2}{M^2} G_{\underset{\sim}{k}'',\omega'',n''} \cdot \frac{kk'}{2} J_n^2(x) J_{n'}(x')$$

$$\beta_{\underset{\sim\sim}{VV}} = \frac{q^2}{M^2} G_{\underset{\sim}{k}'',\omega'',n''} \cdot J_n(x) \cdot$$

$$\left(
\begin{array}{ccc}
\kappa'\kappa J_{n'}(x') J_n(x) & \dfrac{n\omega_c \kappa'}{V} J_{n'}(x') J_n(x) & -k\kappa' \dfrac{dJ_n}{dx} J_{n'}(x') \\[2em]
\dfrac{n'\omega_c \kappa}{V} J_{n'}(x') J_n(x) & \dfrac{n'n\omega_c}{V^2} J_{n'}(x') J_n(x) & \dfrac{-n'\omega_c k}{V} \dfrac{dJ_n}{dx} J_{n'}(x') \\[2em]
-k'\kappa \dfrac{dJ_{n'}}{dx'} J_n(x) & \dfrac{-n\omega_c k'}{V} \dfrac{dJ_{n'}}{dx'} J_n(x) & kk' \dfrac{dJ_n}{dx} \dfrac{dJ_{n'}}{dx'}
\end{array}
\right)$$

and $x \equiv kV/\omega_c$, while n refers to the cyclotron harmonic number. In doing this, the ensemble average $\langle \ \rangle$ has included an average over the phase angles ψ_k and $\psi_{k'}$. That is,

$$\frac{q}{M} \left\langle \sum_{\substack{k' \\ \omega'}} \Phi_{\underset{\sim}{k}',\omega'} \frac{kk'}{\omega_c} \sin(\psi_k - \psi_{k'}) - i\kappa' \frac{\partial}{\partial U} \right.$$

$$- ik'(\cos(\theta - \psi_{k'}) \frac{\partial}{\partial V}$$

$$\left. - \frac{\sin(\theta - \psi_{k'})}{V} \frac{\partial}{\partial \theta} \cdot f_{\underset{\sim}{k}'',\omega''}^{(2)} \right\rangle$$

$$= \int d' \sum_{\substack{k' \\ \omega'}} \frac{q^2}{M^2} \left| \phi_{\underset{\sim}{k}',\omega'} \right|^2 \left\langle \frac{kk'}{\omega_c} \sin(\psi_k - \psi_{k'}) \right.$$

$$- i\kappa' \frac{\partial}{\partial U} - \frac{\partial}{\partial V}\Big(ik'\cos(\theta - \psi_{k'})\Big)$$

$$+ \frac{\partial}{\partial \theta}\Big(\frac{ik'\sin(\theta - \psi_{k'})}{V}\Big) \cdot \exp\Big[\frac{ik'V}{\omega_c}\sin(\theta - \psi_{k'})\Big]$$

$$\cdot G_{\underset{\sim}{k}'',\omega''}(\theta,\theta')\exp\Big[\frac{-ikV}{\omega_c}\sin(\theta' - \psi_k)\Big]$$

$$\cdot \Big[\frac{kk'}{\omega_c}\sin(\psi_{k'} - \psi_k) - i\kappa'\frac{\partial}{\partial U}$$

$$+ ik'\cos(\theta - \psi_k)\frac{\partial}{\partial V} - \frac{ik'\sin(\theta' - \psi_k)}{V}\frac{\partial}{\partial \theta'}\Big]\Big>$$

$$\cdot f_{\underset{\sim}{k},\omega}(\theta')$$

$$+ \int d\theta' \, \Phi_{\underset{\sim}{k},\omega}(\theta) \sum_{\substack{k' \\ \omega'}} \frac{q^2}{M^2}\Big<\Big[\frac{kk'}{\omega_c}\sin(\psi_k - \psi_{k'})$$

$$- \frac{\partial}{\partial U}(i\kappa') - \frac{\partial}{\partial V}\Big(ik'\cos(\theta - \psi_{k'})\Big)$$

$$+ \frac{\partial}{\partial \theta}\Big(\frac{ik'\sin(\theta - \psi_{k'})}{V}\Big)\Big]\exp\Big[\frac{ik'V}{\omega_c}\sin(\theta - \psi_{k'})\Big]$$

$$\cdot G_{\underset{\sim}{k}'',\omega''}(\theta,\theta') \cdot \exp\Big[- \frac{ikV}{\omega_c}\sin(\theta' - \psi_k)\Big]$$

$$\cdot \Big[\frac{kk'}{\omega_c}\sin(\psi_k - \psi_{k'}) - i\kappa\frac{\partial}{\partial U} - ik\cos(\theta' - \psi_k)\frac{\partial}{\partial V}$$

$$- \frac{ik\sin(\theta' - \psi_k)}{V}\frac{\partial}{\partial \theta'}\Big]\Big> \cdot \Big<\phi_{\underset{\sim}{k}',\omega'}\delta f_{\underset{\sim}{k}',\omega'}\Big>,$$

where averaged quantities $\langle .. \rangle$ depends only on $\theta - \theta'$.
The first and second $\int d\theta$ integrals yield $\int C_{\underset{\sim}{k},\omega}(\theta,\theta') \cdot$
$f_{\underset{\sim}{k},\omega}(\theta')d\theta'$ and $B_{\underset{\sim}{k},\omega}(\theta)\phi_{\underset{\sim}{k},\omega}$, respectively.

We notice that the resulting renormalized terms
are consistent with the non-Markovian structure of the
Vlasov equation; in particular, all cyclotron harmonics are
coupled. If one further makes a Markovian approximation,
where $G_{\underset{\sim}{k}'',\omega'',n''}$ is replaced by $G_{\underset{\sim}{k}',\omega',n'}$, it follows
that $C_{\underset{\sim}{k},\omega,n}$ is diagonalized in this case $C_{\underset{\sim}{k},\omega,n}$ is to
be identical to that obtained by Dum and Dupree.[7] In
that paper, the nonlinear dynamics are treated as a
stochastic-acceleration problem for a turbulent-magnetized
plasma.

The total fluctuation $f_{\underset{\sim}{k},\omega,n}$ consists of a com-
ponent $f^{c}_{\underset{\sim}{k},\omega,n}$ that is induced by the electric field, and
another component $f_{\underset{\sim}{k},\omega,n}$ that is generated by the mode-
coupling and is responsible for the localized structures.
To obtain the renormalized dielectric function $\epsilon_{\underset{\sim}{k},\omega}$, we
need the coherent response $f^{c}_{\underset{\sim}{k},\omega,n}$ that satisfies

$$\left[-i(\omega - \kappa U - n\omega_c) + C_{\underset{\sim}{k},\omega,n} \right] f^{c}_{\underset{\sim}{k},\omega,n}$$

$$= \frac{iq}{M} \phi_{\underset{\sim}{k},\omega} \left[\left[\exp\left(\frac{ikV}{\omega_c} \sin(\theta - \psi_k) \right) \left(k \cos(\theta - \psi_k) \frac{\partial}{\partial V} \right. \right. \right.$$

$$\left. \left. + \frac{\partial}{\partial \overline{U}} \right) \right]_n \langle f \rangle - \left(\frac{iM}{q} \right) B_{\underset{\sim}{k},\omega,n}$$

$$\frac{iq}{M} \, \phi_{\underset{\sim}{k},\omega} \left[\exp\left[\frac{ikV}{\omega_c} \sin(\theta - \psi_k) \right] \left[k \, \cos(\theta - \psi_k) \frac{\partial}{\partial V} \right. \right.$$

$$\left. \left. + \kappa \, \frac{\partial}{\partial U} \right] \right]_n \langle f \rangle_M \tag{2:2-11}$$

The last equality indicates that the effect of $B_{\underset{\sim}{k},\omega,n}$ is to modify the average distribution function $\langle f \rangle$, yielding $\langle f \rangle_M$. In the conventional nonlinear theory of wave fluctuations, only the coherent fluctuation $f^c_{\underset{\sim}{k},\omega,n}$ is included. Hence, by substituting $f_{\underset{\sim}{k},\omega,n}$ with $f^c_{\underset{\sim}{k},\omega,n}$, $B_{\underset{\sim}{k},\omega,n}$ can be expressed as

$$B_{\underset{\sim}{k},\omega,n} = \left(\frac{ik}{\omega_c}, \, \frac{\partial}{\partial U}, \, \frac{1}{V} \frac{\partial}{\partial V} V, \, \frac{in'}{V} \right) \cdot \sum_{\substack{k' \\ \omega' \\ n'}} \left[\beta_{\underset{\sim\sim}{VV}} \right] \cdot \begin{pmatrix} \dfrac{ik'}{\omega_c} \\[6pt] \dfrac{\partial}{\partial U} \\[6pt] \dfrac{\partial}{\partial V} \\[6pt] \dfrac{in'}{V} \end{pmatrix}$$

$$\cdot \left(\frac{iq}{M} \right) |\phi_{\underset{\sim}{k}',\omega'}|^2 \sum_m J_{m-n'}(x') J_m(x') G^*_{\underset{\sim}{k}',\omega',m} \left[\kappa' \, \frac{\partial}{\partial U} \right.$$

$$\left. + \frac{m\omega_c}{V} \frac{\partial}{\partial V} \right] \langle f \rangle \tag{2:2-12}$$

When the incoherent fluctuation $\widetilde{f}_{\underset{\sim}{k},\omega,n}$ is included, using the Poisson equation

$$k^2 \phi_{\underset{\sim}{k},\omega} = 4\pi n_0 \left[q \int \delta f^i_{\underset{\sim}{k},\omega} d\underset{\sim}{v}^i - e \int \delta f^e_{\underset{\sim}{k},\omega} d\underset{\sim}{v}^e \right] ,$$

Eqs. (2:2-11) and (2:2-12) of both species yield

$$\phi_{\underset{\sim}{k},\omega} \cdot \left[1 + \frac{4\pi n_0}{k^2} \sum_n \left[\frac{q^2}{M^2} \int \frac{d\underset{\sim}{v}^i}{2\pi} J_n^2(x_i) G^i_{\underset{\sim}{k},\omega,n} \right.\right.$$

$$\cdot (n\omega_{c_i} + \kappa U_i) \langle f_i \rangle$$

$$\left.\left. + \frac{e^2}{m^2} \int \frac{d\underset{\sim}{v}^e}{2\pi} J_n^2(x_e) G^e_{\underset{\sim}{k},\omega,n} (n\omega_{c_e} + \kappa U_e) \langle f_e \rangle \right]\right]$$

$$= \frac{4\pi n_0}{k^2} \left[q \int \delta \tilde{f}^i_{\underset{\sim}{k},\omega} d\underset{\sim}{v}^i - e \int \delta \tilde{f}^e_{\underset{\sim}{k},\omega} d\underset{\sim}{v}^e \right]$$

Thus, the total potential fluctuation

$$\phi_{k,\omega} = \frac{4\pi n_0}{\underset{\sim}{k}^2} \frac{\left(q \int \delta \tilde{f}^i_{\underset{\sim}{k},\omega} dv^i - e \int \delta \tilde{f}^e_{\underset{\sim}{k},\omega} dv^e \right)}{\epsilon_{k,\omega}}$$

$$= \frac{\tilde{\phi}^i_{\underset{\sim}{k},\omega} - \tilde{\phi}^e_{\underset{\sim}{k},\ddot{\omega}}}{\epsilon_{\underset{\sim}{k},\omega}} = \frac{\tilde{\phi}_{\underset{\sim}{k},\omega}}{\epsilon_{\underset{\sim}{k},\omega}} \qquad (2:2-13)$$

where $\epsilon_{\underset{\sim}{k},\omega}$ is the dielectric function containing contributions from the nonlinear wave-particle interactions. Equation (2:2-13) shows that the self-consistent field $\phi_{\underset{\sim}{k},\omega}$ can be viewed as if it were produced by a source field $\tilde{\phi}_{\underset{\sim}{k},\omega}$ caused by the incoherent fluctuations $\tilde{f}_{\underset{\sim}{k},\omega}$.

Since $\tilde{f}_{k,\omega}$ is incoherent with the fluctuating electric field, it satisfies the equation[10]

$$\left[-i(\omega - \kappa U - n\omega_c) + C_{k,\omega,n}\right]\tilde{f}_{k,\omega,n} = 0. \qquad (2:2-14)$$

That is, $f_{k,\omega}$ propagates along the particle orbit, and behaves as a macroparticle. Here, it is apparent that $C_{k,\omega,n}$ is responsible for the deviation from the unperturbed particle orbits.

2.3 Two-Point Correlation Equation

The incoherent fluctuation structure is elucidated by examination of the two-point, one-time correlation function of the phase-space density fluctuation, $\langle\delta f(1,t)\delta f(2,t)\rangle$. This correlation evolves on a slow time scale, since the fast variation from the particle orbiting at cyclotron frequency averages out. Turbulent relative diffusion dominates the evolution of a plasma on this time scale. The necessarily weak relative diffusion at small separation in the presence of a positive-free energy source results in very strong correlation at small separation in phase space.

It is straightforward to obtain an equation of the one-time, two-point correlation function of either species particles from the Vlasov equation,

$$\left[\frac{\partial}{\partial t} + \underset{\sim}{v}_1 \cdot \frac{\partial}{\partial \underset{\sim}{X}_1} + \underset{\sim}{v}_2 \cdot \frac{\partial}{\partial \underset{\sim}{X}_2} + \omega_c \underset{\sim}{v}_1 \times \hat{z} \cdot \frac{\partial}{\partial \underset{\sim}{v}_1} \right.$$

$$\left. + \omega_c \underset{\sim}{v}_2 \times \hat{z} \cdot \frac{\partial}{\partial \underset{\sim}{v}_2}\right] \left\langle \delta f(1) \delta f(2) \right\rangle$$

$$+ \frac{q}{M} \left\langle \left[\underset{\sim}{E}(1) \cdot \frac{\partial}{\partial \underset{\sim}{v}_1} + \underset{\sim}{E}(2) \cdot \frac{\partial}{\partial \underset{\sim}{v}_2}\right] \delta f(1) \delta f(2) \right\rangle$$

$$= - \frac{q}{M} \left[\left\langle \underset{\sim}{E}(1) \delta f(2) \right\rangle \cdot \frac{\partial}{\partial \underset{\sim}{v}_1} \left\langle f(1) \right\rangle \right.$$

$$\left. + \left\langle \underset{\sim}{E}(2) \delta f(1) \right\rangle \cdot \frac{\partial}{\partial \underset{\sim}{v}_2} \left\langle f(2) \right\rangle \right] \qquad (2:3-1)$$

At this point, we could proceed with the re-normalization of the triplet terms by treating each component of each point as shown previously. Then, arguing that variation of the correlation function in the relative coordinates is much stronger than that in the comoving coordinates, we could obtain an approximate renormalized equation for the correlation function. However, in cylindrical coordinates it is very tedious to perform the procedure of subtracting the renormalized equation of one

point from that of the other point to obtain a renormalized

equation in the relative coordinates (i.e., obtain

$\partial/\partial \underset{\sim}{q} \cdot \underset{\approx}{D}(-) \cdot \partial/\partial \underset{\sim}{q}$ by subtracting $\partial/\partial \underset{\sim}{q_1} \cdot \underset{\approx}{D}(1) \cdot \partial/\partial \underset{\sim}{q_1}$

from $\partial/\partial \underset{\sim}{q_2} \cdot \underset{\approx}{D}(2) \cdot \partial/\partial \underset{\sim}{q_2}$). Hence the method described

above is difficult and inefficient. Instead we shall

transform to the relative coordinates at the beginning of

the calculation. Renormalization is then carried out in

the relative-cylindrical coordinate. We note that this

method can indeed preserve the property that decorrelation

of nearby particles is caused by a relative force (Eq.

(2.3-2)).

 First, we introduce the relative coordinates

and the comoving coordinates

$$\underset{\sim}{X}_- = \frac{1}{2}\,(\underset{\sim}{X}_1 - \underset{\sim}{X}_2) \quad , \quad \underset{\sim}{v}_- = \frac{1}{2}\,(\underset{\sim}{v}_1 - \underset{\sim}{v}_2) \quad ,$$

$$\underset{\sim}{X}_+ = \frac{1}{2}\,(\underset{\sim}{X}_1 + \underset{\sim}{X}_2) \quad , \quad \underset{\sim}{v}_+ = \frac{1}{2}\,(\underset{\sim}{v}_1 + \underset{\sim}{v}_2)$$

In addition, let

$$\underset{\sim}{E}(-) \equiv \frac{1}{2}\,(\underset{\sim}{E}(1) - \underset{\sim}{E}(2)) \;,\; \underset{\sim}{E}(+) \equiv \frac{1}{2}\,(\underset{\sim}{E}(1) + \underset{\sim}{E}(2)).$$

We will assume that the plasma is homogeneous,

$$\frac{\partial}{\partial \underset{\sim}{X}_+} \left\langle \delta f(1) \delta f(2) \right\rangle = 0,$$

and that variation of the correlation function is much stronger in the relative coordinates than in the comoving coordinates,

$$\left| \frac{\partial}{\partial \underset{\sim}{v}_-} \left\langle \delta f(1) \delta f(2) \right\rangle \right| \gg \left| \frac{\partial}{\partial \underset{\sim}{v}_+} \left\langle \delta f(1) \delta f(2) \right\rangle \right|$$

Equation (2:3-1) simplifies to

$$\left[\frac{\partial}{\partial t} + \underset{\sim}{v}_- \cdot \frac{\partial}{\partial \underset{\sim}{X}_-} + \frac{q}{M} (\underset{\sim}{v}_- \times \underset{\sim}{B}_0) \cdot \frac{\partial}{\partial \underset{\sim}{v}_-} \right] \left\langle \delta f(1) \delta f(2) \right\rangle$$

$$+ \frac{q}{M} \left\langle \frac{\partial}{\partial \underset{\sim}{v}_-} \underset{\sim}{E}(-) \delta f(1) \delta f(2) \right\rangle$$

$$= - \frac{q}{M} \left[\left\langle \underset{\sim}{E}(1) \delta f(2) \right\rangle \cdot \frac{\partial}{\partial \underset{\sim}{v}_1} \left\langle f(1) \right\rangle \right.$$

$$\left. + \left\langle \underset{\sim}{E}(2) \delta f(1) \right\rangle \cdot \frac{\partial}{\partial \underset{\sim}{v}_2} \left\langle f(2) \right\rangle \right]$$

To renormalize the triplet term $\left\langle \underset{\sim}{E}(-) \delta f(1) \delta f(2) \right\rangle$, it is important to realize that the fast variation of $\delta f(1) \delta f(2)$ will beat with the fast variation of $\underset{\sim}{E}(-)$ yielding a net contribution to the ensemble-averaged triplet. Before ensemble averaging, we note that $\delta f(1) \delta f(2)$ satisfies

$$\left| \underset{\sim}{v}_+ \cdot \frac{\partial}{\partial \underset{\sim}{X}_+} \, \delta f(1) \delta f(2) \right| \gg \left| \underset{\sim}{v}_- \cdot \frac{\partial}{\partial \underset{\sim}{X}_-} \, \delta f(1) \delta f(2) \right|$$

and

$$\left| \underset{\sim}{v}_+ \times \underset{\sim}{B}_0 \cdot \frac{\partial}{\partial \underset{\sim}{v}_+} \, \delta f(1) \delta f(2) \right| \gg \left| \underset{\sim}{v}_- \times \underset{\sim}{B}_0 \cdot \frac{\partial}{\partial \underset{\sim}{v}_-} \, \delta f(1) \delta f(2) \right|$$

when $\left| \underset{\sim}{v}_- \right| \ll \left| \underset{\sim}{v}_+ \right|$. Hence $\delta f(1) \delta f(2)$ evolves according to the equation

$$\left[\frac{\partial}{\partial t} + \underset{\sim}{v}_+ \cdot \frac{\partial}{\partial \underset{\sim}{X}_+} + \frac{q}{M} \underset{\sim}{v}_+ \times \underset{\sim}{B}_0 \cdot \frac{\partial}{\partial \underset{\sim}{v}_+} \right] \delta f(1) \delta f(2)$$

$$+ \frac{q}{M} \left[\underset{\sim}{E}(+) \cdot \frac{\partial}{\partial \underset{\sim}{v}_+} \, \delta f(1) \delta f(2) \right.$$

$$+ \left. \underset{\sim}{E}(-) \cdot \frac{\partial}{\partial \underset{\sim}{v}_-} \, \delta f(1) \delta f(2) \right] = S(1,2)$$

where

$$S(1,2) = -\frac{q}{M} \left[\underset{\sim}{E}(1) \delta f(2) \cdot \frac{\partial}{\partial \underset{\sim}{v}_1} \langle f(1) \rangle \right.$$

$$+ \left. \underset{\sim}{E}(2) \delta f(1) \cdot \frac{\partial}{\partial \underset{\sim}{v}_2} \langle f(2) \rangle \right].$$

Hence, $G^{(0)}$, the linear propagator of the one-point equation, is an approximate propagator for $\delta f(1) \delta f(2)$. We

can then follow the procedure of one-point renormalization that the driven mode $(\delta f(1)\delta f(2))^{(2)}$ is substituted into $\partial/\partial \underset{\sim}{v} \cdot \langle \underset{\sim}{E}(-)(\delta f(1)\delta f(2)) \rangle$, to obtain

$$\frac{q}{M} \left\langle \frac{\partial}{\partial \underset{\sim}{v}} \underset{\sim}{E}(-)\delta f(1)\delta f(2) \right\rangle$$

$$\approx -\frac{q^2}{M^2} \underset{\substack{\underset{\sim}{k} \\ \omega \\ n}}{\Sigma} \left(\frac{1}{2\pi}\right)^4 \underset{\sim}{k} \cdot \frac{\partial}{\partial \underset{\sim}{v}} G^{(0)}_{\underset{\sim}{k},\omega,n} J_n^2 |\phi^{(-)}_{\underset{\sim}{k},\omega}|^2$$

$$\cdot \underset{\sim}{k} \cdot \frac{\partial}{\partial \underset{\sim}{v}} \langle \delta f(1)\delta f(2) \rangle .$$

where $\phi_{\underset{\sim}{k},\omega}(-) = \phi_{\underset{\sim}{k},\omega}\left[1 - \exp[i\underset{\sim}{k}\cdot\underset{\sim}{X}]\right]$. Finally, Eq.$(2:3-2)$ becomes

$$\left[\frac{\partial}{\partial t} + \underset{\sim}{v} \cdot \frac{\partial}{\partial \underset{\sim}{X}} + \frac{q}{M} \underset{\sim}{v} \times \underset{\sim}{B}_0 \cdot \frac{\partial}{\partial \underset{\sim}{v}} \right.$$

$$-\frac{q^2}{M^2} \underset{\substack{\underset{\sim}{k} \\ \omega \\ n}}{\Sigma} \left(\frac{1}{2\pi}\right)^4 \underset{\sim}{k} \cdot \frac{\partial}{\partial \underset{\sim}{v}} \left[J_n^2 G^{(0)}_{\underset{\sim}{k},\omega,n} |\phi_{\underset{\sim}{k},\omega}(-)|^2\right]$$

$$\text{(2:3-3)}$$

$$\left. \cdot \underset{\sim}{k} \cdot \frac{\partial}{\partial \underset{\sim}{v}} \right] \langle \delta f(1)\delta f(2) \rangle = \langle S(1,2) \rangle = S(1,1),$$

where the last equality is because $S(1,1)$ is a smooth function at small separation. The left-hand side

renormalized terms have the form of Fokker-Plank operators
acting on the correlation function. Also, the diffusion
coefficient here is simpler than that obtained previously.
This is because the separation of scales prevents the
operator $\underset{\sim}{k} \cdot \partial/\partial\underset{\sim}{v}$ from mixing with the propagator of co-
moving coordinates.

The source terms of both species can be calcu-
lated explicitly in a way similar to that used in con-
structing the test-particle-model Lenard-Balescu equa-
tion, where we separate

$$\langle \underset{\sim}{E}\delta f\rangle_{\underset{\sim}{k},\omega} \quad \text{into} \quad \langle \underset{\sim}{E}f^c\rangle_{\underset{\sim}{k},\omega} \quad \text{and} \quad \langle \underset{\sim}{E}f\rangle_{\underset{\sim}{k},\omega} .$$

A somewhat more complicated procedure (details shown in
Appendix B) using Eqs. (2:2-11), (2:2-14) yields

$$\langle S^e(1,1)\rangle = [D_{\parallel}^{ee} + D_{\parallel}^{ei}] \left(\frac{\partial\langle f_e\rangle}{\partial U}\right)^2$$

$$+ [F_{\parallel}^{ee} + F_{\parallel}^{ei}]\langle f_e\rangle \frac{\partial\langle f_e\rangle}{\partial U} \qquad (2:3-4)$$

$$S^i(1,1) = [D^{ii} + D^{ie}] : \frac{\partial\langle f_i\rangle}{\partial\underset{\sim}{V}} \frac{\partial\langle f_i\rangle}{\partial\underset{\sim}{V}}$$

$$+ [F^{ii} + F^{ie}] \cdot \langle f_i\rangle \frac{\partial\langle f_i\rangle}{\partial\underset{\sim}{V}} \qquad (2:3-5)$$

where

$$D_{\parallel}^{ee} = \frac{2e^2}{m^2} \sum_{\substack{k \\ \omega}} \frac{\kappa^2 |\tilde{\phi}_{k,\omega}^e|^2}{(2\pi)^4 |\epsilon_{k,\omega}|^2} G_{k,\omega}^{(e)} \ ,$$

$$D_{\parallel}^{ei} = \frac{2e^2}{m^2} \sum_{\substack{k \\ \omega}} \frac{\kappa^2 |\tilde{\phi}_{k,\omega}^i|^2}{(2\pi)^4 |\epsilon_{k,\omega}|^2} G_{k,\omega}^{(e)}$$

$$F_{\parallel}^{ee} = \frac{4e}{m} \sum_{\substack{k \\ \omega}} \frac{\langle \delta \tilde{f}^e \tilde{\phi}^e \rangle_k}{(2\pi)^4 |\epsilon_{k,\omega}|^2} G_{k,\omega}^{(e)} \frac{\text{Im}\chi_e}{\langle f_e \rangle} ,$$

$$F_{\parallel}^{ei} = \frac{4e}{m} \sum_{\substack{k \\ \omega}} \frac{\langle \delta \tilde{f}^e \tilde{\phi}^e \rangle_k}{(2\pi)^4 |\epsilon_{k,\omega}|^2} G_{k,\omega}^{(e)} \frac{\text{Im}\chi_i}{\langle f_e \rangle} \qquad (2:3-6)$$

$$\underset{\approx}{D}^{ii} : \frac{\partial \langle f_i \rangle}{\partial V} \frac{\partial \langle f_i \rangle}{\partial V}$$

$$= \frac{2q^2}{M^2} \sum_{\substack{k \\ \omega \\ n}} \frac{|\tilde{\phi}_{k,\omega}^i|^2}{(2\pi)^4 |\epsilon_{k,\omega}|^2} J_n^2 G_{k,\omega,n}^{(i)} \left[\frac{n\omega_c}{V} \frac{\partial \langle f_i \rangle}{\partial V} \right.$$

$$\left. + \kappa \frac{\partial \langle f_i \rangle}{\partial U} \right]^2$$

$$\underset{\approx}{D}^{ie} : \frac{\partial \langle f_i \rangle}{\partial V} \frac{\partial \langle f_i \rangle}{\partial V}$$

$$= \frac{2q^2}{M^2} \sum_{\substack{k \\ \omega \\ n}} \frac{|\tilde{\phi}_{k,\omega}^e|^2}{(2\pi)^4 |\epsilon_{k,\omega}|^2} J_n^2 G_{k,\omega,n}^{(i)} \left[\frac{n\omega_c}{V} \frac{\partial \langle f_i \rangle}{\partial V} \right.$$

$$\left. + \kappa \frac{\partial \langle f_i \rangle}{\partial U} \right]^2$$

$$\underset{\sim}{F}^{ii} \cdot \frac{\partial \langle f_i \rangle}{\partial \underset{\sim}{V}}$$

$$= \frac{4q}{M} \sum_{\substack{k \\ \omega \\ n}} \frac{\langle \delta \tilde{f}^i \tilde{\phi}^i \rangle_{\underset{\sim}{k}}}{(2\pi)^4 |\epsilon_{\underset{\sim}{k},\omega}|^2} J_n^2 G_{\underset{\sim}{k},\omega,n}^{(i)} \frac{Im\chi_i}{\langle f_i \rangle} \left[\frac{n\omega_c}{V} \frac{\partial \langle f_i \rangle}{\partial V} \right.$$

$$\left. + \kappa \frac{\partial \langle f_i \rangle}{\partial U} \right]$$

$$\underset{\sim}{F}^{ie} \cdot \frac{\partial \langle f_i \rangle}{\partial \underset{\sim}{V}}$$

$$= \frac{4q}{M} \sum_{\substack{k \\ \omega \\ n}} \frac{\langle \delta \tilde{f}^i \tilde{\phi}^i \rangle_{\underset{\sim}{k}}}{(2\pi)^4 |\epsilon_{\underset{\sim}{k},\omega}|^2} J_n^2 G_{\underset{\sim}{k},\omega,n}^{(i)} \frac{Im\chi_e}{\langle f_i \rangle} \left[\frac{n\omega_c}{V} \frac{\partial \langle f_i \rangle}{\partial V} \right.$$

$$\left. + \kappa \frac{\partial \langle f_i \rangle}{\partial U} \right] \tag{2:3-7}$$

and

$$\tilde{\phi}^e_{\underset{\sim}{k}} = \frac{4\pi n_o e}{k^2} \int d^3\underset{\sim}{v} \delta \tilde{f}^e_{\underset{\sim}{k}},$$

$$\tilde{\phi}^i_{\underset{\sim}{k}} = \frac{4\pi n_o q}{k^2} \int d^3\underset{\sim}{v} \delta \tilde{f}^i_{\underset{\sim}{k}},$$

$Im\chi_e$ and $Im\chi_i$ are the imaginary parts of the electron and ion susceptibilities, respectively. The sources are expressed in terms of Fokker-Planck operators. As

explained earlier, these describe the relaxation of the average distribution functions. The diffusion arises from stochastic acceleration of charged particles by the turbulent-electric field. The drag force results from collisionless exchange of momenta between charged particles.

For the electron source terms we have a local cancellation between the diffusion and the drag,

$$[\frac{\partial}{\partial U} D_\parallel^e \frac{\partial}{\partial U} - \frac{\partial}{\partial U} F_\parallel^{ee}]\langle f_e \rangle = 0 \ .$$

This is due to the conservation of particle momenta of localized same-species interactions occurring in a one-dimensional system. An analogy to this is the head-on collisions of two identical particles, in which they appear as to exchange phase-space positions without interacting. Hence, $\langle f_e \rangle$ does not relax because the final state is the same as the initial state. Relaxation of $\langle f_e \rangle$ thus requires the interaction of the electrons with the ions. By contrast, the ion dynamics is three-dimensional, hence the constraint for the one-dimensional interactions is broken. The same-species interactions of ions can now contribute to relax the average distribution function $\langle f_i \rangle$.

When $T_\parallel^i = T_\perp^i$, and $\langle f_i \rangle$ is Maxwellian, we can show (in Appendix B) that the same-species interactions cancel, i.e.,

$$[\frac{\partial}{\partial v} \cdot D^i \cdot \frac{\partial}{\partial v} - \frac{\partial}{\partial v} \cdot F^{ii}]\langle f \rangle^i = 0 \ .$$

The fact that $\langle f_i \rangle$ is isotropic and Maxwellian is crucial for this local cancellation. This is because an isotropic Maxwellian distribution has no free energy by itself, thus the same-species interactions alone cannot relax $\langle f_i \rangle$. In anisotropic collisionless plasmas, the same-species interactions are actually responsible for temperature isotropization. Here, in a current-driven plasma with $T_\parallel^i \neq T_\perp^i$, the isotropization terms are small in comparison to others that are responsible for relaxation of the current. This is because isotropization terms are proportional to the interaction of different harmonics n and m by a very weak coupling

$$(n - m) \frac{\omega_{ci}}{k_\parallel v_{ti}} \cdot \exp[-(n - m)^2 \frac{\omega_{ci}^2}{k_\parallel^2 v_{ti}^2}] \ ,$$

where the argument of the exponential has magnitude much larger than unity. Thus they are hereafter ignored.

Finally, we transform Eq. (2:3-3) to the guiding-center coordinates, and require that

$$\langle \delta f(1)\delta f(2)\rangle^i = 0.$$

This is consistent with the fact that relative evolution, which determines $\langle \delta f(1)\delta f(2)\rangle$, is slowly varying on the gyro-time scale. It then follows that

$$\left\{ \frac{\partial}{\partial t} + U_- \frac{\partial}{\partial Z_-} - \frac{q^2}{M^2} \sum_{\substack{k\\\omega\\n}} \frac{J_n^2}{(2\pi)^4} |\phi_{k,\omega}|^2 G_{k,\omega,n}^{(i)} \cdot \left[\left[\frac{k^4 v^2}{4\omega_{ci}^2} \right. \right. \right.$$

$$\left. + \frac{k^4 R^2}{8} + \frac{\kappa^2 k^2 Z^2}{2} \right] \frac{1}{\omega_{ci}^2} \frac{\partial^2}{\partial R_-^2}$$

$$+ \left[\frac{k^4 v^2}{8\omega_{ci}^2} + \frac{k^4 R^2}{4} + \frac{\kappa^2 k^2 Z^2}{2} \right] \frac{\partial^2}{\partial v_-^2}$$

$$\left. \left. + \left[\frac{k^2\kappa^2 v^2}{2\omega_{ci}^2} + \frac{k^2\kappa^2 R^2}{2} + \kappa^4 Z^2 \right] \frac{\partial^2}{\partial U_-^2} \right] \right\}^i \langle \delta f(1)\delta f(2)\rangle^i$$

$$= \langle S\rangle^i .\qquad(2:3-8)$$

This renormalized equation is only valid for high-frequency fluctuations. This is because in obtaining the simple expression for relative diffusion, we have assumed a

separation of time scales between the comoving motion and relative motion, thus

$$\left| \frac{\partial}{\partial \theta_+} \delta f(1) \delta f(2) \right| \gg \left| \frac{\partial}{\partial \theta_-} \delta f(1) \delta f(2) \right|.$$

Equation (2.3-8) then corresponds to the lowest order of the relative gyro-kinetic ordering, i.e.,

$$\omega_c \frac{\partial}{\partial t} \gg 1.$$

It is straightforward to obtain the equation for the electron-correlation function

$$\left[\frac{\partial}{\partial t} + U_- \frac{\partial}{\partial Z_-} - \frac{e^2}{m^2} \sum_{\substack{k \\ \omega}} |\phi_{k,\omega}|^2 G_{k,\omega}^{(e)} \kappa^4 z_-^2 \frac{\partial^2}{\partial U_-^2} \right]^e \langle \delta f(1) \delta f(2) \rangle^e$$

$$= \langle S \rangle^e \qquad\qquad (2.3-9)$$

Here, we have used $\bar{k}\rho_e \ll 1$ (highly magnetized electrons), hence the electron motion is one-dimensional.

C H A P T E R   I I I

TWO-POINT THEORY OF CURRENT-DRIVEN
ION-CYCLOTRON TURBULENCE (B)

In this chapter, we attempt to study the small-scale structures of ion-cyclotron clumps and investigate global effects due to clumps. For the former, we are able to determine the clump shapes and lifetimes for both species in ion-cyclotron turbulence. For the latter, we can determine the threshold drift velocity for clumps to excite, and its growth rate near marginal instability. Also, we can estimate the saturated turbulence level, and thus anomalous resistivity in stationary turbulence.

3.1 Steady State

In current-driven ion-cyclotron turbulence, the ion-perpendicular velocity is scattered, and the current-free energy is converted into perpendicular ion-thermal energy. During this process the average-distribution functions of electrons and ions vary slowly on a time scale much slower than that of nonlinear evolution. This can be shown as follows.

Nonlinear evolution occurs on a time scale

$$\tau_{NL} \approx \tau_e = \left(\frac{1}{\bar{\kappa}^2 D_{\parallel}^e} \right)^{\frac{1}{3}}$$

where $D_{\parallel}^e$ is the electron parallel diffusion coefficient. The quasi-linear flattening of the electron distribution function and the perpendicular heating of ions occur on the time scales of

$$\tau_{QL}^e \approx \frac{v_{te}^2}{D_{\parallel}^e}$$

and

$$\tau_{heat}^i \approx \frac{v_{ti}^2}{D^i} \approx \frac{v_{te}^2}{D_{\parallel}^e} \cdot \left[\left(\frac{1}{\bar{k}\rho_i} \right)^4 \left(\frac{\bar{\kappa}^{4} v_{te}^2 v_{ti}^2}{\omega_{ci}^4} \right) \right],$$

respectively, where v_{te}^2 and v_{ti}^2 are electron and ion thermal velocity, respectively. For $|e\phi/T_e| \ll 1$, it follows

$$\frac{\tau_{QL}^e}{\tau_{NL}} \gtrsim \omega_{ci}^2 \tau_e^2 \gg \left[\left(\frac{1}{\bar{k}\rho_i} \right)^4 \left(\frac{\bar{\kappa}^{4} v_{te}^2 v_{ti}^2}{\omega_{ci}^4} \right) \right] \omega_{ci}^2 \tau_e^2 \approx \frac{\tau_{heat}^i}{\tau_{NL}} \gg 1.$$

Hence, we can regard the average-distribution functions as stationary over the time scale of interest. In this section, we will calculate the small-scale correlation

functions for these quasi-stationary distribution functions.

Formally, one can invert the operators on the left side of Eqs. (2:3-8) and (2:3-9) (imposing the appropriate boundary conditions), and obtain

$$<\delta f(1)\delta f(2)>^{\sigma} = \tau_{cl}^{\sigma}(\underset{\sim}{X}_-,\underset{\sim}{V}_-)<S>^{\sigma} , \qquad (3:1-1)$$

where τ_{cl}^{σ} is an operator of species σ. Physically, τ_{cl}^{σ} is the time for decorrelation of two nearby phase-space points, separated by $\underset{\sim}{X}_-,\underset{\sim}{V}_-$. This understanding enables one to estimate the eigenvalues of τ_{cl}^{σ} by solving for the relative trajectory of two initially-neighboring phase-space points.

In ion-cyclotron turbulence, electrons are strongly magnetized and their motion is restricted to the vicinity of the same field line, hence the perpendicular motion is negligible. On the other hand, since ion trajectories have moderate Larmor radii, the perpendicular electric field can scatter an ion off a field line. This perpendicular diffusion takes place sufficiently rapidly so that the parallel motion is simply free-streaming. (The relative importance of the perpendicular and the

parallel diffusion of ions depends on the level of fluc-
tuation and the ratio of the perpendicular and the paral-
lel wavenumbers. Experiments[3] and computer simulations[6]
both show strong perpendicular-ion heating, which indi-
cates the dominance of the perpendicular-velocity dif-
fusion.)

A set of coupled equations describing the rela-
tive trajectories can be obtained for each species,

$$\frac{d}{dt} <R_-^2> = \frac{3}{4} Q \frac{<R_-^2>}{\omega_{ci}^2} + \frac{1}{4} \frac{Q}{\omega_{ci}^4} <V_-^2> + \frac{H}{2\omega_{ci}^2} <Z_-^2>$$

$$\frac{d}{dt} \frac{<V_-^2>}{\omega_{ci}^2} = \frac{1}{4} Q \frac{<R_-^2>}{\omega_{ci}^2} + \frac{3}{4} \frac{Q}{\omega_{ci}^4} <V_-^2> + \frac{H}{2\omega_{ci}^2} <Z_-^2>$$

$$\frac{d}{dt} Z_- = U_-$$

(3:1-2)

for ions, and

$$\frac{d^3 <Z_-^2>}{dt^3} = F <Z_-^2>$$

$$\frac{d <R_-^2>}{dt} = 0$$

$$\frac{d <V_-^2>}{dt} = 0$$

(3:1-3)

for electrons, where

$$\begin{pmatrix} Q \\ H \end{pmatrix} = \frac{q^2}{M_i^2} \left(\frac{1}{2\pi}\right)^4 \sum_{\substack{\underset{\sim}{k} \\ \omega \\ n}} J_n^2 |\phi_{\underset{\sim}{k},\omega}|^2 G_{\underset{\sim}{k},\omega,n}^i \begin{pmatrix} k^4 \\ k^2\kappa^2 \end{pmatrix},$$

and

$$F = \frac{e^2}{m_e^2} \left(\frac{1}{2\pi}\right)^4 \sum_{\substack{\underset{\sim}{k} \\ \omega}} |\phi_{\underset{\sim}{k},\omega}|^2 G_{\underset{\sim}{k},\omega}^e \kappa^4$$

The time-asymptotically dominant solutions are

$$\langle Z_-^2(t)\rangle^i = \langle Z_-^2(0)\rangle^i + 2\langle U_-(0)Z_-(0)\rangle^i t + \langle U_-^2(0)\rangle^i t^2$$

$$\langle X_-^2(t)\rangle^i = \frac{3}{4} \exp(t/\tau_i) \left[\bar{k}^2 \langle X_-^2(0)\rangle^i \right.$$

$$+ \frac{\langle V_-^2(0)\rangle^i}{2\omega_{ci}^2} + \left(\frac{\bar{\kappa}}{\bar{k}}\right)^2 \left[\langle Z_-^2(0)\rangle^i \right. \qquad (3:1\text{-}4)$$

$$\left. \left. + 2\langle U_-(0)\rangle^i \tau_i + 2\langle U_-^2(0)\rangle^i \tau_i^2 \right] \right]$$

$$\langle Z_-^2(t)\rangle^e = \frac{1}{3} \exp(t/\tau_e) \, \bar{\kappa}^2 \left[\langle Z_-^2(0)\rangle^e \right.$$

$$+ 2\langle U_-(0)Z_-(0)\rangle^e \tau_e + 2\langle U_-^2(0)\rangle^e \tau_e^2$$

$$\left. + \left(\frac{\bar{k}}{\bar{\kappa}}\right)^2 \frac{X_-^2(0)^e}{2} \right] \qquad (3:1\text{-}5)$$

$$\langle X^2_-(t)\rangle^e = \langle X^2_-(0)\rangle^e \quad .$$

where $\tau_i = \omega_{ci}^2/Q$, $\tau_e = (F)^{-1/3}$ and

$$\langle X^2_-\rangle = \langle R^2_-\rangle + \frac{\langle v^2_-\rangle}{2\omega_c} \quad .$$

Notice that on the time scale of relevance, ions freely stream along the field line and experience turbulent scattering across the field line; while the electron motion is dominated by parallel diffusion. The exponential time-dependence of rapid decorrelation results from the nature of the relative-diffusion coefficients. When $\tau < \tau_i$ (or $t < \tau_e$), the relative motion is slow because of weak relative diffusion. When $t > \tau_i$ (or $t > \tau_e$) the particles have decorrelated, hence the relative motion becomes rapidly varying.

The clump life time $\tau_{cl}(\underset{\sim}{X}_-, \underset{\sim}{V}_-)$ is defined as the time that two nearby phase-space points require to achieve a separation of a distance $\langle|\underset{\sim}{k}|\rangle^{-1}$, so that

$$\bar{k}^2\langle X^2_-(\tau_{cl})\rangle + \bar{\kappa}^2\langle Z^2_-(\tau_{cl})\rangle = 1 \quad . \tag{3:1-6}$$

Substituting X^2_- and Z^2_- from Eqs. (3:1-4) and (3-1?5) into Eq. (3:1-6), we obtain

$$\tau^i_{cl} = \tau_i \ell n \left\{ \frac{4/3}{\overline{k}^2 X^2_- + \dfrac{\overline{k}^2 V^2_=}{2\omega^2_{cl}} + \overline{\kappa}^2 (Z^2_- + 2U_- Z_- \tau_i + 2U^2_- \tau^2_i)} \right\}$$

(3:1-7)

$$\tau^e_{cl} = \tau_e \ell n \left\{ \frac{3}{\dfrac{\overline{k}^2 X^2_=}{2} + \overline{\kappa}^2 (Z^2_- + 2U_- Z_- \tau_e + 2U^2_- \tau^2_e)} \right\}$$

(3:1-8)

The arguments of logarithmic functions are exactly the initial separations of time-asymptotically dominant solutions of $\langle X^2_{\perp-}(t) \rangle^i$ and $\langle Z^2_-(t) \rangle^e$, respectively.

From Eqs. (3:1-7) and (3:1-8), it is possible to characterize phase-space structures (clumps) in ion-cyclotron turbulence. The electron clump, in position space, appears as a cigar-shaped group of electrons aligned along the magnetic field, with the length and radius $(\overline{\kappa})^{-1}$ and $(\overline{k})^{-1}$, respectively; in velocity space, it appears as a thin disc with thickness (in U) and radius (in V) $(\overline{\kappa}\tau_e)^{-1}$ and v_{te}, respectively (Fig. 3.1). The ion clump, in position space appears as a gyrating tether-rod about the guiding center, with the tether length ρ_i, if $\overline{k}\rho_i > 1$, and as a cigar aligned with the magnetic field
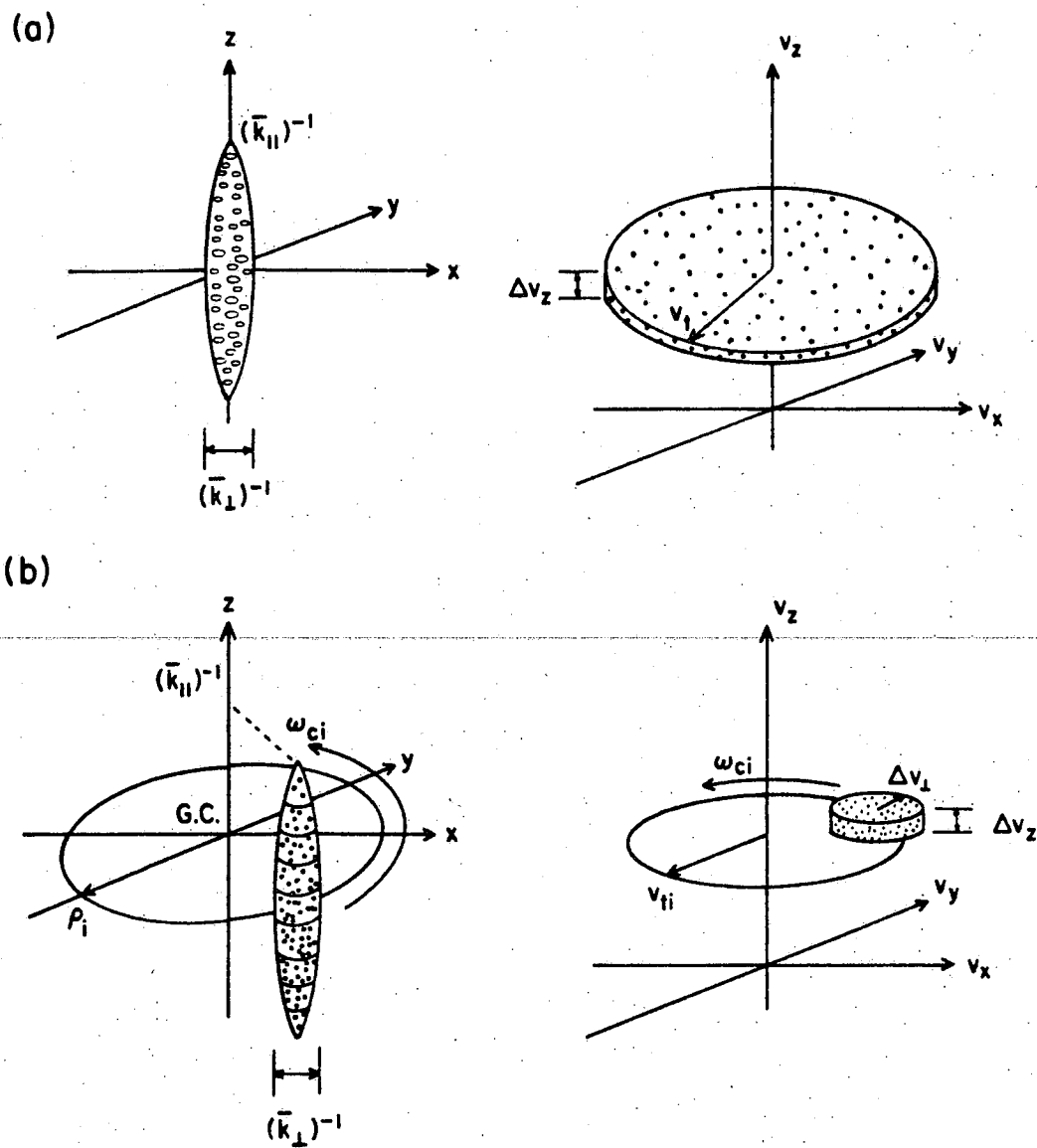
Figure 3-1.   Illustrations for the electron clump and
the ion clump with $\bar{k}_\perp \rho_i < 1$ (a), and the
ion clump, with $\bar{k}_\perp \rho_i > 1$ and the perpendicu-
lar clump velocity of the order of the ion
thermal velocity (b)

if $\overline{k}\rho_i < 1$. Both cigar and rod have radii $(\overline{k})^{-1}$ and lengths $(\overline{\kappa})^{-1}$. In velocity space, the ion clump appears as a gyrating tether-disc perpendicular to the magnetic field, with the disc radius $v_{ti}(\overline{k}\rho_i)^{-1}$ and tether length v_{ti} if $\overline{k}\rho_i > 1$, and as a thin disc of radius v_{ti} if $\overline{k}\rho_i < 1$; the thickness of both discs is $(\overline{\kappa}\tau_i)^{-1}$ (Fig. 3.1).

One may notice that both of the clump lifetimes have similar dependence on the parallel velocities U_-^σ, in that they scale to $1/\kappa\tau_\sigma$, while V_-^i scales to ω_{ci}/k for the ion-clump lifetime. Since ions primarily experience perpendicular scattering, one might expect that V_-^i, instead of U_-^i, would scale to $1/\tau_i$. The reason is discussed here. The ion clump has basic correlation lengths $(\overline{\kappa})^{-1}$ and $(\overline{k})^{-1}$ in the parallel and perpendicular directions, respectively. Furthermore, in the perpendicular direction, the Lorentz force is much stronger than the relative turbulent electric field, thus correlation in the perpendicular velocity scale is determined by the relative gyro-motion and is ω_{ci}/k. In the parallel direction, on the other hand, the dynamics are essentially ballistic streaming. Hence, the parallel velocity correlation length does not directly result from parallel

scattering, but from the fact that the parallel velocity dispersion leads to perpendicular particle scattering by waves of different phase velocities, which causes decorrelation. Since the scattering occurs on the time scale τ_i, thus the parallel velocity correlation scales to τ_i. For electrons, the (relative) turbulent parallel electric field scatters relative parallel velocity, hence U_-^e scales to τ_e. This explains why in the expressions for clump life times the parallel velocities are associated with the decorrelation time, while the perpendicular velocities are not. It is instructive to note that in deriving the expression of ion-clump lifetime, we have used the fact that

$$\left| \omega_{ci} \frac{\partial}{\partial t} \right| \gg 1 \quad \text{or} \quad \tau_i \omega_{ci} \gg 1$$

in Section 2.3. These are equivalent to the assumption that the ion Lorentz force is much stronger than the turbulent electric force field. In the limit of weak magnetic and strong fluctuating electric fields, where the straight-line-orbit limit can be recovered, the above analysis is invalid.

Following Boutros-Ghali, and Dupree,[10] we can evaluate the clump component of the two-point correlation

function,

$$\langle \widetilde{f}\widetilde{f} \rangle^{\sigma} \sim \left[\tau_{cl}^{\sigma}(\underset{\sim}{X}_-, \underset{\sim}{V}_-) - \tau_{\sigma} \right] \langle S \rangle^{\sigma} \qquad (3:1\text{-}9)$$

That is, the nonsingular part of the correlation function has an approximate magnitude $\tau_{\sigma} \langle S \rangle^{\sigma}$.

To investigate moments and extract results, one can integrate over velocities in Eq. (3:1-9). After spatial-temporal Fourier transformation and integration over $\underset{\sim}{V}_1$ and $\underset{\sim}{V}_2$, we have

$$\int d\underset{\sim}{V}_1 d\underset{\sim}{V}_2 \langle \delta\widetilde{f}(1)\delta\widetilde{f}(2) \rangle_{\underset{\sim}{k}}^{e} = -\int d\underset{\sim}{X}_- e^{i\underset{\sim}{k}\cdot\underset{\sim}{X}_-}$$

$$\cdot \int d\underset{\sim}{V}_- \tau_e \ln\left[\frac{\overline{\kappa}^2}{8.15}\left[Z_-^2 + 2U_- Z_- \tau_e + 2U_-^2 \tau_e^2 \right.\right.$$

$$\left.\left. + \frac{\overline{k}^2}{2\overline{\kappa}^2} X_{\perp-}^2 \right]\right] \int d\underset{\sim}{V}_+ \langle S \rangle \qquad (3:1\text{-}10)$$

and

$$\int d\underset{\sim}{V}_1 d\underset{\sim}{V}_2 \langle \delta\widetilde{f}(1)\delta\widetilde{f}(2) \rangle_{\underset{\sim}{k}}^{i} = -\int d\underset{\sim}{X}_- e^{i\underset{\sim}{k}\cdot\underset{\sim}{X}_-}$$

$$\cdot \int d\underset{\sim}{V}_- \tau_i \ln\left[\frac{\overline{k}^2}{2}\left[X_{\perp-}^2 + \frac{V_-^2}{2\omega_{ci}^2} + \frac{\overline{\kappa}^2}{\overline{k}^2}\left[Z_-^2 + 2U_- Z_- \tau_i \right.\right.\right.$$

$$\left.\left.\left. + 2U_-^2 \tau_i^2 \right]\right]\right] \int d\underset{\sim}{V}_+ \langle S \rangle \qquad (3:1\text{-}11)$$

Notice that the integrand has a width $1/\kappa\,\tau_\sigma$ in U_-^σ, hence the integral $\int dU_-^\sigma$ introduces a factor $1/\tau_\sigma$ to cancel the coefficient τ_σ of the clump lifetime. Therefore, the original nonlinear equations of squared fluctuation amplitudes become linear after the velocity integration. Using Poisson's equation, we obtain

$$
\langle \tilde{\phi}^2 \rangle_{\underset{\sim}{k},\omega}^{i} = \frac{8 A^i(\underset{\sim}{k})\, \Lambda_{n_\omega}(k\rho_i)}{\pi k^4} \sum_{\underset{\sim}{k}'} \frac{\dfrac{\Lambda_{n'_\omega}(2k'\rho_i)}{2\Lambda_{n'_\omega}(k'\rho_i)}\ \kappa'(k')^4}{(2\pi)^3 \,|\epsilon_{\underset{\sim}{k}',\omega'}|^2}
$$

$$
\cdot \left[\langle \tilde{\phi}^2 \rangle_{\underset{\sim}{k}',\omega'}^{e}\, (\mathrm{Im}\chi_{\underset{\sim}{k}',\omega'}^{i})^2 \right.
$$

$$
\left. + \langle \tilde{\phi}^2 \rangle_{\underset{\sim}{k}',\omega'}^{i}\, \mathrm{Im}\chi_{\underset{\sim}{k}',\omega'}^{i}\, \mathrm{Im}\chi_{\underset{\sim}{k}',\omega'}^{e} \right] \Bigg|_{\dfrac{\omega - n_\omega \omega_{ci}}{\kappa} \,=\, \dfrac{\omega' - n'_\omega \omega_{ci}}{\kappa'}}
$$

and

$$
(3:1\text{-}12)
$$

$$
\langle \tilde{\phi}^2 \rangle_{\underset{\sim}{k},\omega}^{e} = \frac{8 A^e(\underset{\sim}{k})}{\pi k^4} \sum_{\underset{\sim}{k}'} \frac{\kappa'(k')^4}{(2\pi)^3 \,|\epsilon_{\underset{\sim}{k}',\omega'}|^2}
$$

$$
\cdot \left[\langle \tilde{\phi}^2 \rangle_{\underset{\sim}{k}',\omega'}^{i}\, (\mathrm{Im}\chi_{\underset{\sim}{k}',\omega'}^{e})^2 \right.
$$

$$
\left. + \langle \tilde{\phi}^2 \rangle_{\underset{\sim}{k}',\omega'}^{e}\, \mathrm{Im}\chi_{\underset{\sim}{k}',}^{i}\, \mathrm{Im}\chi_{\underset{\sim}{k}',\omega'}^{e} \right] \Bigg|_{\dfrac{\omega}{\kappa} \,=\, \dfrac{\omega'}{\kappa'}} \qquad (3:1\text{-}13)
$$

where terms proporation to $\langle \tilde{\phi}^2 \rangle_{\underset{\sim}{k}',\omega'}^{e}(\mathrm{Im}\chi^i)^2$, $\langle \tilde{\phi}^2 \rangle_{\underset{\sim}{k}',\omega'}^{i}\,\mathrm{Im}\chi^i\,\mathrm{Im}\chi^e$ in Eq. (3:1-12) and $\langle \tilde{\phi}^2 \rangle_{\underset{\sim}{k}',\omega'}^{i}\,\mathrm{Im}\chi^i\,\mathrm{Im}\chi^e$,

$<\phi^2>^i_{\underset{\sim}{k}',\omega'}$, $(Im\chi^e)^2$ in Eq. (3:1-13) correspond to D^{ie}, F^{ie} and D^{ei}, F^{ei}, respectively.

$$A^\sigma(\underset{\sim}{k}) = \int d\underset{\sim}{v} \int d\underset{\sim}{X} e^{i\underset{\sim}{k}\cdot\underset{\sim}{X}}[\tau^\sigma_{cl} - \tau_\sigma],$$

and

$$_n(k\rho_i) = I_n(k^2\rho_i^2)e^{-k^2\rho_i^2} .$$

The summation over n has one dominant term $n = n_\omega$, for a given ω, because the ions can only interact with fluctuations with Doppler-shifted phase velocity $\omega - n\omega_c/\kappa$ near the ion thermal velocity. Since κ is small ($\kappa << \omega_{ci}/v_{ti}$) in ion-cyclotron turbulence, only one harmonic is resonant.

To evaluate the $\underset{\sim}{k}'$ integral, we note that $1/|\epsilon_{\underset{\sim}{k}',\omega'}|^2$ can be expressed as $1/|Re\epsilon_{\underset{\sim}{k}',\omega'}|^2 + |Im\epsilon_{\underset{\sim}{k}',\omega'}|^2$, which is peaked where both $Re\epsilon_{\underset{\sim}{k}',\omega'}$ and $Im\epsilon_{\underset{\sim}{k}',\omega'}$ are minimal. Since the magnitude of $|Re\epsilon_{\underset{\sim}{k}',\omega'}|$ is generally larger than that of $|Im\epsilon_{\underset{\sim}{k}',\omega'}|$ (when $T^i_\parallel \le T^i_\perp$), the minimum of $|\epsilon_{\underset{\sim}{k}',\omega'}|^2$ is located near where $|Re\epsilon_{\underset{\sim}{k}',\omega'}| = 0$ and $|Im\epsilon_{\underset{\sim}{k}',\omega'}|$ is minimal. Hence the $\underset{\sim}{k}'$ integral can be evaluated at the zero of $Re\epsilon_{\underset{\sim}{k}',\omega'}$

(for situations where the magnitude of $|\mathrm{Re}\epsilon|$ is not necessarily larger than that of $|\mathrm{Im}\epsilon|$, see Appendix C).

As a result, ion-cyclotron clumps are associated with ion-cyclotron waves, for which $\mathrm{Re}\,\epsilon_{\underset{\sim}{k},\omega} = 0$. In the limit $T_{\perp}^{i} \gg T_{\parallel}^{i}$, the magnitude of $|\mathrm{Im}\epsilon_{\underset{\sim}{k},\omega}|$ is comparable to $|\mathrm{Re}\epsilon_{\underset{\sim}{k},\omega}|$ because the normal mode frequencies are approaching cyclotron harmonics where the wave dissipation is the greatest. Hence, in the spectrum sum the approximation $\mathrm{Re}\,\epsilon_{\underset{\sim}{k}',\omega'} = 0$ is not valid, and the ballistic frequencies do not coincide with the normal mode frequencies. In fact, the long-range character of waves disappears due to the highly dissipative media. Ion cyclotron turbulence then consists of only the clump fluctuations, analogous to ion-acoustic turbulence with equal ion and electron temperatures. In this regime, one must solve the integral equations numerically. Hereafter, we shall confine ourselves to the wave-clump regime.

Thus, using the pole approximation, evaluating $\underset{\sim}{k}$ at $\underset{\sim}{k}_{\omega}$, and assuming that only one harmonic is dominant for a given ω, we obtain the expression

$$
<\phi^2>_{\underset{\sim}{k},\omega}^{e}\Big|_{\underset{\sim}{k}=\underset{\sim}{k}_{\omega}} = \left[\frac{a^{e}k^2\lambda_D^2}{|\mathrm{Im}\epsilon_{\underset{\sim}{k},\omega}|} \left[(\mathrm{Im}\chi_{\underset{\sim}{k},\omega}^{e})^2 <\widetilde{\phi}^2>_{\underset{\sim}{k},\omega}^{i} \right.\right.
$$

$$
\left.\left. + \mathrm{Im}\chi_{\underset{\sim}{k},\omega}^{e}\mathrm{Im}\chi_{\underset{\sim}{k},\omega}^{i}<\widetilde{\phi}^2>_{\underset{\sim}{k},\omega}^{e} \right]\right]\Big|_{\underset{\sim}{k}=\underset{\sim}{k}_{\omega}} \qquad (3:1-14)
$$

$$\langle\phi^2\rangle^i_{\underset{\sim}{k},\omega}\Big|_{\underset{\sim}{k}=\underset{\sim}{k}_\omega} = \left[\frac{a^i \underset{\sim}{k}^2\lambda_D^2}{|Im\epsilon_{\underset{\sim}{k},\omega}|}\left[(Im\chi^i_{\underset{\sim}{k},\omega})^2\langle\tilde{\phi}^2\rangle^e_{\underset{\sim}{k},\omega}\right.\right.$$

$$\left.\left. + Im\chi^e_{\underset{\sim}{k},\omega}Im\chi^i_{\underset{\sim}{k},\omega}\langle\tilde{\phi}^2\rangle^i_{\underset{\sim}{k},\omega}\right]\right]\Big|_{\underset{\sim}{k}=\underset{\sim}{k}_\omega} . \qquad (3:1-15)$$

Here, $a^e \sim 0.7$, $a^i \sim 0.15/\bar{k}^2\rho_i^2 \sim 0.1$, obtained from $A^e(\underset{\sim}{k}_\omega)$ and $A^i(\underset{\sim}{k}_\omega)$, respectively. A condition for stationary turbulence,

$$(a^e + a^i)\underset{\sim}{k}^2\lambda_D^2 Im\chi^e_{\underset{\sim}{k},\omega}Im\chi^i_{\underset{\sim}{k},\omega} = -|Im\epsilon_{\underset{\sim}{k},\omega}| = Im\epsilon_{\underset{\sim}{k},\omega},$$

$$(3:1-16)$$

follows directly. The choice of sign is based on the physical motivation that the waves must be overdamped in the presence of a (nonlinear) noise source. Moreover, the structure of Eq. (3:1-16) persists in other plasma-turbulence problems, such as the wave-clump regime of ion-acoustic turbulence, drift-wave turbulence, etc.

The frequency linewidth due to the finite collective dissipation $Im\epsilon_{\underset{\sim}{k},\omega}$ can be expressed as

$$\Delta\omega_{\underset{\sim}{k}} = \left|Im\epsilon_{\underset{\sim}{k},\omega}\Big/\frac{\partial Re\epsilon_{\underset{\sim}{k},\omega}}{\partial\omega}\right|\Big|_{\omega=\omega_{\underset{\sim}{k}}} \qquad (3:1-17)$$

For a given mass ratio, temperature ratio and drift velocity, $\Delta\omega_{\underset{\sim}{k}}$ may then be estimated numerically.

Physically, the above results may be summarized as follows. First, the multispecies plasma can relax its configuration to drive formation of small-scale fluctuations. This relaxation mechanism is similar to that in the test particle model, where only the interaction of different particle species contributes to this relaxation. Second, interactions that contribute to the driving source arise from the collective dissipation of wave-particle interactions and are proportional to $\text{Im}\chi^i_{\underset{\sim}{k},\omega}$ and $\text{Im}\chi^e_{\underset{\sim}{k},\omega}$. Third, waves that are emitted from clumps must be dissipated by the plasma in order to maintain stationary turbulence. Balancing the dissipation $\text{Im}\epsilon_{\underset{\sim}{k},\omega}$ with the driving source, Eq. (3:1-16) follows, i.e.,

$$\text{Im}\epsilon_{\underset{\sim}{k},\omega} \propto \text{Im}\chi^e_{\underset{\sim}{k},\omega} \text{Im}\chi^i_{\underset{\sim}{k},\omega} \ .$$

Experimentally, one is concerned about the possibility of measuring the clump fluctuations in ion cyclotron turbulence. For the regime $T^i_\perp \gg T^i_\parallel \sim T^e$, wave fluctuations are weakly damped; the mixture of wave and clump fluctuations may make a clear identification of clumps difficult. However, if the fluctuation level of turbulence is sufficiently high so that the collective dissipation is large enough to damp the wave fluctuations,

then the clump fluctuations will be more likely to be detected. For the regime $T_{\perp}^i \gg T_{\parallel}^i \approx T^e$, turbulence is dominated by clump fluctuations and a direct measurement of clump fluctuations should be possible.

Next, one may be concerned about which species of clump fluctuation is more likely to be measured. The probability of measuring them is proportional to a statistical average of clump amplitudes. Therefore the relative size of $<\tilde{\phi}^2>_{k,\omega}^e$ to $<\tilde{\phi}^2>_{k,\omega}^i$ is a reasonable measure of likelihood of which species of clump fluctuation will be detected. From Eqs. (3:1-14) and (3:1-15), it is straightforward to obtain that

$$\frac{<\tilde{\phi}^2>_{k,\omega}^e}{<\tilde{\phi}^2>_{k,\omega}^i} = \frac{a^e |Im\chi_{k,\omega}^e|}{a^i |Im\chi_{k,\omega}^i|} \approx \frac{a^e}{a^i} = \frac{0.7}{\frac{0.15}{(\bar{k}\rho_i)^2}} \approx 7 \quad . \qquad (3:1-18)$$

The fact that $a^i \ll a^e$ is due to the effects of finite Larmor-radii of ions, which greatly weaken the driving source and also reduce the perpendicular velocity correlation length of ion clumps. As a consequence, the electron clump fluctuations are more likely to be observed than ion clump fluctuations.

3.2 Clump Instability

A state of stationary turbulence can be attained when damping of collective resonances balances emission. Both processes are related to the amplitude-dependent susceptibilities $\mathrm{Im}\chi^e_{\underset{\sim}{k},\omega}$ and $\mathrm{Im}\chi^i_{\underset{\sim}{k},\omega}$. When an imbalance occurs, the plasma will adjust its fluctuation level so as to satisfy the steady-state condition. Below the threshold-drift velocity, the free energy is insufficient for excitation of fluctuations, and the steady-state fluctuation level is that of thermal noise. Beyond the threshold drift velocity, the free energy available can be used to excite the enhanced local phase-space fluctuations. This threshold-drift velocity is in general smaller than the threshold-drift velocity for linear instability because the clump instability can occur for $\mathrm{Im}\,\epsilon < 0$.

To obtain the threshold drift of the nonlinear instability, we can express Eq. (3:1-16) as

$$\mathrm{Im}\chi^e_{\underset{\sim}{k},\omega} = \frac{|\mathrm{Im}\chi^i_{\underset{\sim}{k},\omega}|}{1 + (a^e + a^i)\underset{\sim}{k}^2\lambda_D^2|\mathrm{Im}\chi^i_{\underset{\sim}{k},\omega}|} \tag{3:2-1}$$

where $\mathrm{Im}\chi^e_{\underset{\sim}{k},\omega}$ contains the free-energy source, the drift velocity v_D. When $T^i_\parallel \sim T^i_\perp$, the expressions for $\mathrm{Im}\chi^e_{\underset{\sim}{k},\omega}$

and $\left| \text{Im}\chi^i_{\underset{\sim}{k},\omega} \right|$ are

$$\text{Im}\chi^e_{\underset{\sim}{k},\omega} \sim \left[\frac{v_D}{v_{te}} - \frac{\omega}{\kappa v_{te}} \right] \left(\frac{1}{\underset{\sim}{k}^2 \lambda_D^2} \right)$$

$$\text{Im}\chi^i_{\underset{\sim}{k},\omega} \sim \frac{-\omega}{\kappa v_{t\parallel i}} \left(\frac{T^e}{T^i_\perp} \right) \Lambda_{n_\omega}(k^2 \rho_i^2) \exp\left[\frac{-(\omega - n_\omega \omega_{ci})^2}{\kappa^2 v_{t\parallel i}^2} \right] \left[\frac{1}{\underset{\sim}{k}^2 \lambda_D^2} \right]$$

with ω and k satisfying $\text{Re}\,\epsilon_{k,\omega}$. A straightforward sub-stitution of the above expressions into Eq. (3:2-1) yields

$$\frac{v^{thr}}{v_{te}} \sim \frac{\omega}{\kappa v_{te}}$$
$$+ \frac{\frac{\omega}{\kappa v_{t\parallel i}} \left(\frac{T^e}{T^i} \right) \Lambda_{n_\omega} \exp\left[- \frac{(\omega - n_\omega \omega_{ci})^2}{\kappa^2 v_{t\parallel i}^2} \right]}{1 + \sqrt{\pi} (a^e + a^i) \frac{\omega}{\kappa v_{t\parallel i}} \left(\frac{T^e}{T^i} \right) \Lambda_{n_\omega} \exp\left[- \frac{(\omega - n_\omega \omega_{ci})^2}{\kappa^2 v_{t\parallel i}^2} \right]}$$

$$(3:2-2)$$

While the linear threshold-drift velocity is

$$\left[\frac{v^{thr}}{v_{te}} \right]^L \sim \frac{\omega}{\kappa v_{te}} + \frac{\omega}{\kappa v_{t\parallel i}} \left(\frac{T^e}{T^i} \right) \Lambda_{n_\omega} \exp\left[\frac{-(\omega - n_\omega \omega_{ci})^2}{\kappa^2 v_{t\parallel i}^2} \right]$$

$$(3:2-3)$$

The factor $(a^i + a^e)$ in Eq. (3:2-2) accounts for the reduction of threshold-drift velocity.

The reduction of the threshold-drift velocity may be substantial if $(\underset{\sim}{k}^2 \lambda_D^2) \mathrm{Im} \chi^i_{\underset{\sim}{k},\omega} \sim 0(1)$, that is when $|\omega - n_\omega \omega_{ci}/\kappa v_{t_{\parallel i}}| < 1$, in which case the second term on the right of Eq. (3:2-2) can be sizably reduced. When $T^i_\perp > T^i_\parallel \sim T^e$, the wave fluctuations emitted by clumps tend to approach this regime, hence the clump effect may be enhanced. In Fig. 2 we plot both of the linear and nonlinear threshold-drift velocites versus $T^i_\perp/T^e \sqrt{m_e/M_i}$. As the latter increases both the threshold velocities increase, but the reduction Δv^{thr} does not increase as rapidly. When $T^i_\perp/T^e \sqrt{m_e/M_i} \sim 0.10$, there is a maximum Δv^{thr} with $\Delta v^{thr}/v^{thr} \sim 7\%$. This is because, upon minimizing the threshold velocity, the parallel-phase velocity ω_k/κ of the nonlinearly-excited fluctuations increases with $T^i_\perp/T_e \sqrt{m_e/M_i}$ more rapidly than that of the linear modes. According to Eq. (3:2-2), this increment in ω_k/κ tends to offset the reduction of v^{thr} due to finite ion dissipation. This explains why the reduction Δv^{thr} saturates even in the case of strong ion dissipation.

By contrast, the ion-acoustic branch wave-clump turbulence is quite different. The ion-acoustic waves have an almost constant parallel-phase velocity.
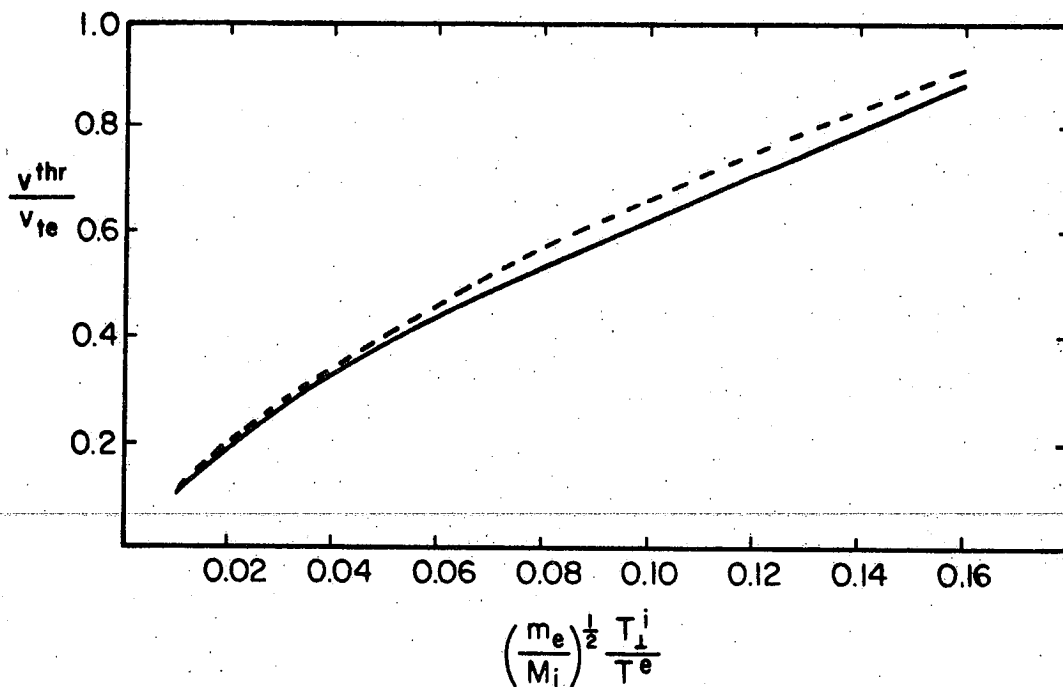
Figure 3-2. Threshold drift velocity of ion-cyclotron
clumps normalized to the electron thermal
velocity v^{thr}/v_{te} as a function of
$(m_e/M_i)^{1/2} T_\perp^i/T^e$. Nonlinear and linear
results are shown by the solid and dash
lines, respectively

Hence, the first term of Eq. (3:2-2) is constant, and the nonlinear threshold-drift velocity is determined by the enhanced ion dissipation. Reduction of threshold drift can thus be very significant[11],[17] (Appendix D).

If the drift velocity is above the nonlinear-threshold drift, the fluctuation will grow and hence the amplitude-dependent collective-resonance dissipation will increase till steady state results. The growing correlation function satisfies the equation.

$$\left[\gamma + \frac{1}{\tau_{c1}} \right] <\delta f_{(1)} \delta f_{(2)}>^{\sigma} \approx <S>^{\sigma} \tag{3:2-4}$$

$$<\delta f_{(1)} \delta f_{(2)}>^{\sigma} \approx \frac{\tau_{c1}^{\sigma}}{1 + \gamma \tau_{c}^{\sigma}} <S>^{\sigma} \tag{3:2-5}$$

These expressions are valid when the nonlinear growth rate γ is smaller than the shifted frequency $\omega - n\omega_c$. This has been assumed from the outset to guarantee a separation of time scales. It will be shown that the nonlinear growth rate γ scales with the particle trapping-time. Hence, so long as the fluctuation amplitude is small enough, the condition for separation of time scales can always be met. Following the same procedure as that in the previous section, one finds

$$\text{Im}\epsilon_{\underset{\sim}{k},\omega} = \left[\frac{a^i}{1 + \gamma\tau_i} + \frac{a^e}{1 + \gamma\tau_e}\right] \text{Im}\chi^i_{\underset{\sim}{k},\omega} \text{Im}\chi^e_{\underset{\sim}{k},\omega} (k^2\lambda_D^2) .$$

$$(3:2-6)$$

In the limit of weak growth, $\gamma\tau_i$, $\gamma\tau_e < 1$, so $1/1 + \gamma\tau_i \sim 1 - \gamma\tau_i$ and $1/1 + \gamma\tau_e \sim 1 - \gamma\tau_e$. This yields

$$\gamma(a^i\tau_i + a^e\tau_e) = \frac{(v_D - v_c)}{\text{Im}\chi^e} \frac{\partial}{\partial v_D}\left|\text{Im}\chi^e\right| . \qquad (3:2-7)$$

where v_c is the critical drift velocity for maintaining the stationary turbulence at a certain fluctuation level, and hence is amplitude-dependent. The growth rate scales with the test-particle diffusion times, weighted by the relative sizes of the clumps of the corresponding species. When $\tau_e \sim \tau_i$, $a^e\tau_e \gg a^i\tau_i$ the clump-growth rate is that of an electron-decorrelation time.

If the electron-drift velocity significantly exceeds the threshold, and $\gamma\tau_e$, $\gamma\tau_i \gtrsim 1$ then

$$\gamma \approx \left[\frac{a^i}{\tau_i} + \frac{a^e}{\tau_e}\right] \frac{\text{Im}\chi^e \text{Im}\chi^i k^2\lambda_D^2}{\text{Im}\epsilon} \sim \left[\frac{a^i}{\tau_i} + \frac{a^e}{\tau_e}\right] (a^i + a^e)^{-1}$$

$$(3:2-8)$$

For ion-cyclotron turbulence, $a^i/\tau_i \ll a^e\tau_e$, hence

$$\gamma \sim \frac{1}{\tau_e} \qquad\qquad\qquad\qquad (3:2-9)$$

Notice that Eq. (3:2-6) is quite general. In the case
of ion-acoustic turbulence, $a^i = a^e$ but $\tau_e \ll \tau_i$, hence
in the limit of small growth, the growth rate scales with
the ion-decorrelation time τ_i. However, in the case of
strong growth, the growth rate scales with the electron
decorrelation time τ_e.

3.3 Saturation Level and Anomalous Resistivity

In ion-cyclotron turbulence, perpendicular non-
linear-ion scattering and heating is proposed as the
dominant mechanism for saturation. Energetically, this
nonlinear process transforms the electron current energy
into the ion perpendicular thermal energy. Dynamically,
this nonlinear effect leads to a broadened wave-ion
resonance. The width of resonance, which is dependent
upon the fluctuation level, yields a correction to the
linear-ion dissipation. If the electron-drift velocity
v_D does not significantly exceed the threshold velocity,
the saturation level can thus be estimated with a per-
turbation expansion around the marginally stable state.

The saturation level (or the resonance width)
can be estimated using Eq. (3:1-16), the steady state

condition and $\mathrm{Re}\,\epsilon_{\underset{\sim}{k},\omega} = 0$ as a function of the drift veloc-ity excess beyond the threshold. Since the anisotropic-ion distribution can lead to more effective wave-ion interactions as explained earlier, we shall confine our-selves to the case where $T_\parallel^e = T_\parallel^i = T_\perp^e < T_\perp^i$. Then Eq. (3:1-16) and $\mathrm{Re}\,\epsilon_{\underset{\sim}{k},\omega} = 0$ can be expressed explicitly as

$$-Z'\left(\frac{\omega - \kappa v_D}{\kappa v_{te}}\right) + \frac{2T^e}{T_\perp^i}\,\Lambda_{n_\omega}\left[\frac{\omega + \frac{i}{\tau_i}}{\kappa v_{t_{\parallel i}}}\right] Z\left(\frac{\omega - n_\omega \omega_{c1} + \frac{i}{\tau_i}}{\kappa v_{t_{\parallel i}}}\right)$$

$$- \Lambda_{n_\omega} Z'\left(\frac{\omega - n_\omega \omega_{ci} + \frac{1}{\tau_i}}{\kappa v_{t_{\parallel i}}}\right)$$

$$= i\,\frac{(a^e + a^i)}{2}\,\mathrm{Im}Z'\left[\frac{\omega - \kappa v_D}{\kappa v_{te}}\right]\Lambda_{n_\omega}\,\mathrm{Im}Z'\left[\frac{\omega - n_\omega \omega_{ci} + \frac{1}{\tau_i}}{\kappa v_{t_{\parallel i}}}\right]$$

$$+ \frac{T^e}{T^i}\,\mathrm{Im}\left[\frac{\omega + \frac{1}{\tau_i}}{\kappa v_{t_{\parallel i}}}\right] \cdot Z\left[\frac{\omega - n_\omega \omega_{ci} + \frac{1}{\tau_i}}{\kappa v_{t_{\parallel i}}}\right] \qquad (3\!:\!3\text{-}1)$$

where the function Z is the plasma dispersion function. From the paragraph immediately following Eq. (3:1-5), ion decorrelation time τ_i is defined to be amplitude-dependent and can be estimated as

$$\frac{1}{\tau_i} \sim \frac{\pi c^2 \bar{k}^4}{2B_o^2 \bar{\kappa} v_{t_{\parallel i}}}\,\langle \phi^2(x)\rangle \quad . \qquad (3\!:\!3\text{-}2)$$

Since the ions are fluid-like, the dominant dependence
on $1/\tau_i$ is in the Z functions. Let $1/\tau_i = 0$, we can ob-
tain the threshold drift v^{thr} by solving the real and
imaginary part of Eq. (3:3-1). In doing this, we have
assumed that the fundamental harmonic is dominant and
have evaluated $\bar{k}\rho_i$ at where Λ_o peaks. When $1/\tau_i$ is
finite, we let $v_D = v^{thr} + \Delta v_D$, $\omega = \omega_o + \Delta\omega$, $\kappa = \kappa_o + \Delta\kappa$
where ω_o, κ_o are the frequency and parallel wavenumber
of marginal stability. Using a perturbation expansion
around the marginally stable state, we obtain an approxi-
mately linear relation between $\Delta v_D/v_{te}$ and $1/\tau_i$.

$$\frac{\Delta v_D}{v_{te}} = Y \cdot \frac{1}{\kappa v_{t_{\parallel i}} \tau_i} \qquad (3:3-3)$$

where Y is a function of $\sqrt{m_e/M_i}$ T^i/T^e, and is shown in
Fig. 3-3. Eq. (3:3-3) is recognizable as the expression
$\gamma = 1/\tau_i$, where γ is the clump-enhanced growth rate. The
saturation level can hence be estimated as a function of
$\Delta v_D/v_{te}$ and $\sqrt{m_e/M_i}$ T^i/T^e,

$$\frac{e^2 <\phi^2(x)>}{T_e^2} = \frac{2}{\pi} \frac{m_e}{M_i} \left(\frac{T^i_i}{T^e}\right) \left(\frac{1}{\bar{k}\rho_i}\right)^4 \left(\frac{\bar{\kappa} v_{te}}{\omega}\right)^2 \left(\frac{\Delta v_D}{v_{te}}\right) Y^{-1} \qquad (3:3-4)$$
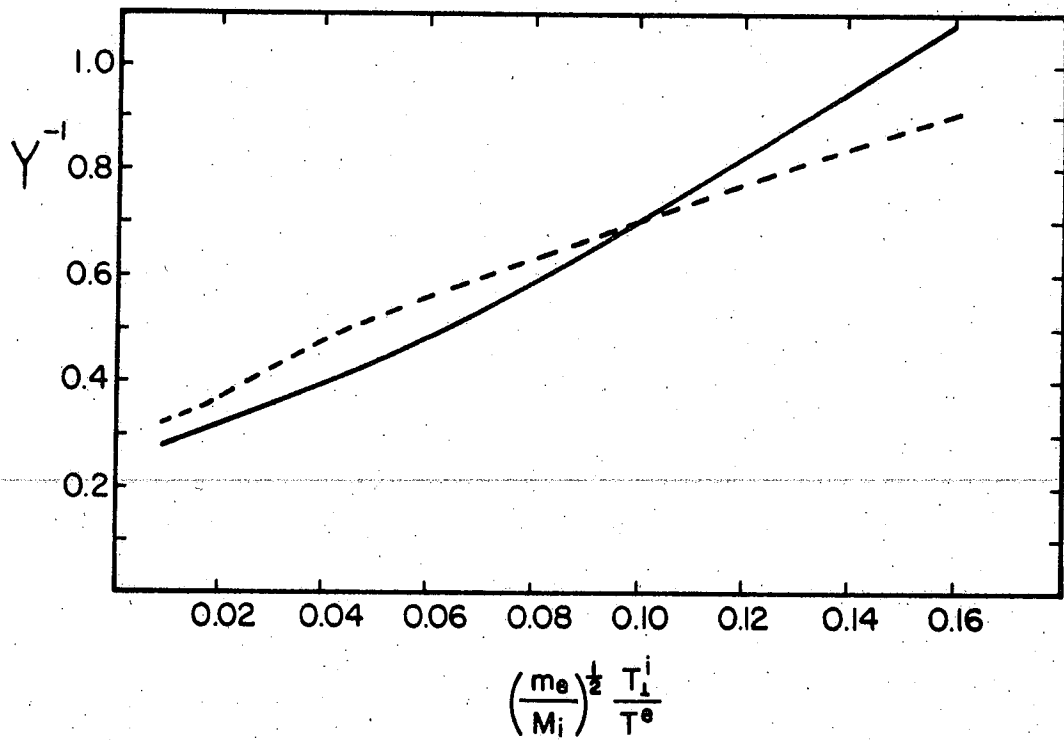
Figure 3-3. Ratio of the excess of drift velocity $\Delta v_D/v_{te}$ to the ion trapping rate $1/k_\perp v_{t\|i}\tau_i$ as a function of $(m_e/M_i)^{1/2} T_\perp^i/T^e$. Results of the clump theory and the conventional nonlinear theory are shown by the solid and dash line, respectively.

In Fig. 3-4, we show $e^2 <\phi^2(x)>/T_e^2 (\Delta v_D/v_D)$ as a function of $\sqrt{m_e/M_i}\ T^i/T^e$. The conventional nonlinear theory of wave fluctuations predicts that $e^2 <\phi^2(x)>/T_e^2$ increases almost linearly with $\sqrt{m_e/M_i}\ T^i/T^e$. However, $e^2 <\phi^2(x)>/T_e^2$ obtained using the clump theory increases more rapidly than that of conventional nonlinear theory, until $\sqrt{m_e/M_i}\ T^i/T^e = 0.045$. Then, after reaching a maximum value at $\sqrt{m_e/M_i}\ T^i/T^e \approx 0.05$, $e^2 <\phi^2(x)>/T_e^2$ begins to decrease slightly. This is because $e\sqrt{<\phi^2(s)>}/T_e$ is inversely proportional to the parallel phase velocity $\omega/\kappa v_{te}$, Eq. (3:3-4), which increases more rapidly in the clump theory than that in the conventional nonlinear theory (see paragraph immediately following Eq. (3:2-3).

Among various anomalous transport coefficients, anomalous resistivity and heating are the most significant results of the clump theory. The anomalous resistivity results from a drag force, which is essential to maintain a steady current against a D.C. parallel electric field. In addition, this theory predicts a negligible turbulent diffusion of the electron distribution function, since this diffusion coefficient is proportional to the ion-clump amplitude, which is
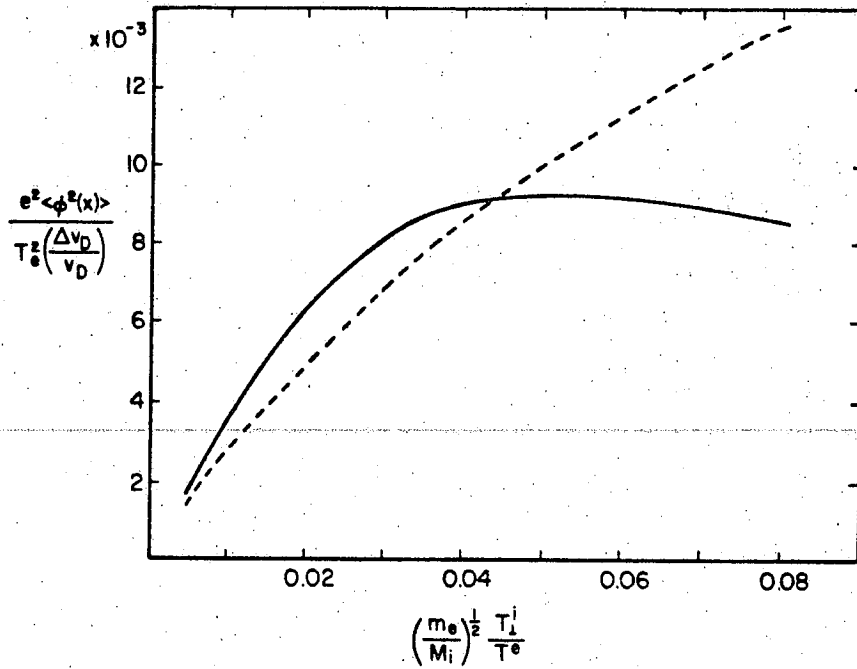
Figure 3-4. Saturation level of the potential fluctuation $e^2 <\phi^2(x)>/T_e^2$ normalized to $(\Delta v_D/v_D)$ as a function of $(m_e/M_i)^{1/2}\, T_\perp^i/T^e$. Results of the clump theory and the conventional nonlinear theory are shown by the solid and dash lines, respectively.

relatively small, as shown in the previous section. This indicates that there is relatively weak electron heating and that most of the electron-beam energy is converted into ion-perpendicular heating. By marked contrast, the conventional quasi-linear theory prediction contains only the diffusion, and cannot treat a situation of a steady current. That theory also predicts that electron heating is greater than or equal to ion heating, because of the fact that $\bar{k}^2 \rho_i^2 \gtrsim 1$ and $(\bar{k}/\bar{\kappa})^2\, m_e/M_i \sim 1$ for ion-cyclotron turbulence, thus electron diffusion coefficient is larger than that of ions. Therefore, the wave and clump theories differ significantly in their prediction for the energy conversion of the electron current.

Anomalous resistivity is obtained by taking the first moment of the electron-average distribution function. At steady state, where a D.C. electric field is necessary, it follows,

$$\frac{eE_o}{m} \int U\, \frac{\partial \langle f_e \rangle}{\partial U}\, d\underset{\sim}{V}$$

$$= \frac{e}{m} \int d\underset{\sim}{V} \left\{ \sum_{\substack{\underset{\sim}{k} \\ \omega}} \frac{U}{(2\pi)^4 |\epsilon_{\underset{\sim}{k},\omega}|^2} \left[\frac{\omega_{pe}^2}{e k_{\underset{\sim}{}}^2}\, \kappa^2 \right.\right.$$

$$\left. \cdot \frac{\partial}{\partial U} \left[G^e_{\underset{\sim}{k},\omega} \langle \tilde{\phi}^2 \rangle^i_{\underset{\sim}{k},\omega} \right] \frac{\partial \langle f_e \rangle}{\partial U} \right.$$

$$\left.\left. - \mathrm{Im}\chi^i_{\underset{\sim}{k},\omega}\, \kappa\, \frac{\partial}{\partial U} \langle \delta \tilde{f}^e\, \tilde{\phi}^e \rangle_{\underset{\sim}{k},\omega} \right] \right\} . \qquad (3:3-5)$$

The diffusion term is small because it is proportional to the amplitude of ion clumps. Thus, the drag force yields,

$$\frac{eE_o}{m} \approx \overline{Im\chi^i_{\underset{\sim}{k},\omega}} \left[\frac{e^2 <\phi^2(x)>}{T_e^2} \right] \; \overline{\kappa} v_{te}^2 \quad , \tag{3:3-6}$$

where $\overline{Im\chi^i_{\underset{\sim}{k},\omega}}$ is the spectrum-averaged ion dissipation. With η_A defined by $E_o = \eta_A(n_o e v_D)$, we have the anomalous resistivity η_A,

$$\eta_A = \frac{4\pi\,\omega_{ci}}{\omega_{pe}^2} \left[\frac{\dfrac{m_e}{M_i}\left(\dfrac{T^i}{T^e}\right)^2}{1.5(\overline{k}\rho_i)^4} \left[\frac{\kappa v_{te}}{\omega} \right]^3 \cdot \left(\overline{Im\chi^i_{k,\omega}} \right) \left[\frac{\Delta v_D}{v_D} \right] Y^{-1} \right] \tag{3:3-7}$$

In Fig. 3-5, we show the properly normalized anomalous resistivity

$$\frac{\eta_A}{\dfrac{4\pi\,\omega_{ci}}{\omega_{pe}^2}\dfrac{\Delta v_D}{v_D}} \quad vs. \quad \left(\frac{m_e}{M_i} \right)^{1/2} \frac{T^i}{T_e}$$

A comparison between the anomalous resistivity of the clump theory and that of the conventional nonlinear theory of wave fluctuations is also shown in Fig. 3-5. The conventional nonlinear theory predicts an ever-increasing (but more slowly) resistivity as a function of $(m_e/M_i)^{1/2} \cdot T^i/T^e$, while the clump theory predicts a much higher
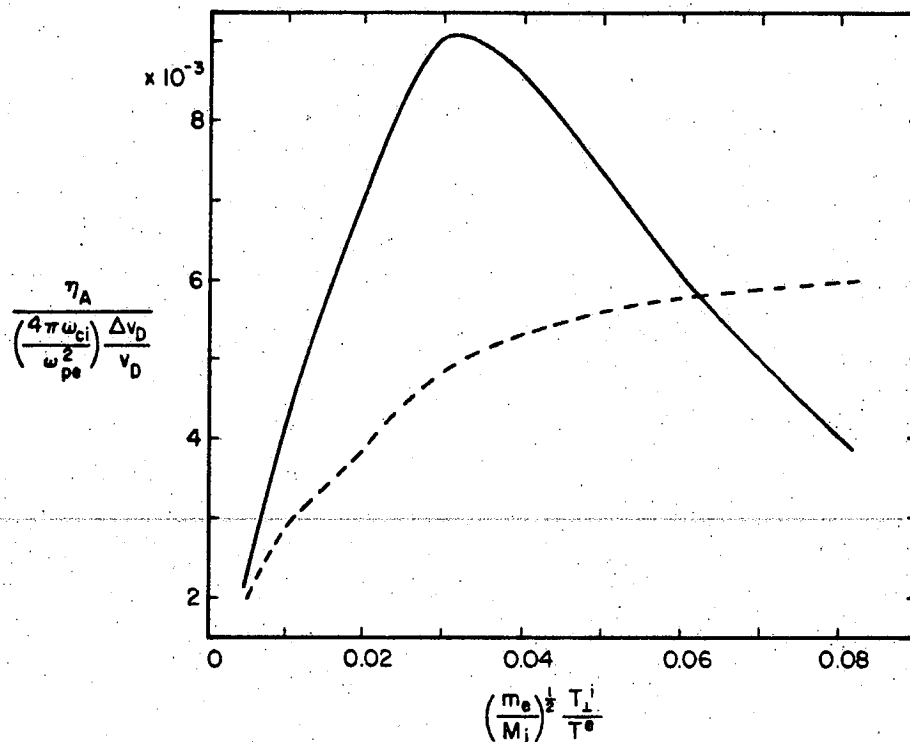
Figure 3-5. Anomalous resistivity η_A normalized to $(4\pi \omega_{ci}(\omega_{pe}^2)) \Delta v_D/v_D$ as a function of $(m_e/M_i)^{1/2} T_\perp^i/T^e$. Results of the clump theory and the conventional nonlinear theory are shown by the solid and dash lines, respectively.

value of resistivity at $(m_e/M_i)^{1/2} T^i/T^e \sim 0.03$. Then, the anomalous resistivity begins to decrease.

The saturation level and anomalous resistivity predicted in this theory are in good agreement with those obtained from the preliminary results of particle simulations.[17] It is also noticed that this theory predicts that the fluctuation level $e\phi/T_e$ is quite moderate ($\lesssim 0.1$) for the wave-clump regime of ion-cyclotron turbulence. This conclusion suggests that a study of the clump regime of ion-cyclotron turbulence may be necessary to explain the anomalous transport associated with ion-cyclotron turbulence in the observations.

3.4   Summaries and Conclusions

In this paper, we investigate the nonlinear theory of ion-cyclotron turbulence in the regime of strong wave-particle interaction. This type of turbulence contains two major constituents, the wave and nonwave (clump) fluctuations, in contrast to the case that is dominated by the nonwave fluctuations. Wave-wave interaction has been neglected because ion cyclotron waves are of the nondecay type that requires very high turbulence levels for wave-wave interaction, and also because we have

focused our investigation on the small-scale structures of the phase space. The principal results of this study are:

(1) Renormalized one-point and two-point equations describing magnetized Vlasov turbulence have been derived. Since particle motions evolve on two different time scales, the renormalized two-point equation describes the slow, relative motion, the renormalized one-point equation describes the rapid cyclotron motion and yields a renormalized dielectric function.

(2) Shapes of ion and electron clumps have been predicted. The electron clump appears cigar-shaped aligned along the magnetic field in position space, and appears as a thin disc perpendicular to the magnetic field in velocity space. The ion clump, when $\bar{k}\rho_i > 1$, appears as a gyrating tether-rod about the guiding center in position space and a gyrating tether-disc in velocity space, when $\bar{k}\rho_i < 1$, the ion clump appears cigar-shaped aligned along the magnetic field in position space, and appears as a thin disc perpendicular to the magnetic field in velocity space (Fig. 3-1).

(3) The clump amplitude of ions is much less than that of electrons because of ion finite-Larmor radius effects.

(4) When $T_\perp^i \geq T_\parallel^i \sim T^e$, ion-cyclotron turbulence
is of the wave-clump type. When $T_\perp^i \gg T_\parallel^i \sim T^e$, transi-
tion to the clump-dominant type of turbulence occurs.
This transition takes place approximately when $(m_e/M_i)^{1/2}$
$\cdot\ T_\perp^i/T_\parallel^e \geq 0.1$, where waves are heavily damped.

(5) A necessary condition for the maintenance
of stationary ion-cyclotron turbulence is given in Eq.
(3:1-16), and is a Vlasov-theory analogue to the pre-
diction of the fluctuation-dissipation theorem of the
test-particle model. This results from the fact that the
collective dissipation must balance incoherent noise
emission from macroparticles at steady state. This ex-
pression is valid for turbulence of the wave-clump type.

(6) The nonlinear growth rates in different
regimes have been obtained, and are given in Eqs. (3:2-7)
and (3:2-8). Nonlinear instabilities grow on the time
scales of the particle decorrelation times.

(7) The clump modifications to the instability
threshold in the wave-clump regime are small (reduction
of threshold drift velocity is within 7 percent, Fig. 3-2).
However, the modifications to the fluctuation level at
saturation and the anomalous resistivity are more sig-
nificant. Also, while the quasi-linear theory predicts

that electron parallel heating is larger than, or equal to, ion perpendicular heating for ion-cyclotron turbulence ($\bar{k}^2/\bar{\kappa}^2 \approx M_i/m_e$, $\bar{k}^2 \rho_i^2 \geq 1$), this theory predicts that ion perpendicular heating is the dominant mechanism for extraction of electron-beam energy.

In deriving the global conditions for steady state turbulence, two interesting questions arise. First, supposing that the drift velocity v_D slightly exceeds the threshold velocity v^{thr}, then only the fluctuations $<\tilde{\phi}^2>_{\underset{\sim}{k}}^{\sigma}$ within a narrow window of the wavenumber spectrum can be excited. However, the wavenumber spectra obtained from Eqs. (3:1-10) and (3:1-11) are broad and independent of v_D. Second, the spectrum of $<\phi^2>_{\underset{\sim}{k},\omega}$ obtained from Eq. (3:1-1), by integrating the velocity and using Poisson's equation, is different from that obtained from the expression,

$$<\phi^2>_{\underset{\sim}{k},\omega} = [<\tilde{\phi}^2>_{\underset{\sim}{k},\omega}^i + <\tilde{\phi}^2>_{\underset{\sim}{k},\omega}^e]/|\epsilon_{\underset{\sim}{k},\omega}|^2 .$$

The latter expression has peaks near normal modes, $|\epsilon_{\underset{\sim}{k},\omega}|^2 \approx 0$, while the former expression does not.

The answer to the first question is simply that as soon as fluctuations within the narrow window of the

wavenumber spectrum are excited, they will spread out
and cover the whole range of spectrum by mode coupling
processes. The answer to the second question is as fol-
lows. The expression Eq. (3:1-1), is only valid for the
relative separation $|\underset{\sim}{x}_-| \lesssim 1/|\overline{\underset{\sim}{k}}|$. This limits validity
of the long-wavelength ($|\underset{\sim}{k}| \leq |\overline{\underset{\sim}{k}}|$) side of the spectrum
resulting from Eq. (3:1-1). Since the poles of $|\epsilon_{\underset{\sim}{k},\omega}|^2$
are generally located in this range of the spectrum,
hence the expression of $<\phi^2>_{\underset{\sim}{k},\omega}$ obtained from one method
should not be compared with that from the other in this
range.

It is natural to ask the question, what happens
when both ion-cyclotron turbulence ($k/\kappa \gg 1$, $k\rho_i \sim 1$) and
ion-acoustic turbulence ($k/\kappa \leq 1$) exist at the same time?
For a magnetized plasma with $T_\perp^i > T^e > T_\parallel^i$, the threshold-
drift velocities of both are comparable. When one type
of fluctuation is excited the other may also be excited.
The presence of both types of fluctuations not only can
change the structures of clumps, but their interplay
leads to that the dissipation of one branch is determined
by the other branch. Furthermore, ion-acoustic turbu-
lence is intrinsically clump-dominated. When ion-
cyclotron turbulence is coupled to ion-acoustic turbulence,
its clump character can be greatly modified.

This kind of plasma turbulence with both ion-cyclotron and ion-acoustic fluctuations is a generalization of what has been investigated in this paper, and is now under investigation. The results will be published in the future.

C H A P T E R I V

TWO-DIMENSIONAL SHEAR FLOW TURBULENCE

4.1 Introduction

In this chapter, we will study free shear flow driven low-frequency turbulence of strongly magnetized plasmas, in the limit of vanishing magnetic shear. Thus, the problems are two-dimensional. Furthermore, in low-β plasmas, low-frequency fluctuations are usually electrostatic[2] (i.e., for $\beta \ll 1$, magnetic fluctuations are usually negligible), and incompressible.[22] In this case, the plasmas are dynamically equivalent to two-dimensional incompressible fluids.

In the following study, we will consider magnetized plasmas in the limits mentioned above, that is, a system which can be treated as a two-dimensional incompressible fluid. Our motivations for the investigation in these limits are twofold. First, we feel that a deep understanding of electrostatic turbulence is necessary before one attempts to study electromagnetic problems, which are usually more relevant but also more complicated.

Second, since fluid turbulence is simpler, in that well-controlled experiments and computer simulations can be conducted with great precision, theoretical prediction can have a ground with which to compare.

With these notions, we may start our investigation on two-dimensional fluid turbulence by briefly examining the following simple system.

Consider two streams of uniform, and parallel flows characterized by their velocities U_1 and U_2, and a plane of interface parallel to the flows. Any perturbed motion across this interface can immediately be amplified due to the shear motion at the interface. The inhomogeneity of the mean flow at this plane provides free energy for exitation of turbulence. Soon, when the turbulence motion is sufficiently violent and thus enhance local gradients of the flow, turbulence energy will then be quickly dissipated by molecular viscosity. Maintenance of turbulence, in general, relies again on the inhomogeneity of the mean flow to provide free energy. This is why turbulence of practical importance in the nature is frequently associated with inhomogeneous flows, i.e., shear flows.

Shear flow turbulence near walls is different from that away from walls (free shear flow). The former

usually can exchange momentum with the walls via viscosity,[23] which may then lead to a phase shift, possibly a positive feedback, and thus an instability. The latter generally results from an interchange instability of vortex tubes at the vorticity maximum[23] of the mean flow. At this region, the restoring force[24] of vortex tubes, upon interchange of their positions, vanishes, thus instability can occur and the shear can relax.

In this chapter, we study two types of <u>free</u> shear flow turbulence in two-dimensional incompressible fluids:

(a) Mixing-layer turbulence

(b) Wake or jet turbulence.

For mixing-layer turbulence, interactions among the mean flow and large-scale fluctuations[25] govern the turbulence evolution. We are interested in the time dependence of the shear flow layer and turbulence energy, and note that the former has been observed[26] to expand linearly in time. We use quasi-linear theory to examine their behavior, and find that our results are consistent with those of experiments[27] and computer simulations. For wake or jet turbulence, small-scale fluctuations comprise the main body of turbulence. In a two dimensional

model, we examine small-scale vorticity correlation, and find that the two-point correlation function is strongly peaked at small spatial separation. This is similar to the clump of a one-dimensional Vlasov's plasma.[10,13] We also obtain an anisotropic spectrum, where anisotropy is due to distortion by the shear motion of mean flow. The remainder of this chapter is organized as follows:

In Section 2, we present a survey of the experimental and computational evidence, which shows a distinction between two types of free shear flow turbulence. In Section 3, we review the earlier theoretical attempts at explaining mixing-layer turbulence. We point out the inconsistency of their assumptions when compared with experimental and computational observations. Having gained insights from observations, in Section 4, we are able to pose the appropriate problems, which is addressed analytically. In Section 5, we briefly review the necessary conditions for two-dimensional shear flow (linear) instability. We also present a new theorem regarding the necessary condition for linearly neutrally stable modes in two-dimensional shear flows. In Section 6, we focus on mixing-layer turbulence. We first discuss the linear stability analysis of the mixing layer and the

renormalization scheme for the nonlinear one-point vorticity equation. Subsequently, we examine the quasi-linear evolution of the shear layer and turbulence energy. In this analysis, turbulence diffusion due to the linearly unstable fluctuations is properly taken into account. In Section 7, we investigate the possibility of vorticity clump fluctuations in wake and jet turbulence. Finally, conclusions are discussed and summarized in Section 8.

4.2 Observational Motivations

a. Experimental

In shear flow visualization experiments,[26] it is usually observed that large-scale (comparable to the scale length of mean flows) coherent waves are excited at an initial phase; the instabilities are associated with the inflection points of mean flow profiles. For mixing-layer mean flows, the large-scale coherent vortices[26] (Fig. 4-2), persist for a time much longer than the time scale of vortex rotation. They have the same signs and are located at the center of mean flows. For types of mean flows such as jets or wakes, vortices[28,29] appear

in pairs and have different signs. These vortices will then break up into turbulent fluctuations before long. This is clearly illustrated by the example of a jet[28] coming out from a circular nozzle (Fig. 4-1) at very high Reynolds number, $R_e = 10^4$.

In an interesting visualization experiment conducted by Brown and Roshko,[26] they found that the coherent vortices can still remain in the mixing-layer flow as the Reynolds numbers were varied from 1.2×10^5 to 3×10^4 (Fig. 4-2). At smaller Reynolds numbers, it is not surprising that small-scale fluctuations are suppressed by viscosity and only large-scale vortices survive. However, at higher Reynolds numbers, the large-scale coherent vortices still exist, superposed on the small-scale fluctuations. In one of their experiments[30] on mixing-layer flow, large vortices can still be observed at a Reynolds number as high as $R_e = 3 \times 10^6$. This amazing observation indeed suggests that the existence of large vortices be a genuine feature of mixing-layer turbulence, as opposed to the conventional skeptism as to whether the mixing-layer flow is really turbulent, or whether Reynolds numbers are high enough. Also, a recent experiment by Bandyopadhyay[31] had Hussain show

(a)
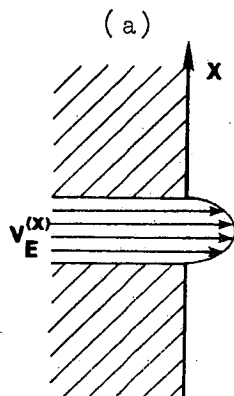
(b)

Figure 4-1. Typical jet mean flow profile (a), and
evolution of jet turbulence at high Reynolds
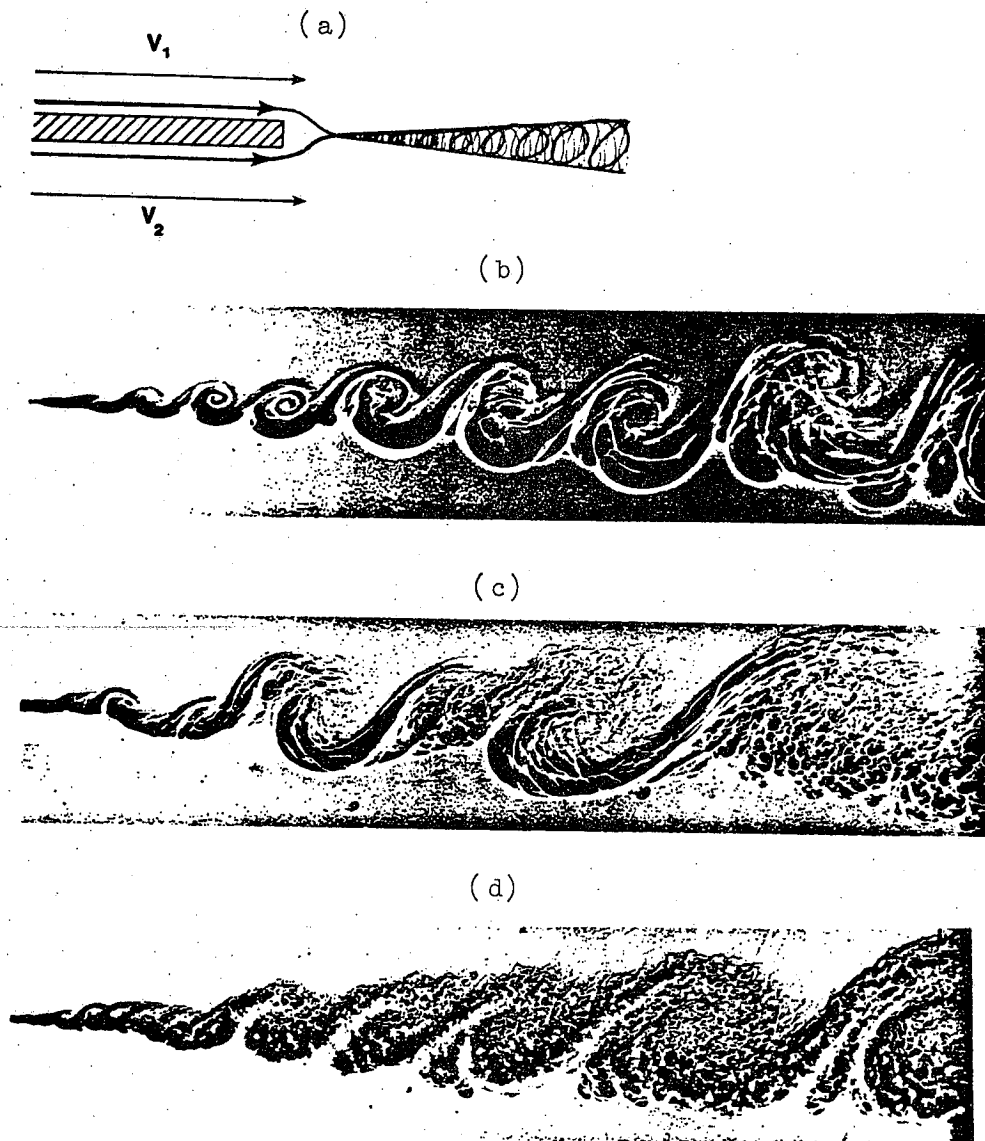numbers (b).

(a)

V_1

V_2

(b)

(c)

(d)

Figure 4-2. Typical setup for mixing-layer turbulence (a),
and evolution of mixing-layer turbulence at
Reynolds numbers equal to 3×10^4 (b),
6×10^4 (c), and 1.2×10^5 (d).

that among a variety of free shear flow turbulence, only

the mixing-layer turbulence exhibits different character.

This experiment examines velocity-field spatial correla-

tion between large-scale fluctuations and the low-frequency

modulation of small-scale fluctuations. It shows that

these two quantities, except in the case of mixing-layer

turbulence, are always in phase everywhere in the flow.

However, in mixing-layer turbulence, the phase between

these two quantities varies from one location to another.

This observation implies that the energy-exchange mech-

anism between fluctuations of disparate length scales in

mixing-layer turbulence is different from that of other

types of turbulence. It also suggests that the large-

scale fluctuations are not directly coupled with the

small-scale fluctuations in mixing-layer turbulence,

whereas in jet or wake turbulence fluctuations of distinct

scales may be more strongly coupled.

There are also visualization experiments[29] on

wake turbulence by Taneda. For low Reynolds numbers,

i.e., $R_e < 150$, they observed that the vortex street

excited from the initial linear instability persists for

a long time. However, for Reynolds numbers $R_e > 150$, the

initial vortex street will now break up into a turbulence

state, as mentioned earlier. Nonetheless, large vortices are observed to reappear from the chaotic state, and then break up again. Presumably, the cycles of vortex breaking and reforming can continue for a long time. In this report, whether these vortices and turbulence are two or three-dimensional is not discussed.

b. Computational

Aref,[28] et al., have computationally studied vortex-cloud-in-cell simulations for two-dimensional flows. They begin the run with a thin vortex layer, and observe it relax. Initially, linear instability develops (excitation of large-scale fluctuations), and subsequently groups of vortices are formed. Simultaneously, these vortex clusters are scattered from the center of the shear layer, hence the mean flow then expands. Interactions of adjacent vortex groups pull in the irrotational flow (entrainment), hence vortex clusters grow and the mean flow expands further. In this study, Aref, et al. point out that the large-scale coherent vortex observed in the visual experiment is not a single vortex. It is merely an illusion of the dye used in the experiment, which is entrained by many smaller vortices in a cluster,

tracing a seemingly simple pattern. They claim that the
vortices producing the dye pattern can be more complex
than the distribution of dye would suggest, and that a
cluster of vortices would probably appear as a single
vortex structure in the dye experiment.

There is also an interesting two-dimensional
computer simulation on wake turbulence by Zabusky,[32]
et al. They observed that the paired vortices of dif-
ferent signs start to roll up at the initial linear phase.
Subsequently, the mean flow is broadened; the instability
slows down, and transition to the nonlinear phase occurs.
The constant vorticity contours are now stretched to
form long, thin filaments. Eventually they break and
form small islands. In this report, they claim that the
reformation of larger vortices due to vortex pairing is
also observed. Furthermore, the energy spectrum is mea-
sured, $E(k) \propto k^{\alpha}$, for large wavenumbers, where $-4 < \alpha$
< -3.

c. Discussion

In mixing layer turbulence, even though Aref,
et al., argue that the regularly patterned coherent vor-
tices in the visual experiments do not reflect the real

distribution of small vortices, the dye pattern does reveal the integrated large-scale flow pattern, superposed on the small-scale fluctuations. This is consistent with Brown's observations for the high Reynolds number cases.

For the wake turbulence experiment by Taneda, we think the fact that the large-scale two-dimensional vortex pattern reforms itself from a turbulence state is of significance. Conventionally, it is assumed that the turbulent motion in a wake is three-dimensional. However, it is difficult for us to conceive how three-dimensional turbulent fluctuations, after vortex tubes being stretched and entangled, should organize themselves to form the large-scale two-dimensional flow pattern. Unfortunately, in the report of this experiment, the authors did not mention whether the turbulence was two or three-dimensional. We believe that, for the intermediate values of Reynolds numbers ($R_e \sim 300$) of their flows, the fluctuations are probably two-dimensional. At very high Reynolds numbers, as shown in Fig. 4-1, turbulence is probably three-dimensional, and the reformation of large-scale vortices may not be possible.

Now, it is interesting to compare the vortices observed in mixing-layer turbulence with those in wake

turbulence. The former are generated continuously and
show little difference from the linearly excited initial
vortices; however, the latter are intermittently dis-
rupted by turbulent fluctuations. Hence, we tend to be-
lieve that the large-scale vortices of mixing-layer tur-
bulence are generated by the linear instability associated
with the inflection point of the flow, and that the large-
scale vortices of wake turbulence are a result of non-
linear rearrangement of small vortex tubes. Because of
the conservation of vorticity (assuming Reynolds number
is large enough), part of the fluctuation energy trans-
ferred back and forth between the large-scale and small-
scale vortices. This may lead to the intermittent ap-
pearance of large-scale vortices.

To further elaborate on these two types of tur-
bulence, we notice that the large-scale vortices of mixing
layers are of the same sign, and interactions between
adjacent vortices are attractive. Hence, the vortices
tend to confine in the center of the mean flow so that
the mean flow expands slowly. Moreover, the counter
streaming flows of a mixing layer, which occupy a large
volume on either side of the layer in comparison to the
volume of the shear layer itself, serve as a large free

energy reservoir. Therefore, the system has enough free
energy to continuously and adiabatically excite the
large-scale fluctuations. On the other hand, the vor-
tices of wakes or jets appear in pairs of opposite signs.
They tend to expel each other, hence the mean flow is
broadened (losing energy) rapidly. Furthermore, there
is only a finite amount of free energy stored in the
finite volume shear layers of the mean flows. Thus,
large-scale vortices, which require substantial fluctua-
tion energy, cannot be continuously excited. Therefore,
small-scale fluctuations will then take over and domi-
nate the turbulence.

4.3 Earlier Theoretical Treatments

Theoretical attempts[26,27] at understanding shear
flow turbulence have been made previously. Most of the
studies assume that turbulence consists of three basic
components: two-dimensional mean flows, large-scale
fluctuations, and three-dimensional small-scale fluctua-
tions. The large-scale fluctuations are generally be-
lieved to be associated with the instability due to the
vorticity maximum of the mean flows. The small-scale
fluctuations interact with the mean flow and large-scale

fluctuations through local shearing of the mean flow and mode coupling, respectively.

In the earlier studies,[33] investigators considered a model where these three components could directly interact with one another. The nonlinear coupling of the fluctuations of different length scales was modelled by closure schemes. Here, an assumed global shape function for the small-scale turbulent stresses was used. The relative amplitudes of the components of turbulent stresses were determined from the locally homogeneous shear problem, i.e., turbulence with a linear mean flow profile. The shape for large-scale fluctuations was determined by a driven Rayleigh's equation, where Reynolds stresses were the source. As a result, they obtained a set of coupled equations, describing the mean flow kinetic energy, large-scale fluctuation amplitude, and turbulent stress amplitude. In this theory, the three components of turbulence are equally important in the determination of the turbulence evolution. In particular, it is assumed that the three components can simultaneously and instantaneously interact with one another.

However, as shown in the earlier experiments, mixing-layer turbulence is probably governed by the

interaction between the mean flow and large-scale fluctuations. This is probably necessary to explain the observed similar evolution for the flows of high Reynolds numbers and those of low Reynolds numbers. Therefore, this earlier theory may not be appropriate for application to mixing-layer turbulence. Furthermore, a numerical calculation[34] of mixing-layer turbulence, based on the reduced coupled equations derived from this theory, was performed. The result shows that after the initial transient state, turbulence energy is eventually concentrated in the small-scale fluctuations. This result, we think, probably is due to the overestimated coupling between the large and small-scale fluctuations in this theory. The result of this numerical calculation has actually cast a serious doubt as to the validity of a theory such as this.

The difficulty of this theory in fact arises from the assumption that fluctuations of disparate length-scales can directly and instantaneously interact with each other. In mixing-layer turbulence, the large-scale fluctuations that are excited by the mean flow contain most of turbulence energy. They should be responsible for the scrambling mechanism which removes wave energy

from other large-scale unstable modes, thus transferring
energy to smaller-scale fluctuations. As pointed out by
Kraichnan,[35] random large-scale fluctuations should not
feed energy to (or affect dynamics of) small-scale fluc-
tuations directly because of the invariance of Galilean
transformation. The only way to couple them is by a
coupling through the fluctuations of intermediate length-
scales. After several stages of local (in lengthscale)
interactions, energy can then reach small-scale fluctua-
tions. This is exactly the picture of cascade,[36] where
interactions between fluctuations of disparate length-
scales are neither direct nor instantaneous.

Since several cascades are needed to allow
the large and small-scale fluctuations to communicate
(interact), details of the small-scale fluctuations may
influence the large-scale dynamics very little. That is,
the dynamics of the source of fluctuations are insensi-
tive to the small-scale sink. (This is analogous to
the facts that the energy flow in the inertial range is
independent of viscosity, and that turbulence diffusion
is independent of molecular diffusion.) In a model to
be developed later, we properly account for this fact
such that the turbulent diffusion of large-scale unstable
modes is contributed by other large-scale modes.

For wake or jet turbulence, the small-scale vorticity fluctuations comprise the main body of turbulence. At very high Reynolds numbers, turbulence is three-dimensional and driven by the local shearing of mean flows. Probably this earlier theory works better in these cases.[37] This is because large-scale fluctuations plays a minor role in this type of turbulence. The overestimation of the coupling between large and small-scale fluctuations (thus enhancing turbulent diffusion) may significantly affect the transient state (speed up the energy transfer), but not the stationary turbulence state.

4.4 Problems Posed to Be Studied Analytically

The complexity of turbulence makes any purely analytical treatment impractical, if not impossible. However, when appropriately taking into account observations from experiments or computer simulations, theoretical progress may very well be made. Below, we will address two model problems for mixing-layer turbulence, and jet (and wake) turbulence, separately.

For mixing-layer turbulence, both experiments and computer simulations hint that the large-scale

fluctuations play a role in the self-preserving evolution of turbulence. Therefore, two questions of central interest arise: What makes the flows evolve self-similarly, and what makes the shear layer expand linearly in time?

The answer to the first question can be qualitatively answered from an energetic point of view as follows. The mean flow has an infinite free energy reservoir and provides fluctuation energy needed to sustain a quasi-equilibrium state. Once this state is reached, the system may tend to remain in the same configuration. This is possibly why the self-preservation occurs. The question now becomes whether the mean flow can evolve slowly enough to ensure a quasi-equilibrium state. This can only be answered if the second question is resolved.

For the other type of free shear flow turbulence small-scale nonwave fluctuations dominate the turbulence. This is because only a finite amount of free energy is stored in the mean flows. When the energy source is consumed and fluctuation energy increases, turbulent diffusion can then defeat the driving force associated with the inflection point of mean flows. The large-scale fluctuations are thus damped. By contrast, the small-scale fluctuations can draw energy from the

mean flows in different ways, and thus possibly be sustained.

It is generally believed that the small-scale fluctuations in fluid turbulence are three-dimensional,[25] and that vortex stretching[38] is an important mechanism for generation of small-scale vorticity fluctuations. However, we want to confine this study to turbulence in a invicid two-dimensional fluid, merely because it is simple enough to make a reliable analysis, and yet rich enough to contain interesting physics. This situation corresponds to wake (or jet) turbulence in an intermediate Reynolds number regime (R_e equal to several hundreds) as observed in experiments. In this regime, Reynolds numbers are high enough to approximate invicid flows and low enough to ensure two-dimensional motion.

A two-dimensional invicid flow obeys the equation,[39]

$$\frac{d}{dt} \left(\nabla_\perp \times \underset{\sim}{v} \cdot \hat{z} \right) = 0$$

conservation of vorticity. In wake or jet turbulence, velocity field fluctuations are almost spatially random, except in some intermittent occasions where large

vortices may reappear. Thus, a vortex element is convected by the velocity field, induced by other vortex elements, in an approximately random manner. This situation is very similar to what happens to the phase-space density element of a one-dimensional plasma,[10] where the density element is subjected to approximately stochastic acceleration. At small separation, two vortex (or phase-space density) elements experience the same convection (or acceleration), hence tend to travel together. The analogy can possibly be extended further to situations where the relaxation of mean vorticity drives small-scale vorticity fluctuations (see Chapter II).

However, caution has to be exercised in extending the analogy. In one-dimensional single-species plasmas, the average distribution function cannot relax due to the conservation laws of particle energy and momentum (i.e., in a one-dimensional elastic collision process of identical particles, the final state equals the initial state, hence the system does not relax). Consequently, the small-scale phase-space granulations are not spontaneously generated. Yet, collisions between vortices are not elastic, thus the vorticity granulation, in principle, can be driven by the relaxation of

the average vorticity. In this study, we are interested
in investigating the possibility of small-scale vortex
generation and its implications. We do not attempt to
explain how the large vortices can intermittently reap-
pear. Nevertheless, a brief discussion on this subject
will be addressed.

4.5 Evolution Equation and Linear
    Stability Analysis

In this section, we begin with deriving an
equation (conservation of vorticity) for two-dimensional
incompressible flows, and then discuss the linear stabil-
ity criteria. It is then followed by a discussion of the
physical interpretation[24] given by Orszag, et al., for
the origin of instability. Finally, we give a new theorem
for the necessary condition for the existence of neutrally
stable eigenmodes.

A Newtonian fluid satisfies the Navier-stokes
equation,[39]

$$\left(\frac{\partial}{\partial t} + \underset{\sim}{v} \cdot \nabla\right)\underset{\sim}{v} = -\frac{1}{m}\nabla(p + \psi) + \nu\nabla^2\underset{\sim}{v}, \qquad (4:5\text{-}1)$$

where p and ψ are the pressure and external-force poten-
tial, respectively, and m and ν are the mass density and

kinematic viscosity, respectively. For Boussinesq
fluids,[40] the density m can be taken within the gradient
operator in Eq. (4:5-1). Taking a curl of both sides of
this equation, the incompressible fluid is then described
by an evolution equation for vorticity, $\rho \equiv \nabla \times v$. That
is,

$$\left(\frac{\partial}{\partial t} + v \cdot \nabla\right)\rho = \rho \cdot \nabla v + \nu \nabla^2 \rho \, , \qquad (4:5-2)$$

where the first term on the right corresponds to vortex
stretching due to velocity shear.

For two dimensional flows, the vortex stretch-
ing term vanishes, and Eq. (4:5-2) becomes

$$\left[\frac{\partial}{\partial t} + \hat{z} \times \nabla_\perp \phi \cdot \nabla_\perp\right]\nabla_\perp^2 \phi = \nu \nabla_\perp^2 \nabla_\perp^2 \phi, \qquad (4:5-3)$$

where ϕ is the stream function, defined as $\hat{z} \times \nabla_\perp \phi \equiv v$,
and $\nabla_\perp$ is a two-dimensional gradient. Hence $\nabla_\perp^2 \phi = \rho$, the
magnitude of vorticity. For invicid fluids, Eq. (4:5-3)
can further be simplified to,

$$\frac{d\rho}{dt} = 0 \, , \qquad (4:5-4)$$

conservation of vorticity.

Given a parallel equilibrum (mean) flow in the y direction, which varies spatially in the x direction, i.e.,

$$\underset{\sim}{V}_E = V_E(x)\hat{y},$$

Eq. (4:5-4) can be expressed as

$$\left[-i\omega + ikV_E(x)\right]\nabla_\perp^2 \phi_{k,\omega} - ik\frac{d^2V_E}{dx^2}\phi_{k,\omega}$$

$$+ i\underset{\substack{k'\\\omega'}}{\Sigma}\left[(ik')\phi_{k',\omega'}\frac{d}{dx}\nabla_\perp^2\phi_{k'',\omega''}\right.$$

$$\left. - ik''\frac{d\phi_{k',\omega'}}{dx}\nabla_\perp^2\phi_{k'',\omega''}\right] = 0, \qquad (4:5-5)$$

After a spatial-temporal Fourier transformation has been performed. The linearized form of Eq. (4:5-3) is then,

$$\left[\frac{d^2}{dx^2} - k^2 + \frac{d^2V_E}{dx^2} \Big/ (\omega - kV_E)\right]\phi_{k,\omega} = 0 \qquad (4:5-6)$$

This equation is recognized as Rayleigh's equation.

The stability of solutions depends on the mean flow profiles, $V_E(x)$. Two important theorems[41] regarding to the necessary mean flow profiles for instability are given below.

(A) Rayleigh's inflection point theorem. A necessary condition for instability is that the mean flow profile should have an inflection point, x_s, where $(d^2 V_E / dx^2) \big|_{x = x_s} = 0$.

(B) Fjortoft's theorem. A necessary condition for instability is that $(d^2 V_E(x)/dx^2)(V_E(x) - V_E(x_s)) < 0$ somewhere in the field of flow.

The first theorem actually states that a mean-vorticity extremum is needed for instability. The second theorem sharpens the first one, requiring that the mean vorticity extremum be a maximum.

Orszag and Petera gave a physical picture interpreting the need of a mean vorticity extremum for instability as follows. In a flow that does not have vorticity extremum, the restoring force is always available to stop the instability associated with interchange of vortex tubes. In Figs. 4-3a, b, c, we show how this restoring force occurs. The parallel two-dimensional shear flow can be viewed as infinitely many discrete line vortices (directed in the y direction) whose magnitudes depend on x (Fig. 4-3a). Supposing that vortex I moves up one level as shown in Fig. 4-3b, using the Brot-Savart law to obtain the vortex induced velocities, we
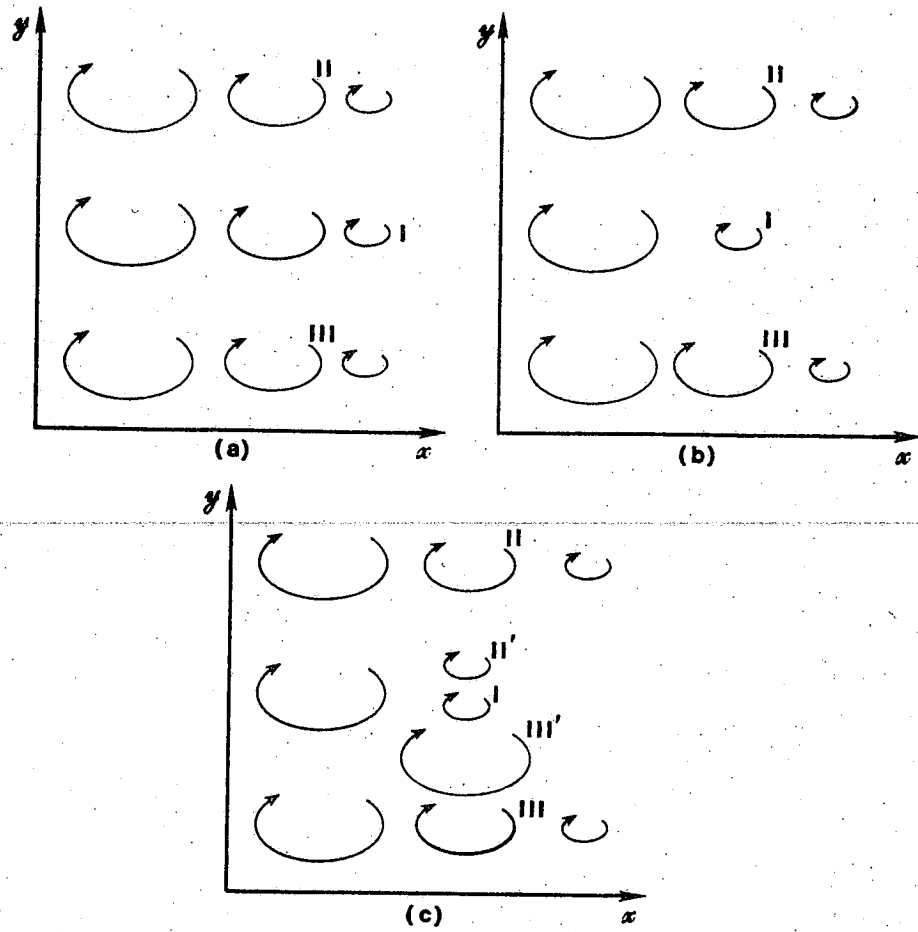
Figure 4-3. Physical picture for the restoring force of vortex elements.

find that vortex III tends to bring down the large vortex

III', and II to bring up the small vortex II' (Fig. 4-3c).

Clearly, the net result of vortices II' and III' on I is

to push it down to its original level, thus providing a

restoring force. Therefore, the necessary condition for

instability is that at some point in the flow field,

the restoring force vanishes. It ultimately requires a

vorticity extremum for this to occur. Notice that

Fjortorf's theorem can not be obtained from this argu-

ment. This is because the theorem is a second order ef-

fect. (A similar argument was first given by Lin.[23])

In the following section, we will present a new

theorem about the necessary condition for neutrally stable

solutions of Rayleigh's equation. The technique developed

in proving this theorem will prove to be useful, in Sec-

tion 4. , in showing the positivity of the driving source

for the vorticity correlation function.

Theorem: For any mean flow which has no more

than two resonance points, the necessary condition for

any neutrally stable solution, whose phase velocity ω/k

resonates with the mean flow $V_E(x)$ somewhere in the flow

field, to exist is that all the resonance points are in-

flection points.

Proof: Separating the real and imaginary parts
of Eq. (4:5-6), we obtain

$$\left[\frac{d^2}{dx^2} - k^2 + k \frac{d^2 V_E}{dx^2} \frac{(\omega_r - kV_E)}{(\omega_r - kV_E)^2 + \omega_i^2} \right] \operatorname{Re} \phi_{k,\omega}(x)$$

$$= k \frac{d^2 V_E}{dx^2} \frac{\omega_i}{(\omega_r - kV_E)^2 + \omega_i^2} \operatorname{Im} \phi_{k,\omega}(x) \qquad (4:5-7)$$

$$\left[\frac{d^2}{dx^2} - k^2 + k \frac{d^2 V_E}{dx^2} \frac{(\omega_r - kV_E)}{(\omega_r - kV_E)^2 + \omega_i^2} \right] \operatorname{Im} \phi_{k,\omega}(x)$$

$$= -k \frac{d^2 V_E}{dx^2} \frac{\omega_i}{(\omega_r - kV_E)^2 + \omega_i^2} \operatorname{Re} \phi_{k,\omega}(x). \qquad (4:5-8)$$

Recognizing the operators on the left-hand sides of
Eqs. (4:5-7) and (4:5-8) are the same, we can define a
propagator $G_{k,\omega}^c(x,x')$ for this operator, that is,

$$\left[\frac{d^2}{dx^2} - k^2 + k \frac{d^2 V_E}{dx^2} \frac{(\omega_r - kV_E)}{(\omega_r - kV_E)^2 + \omega_i^2} \right] G_{k,\omega}^c(x,x')$$

$$\qquad (4:5-9)$$

$$= \delta(x - x'). \qquad (4:5-9)$$

As a result, $\operatorname{Re} \phi_{k,\omega}$ and $\operatorname{Im} \phi_{k,\omega}$ can formally be solved
in terms of $G_{k,\omega}^c(x,x')$, i.e.,

$$\operatorname{Re} \phi_{k,\omega}(x) = \int dx' G_{k,\omega}^c(x,x')$$

$$\cdot \left[k \frac{d^2 V_E}{d(x')^2} \frac{\omega_i}{(\omega_r - kV_E)^2 + \omega_i^2} \operatorname{Im} \phi_{k,\omega}(x') \right] \quad (4:5-10)$$

$$\mathrm{Im}\,\phi_{k,\omega}(x)$$

$$= -\int dx'\, G^c_{k,\omega}(x,x') \left[k\, \frac{d^2 V_E}{d(x')^2}\, \frac{\omega_i}{(\omega_r - kV_E)^2 + \omega_i^2}\, \mathrm{Re}\,\phi_{k,\omega}(x') \right] \tag{4:5-11}$$

For neutrally stable modes, $\omega_i \to 0$, and

$$\frac{\omega_i}{(\omega_r - kV_E)^2 + \omega_i^2} = \pi\, \delta(\omega - kV_E(x))$$

$$= \sum_\alpha \frac{1}{|dV_E(x_\alpha)/dx_\alpha|}\, \delta(x - x_\alpha) \tag{4:5-12}$$

where α is the index for a resonance point. For the present theorem, $\alpha = 1$ or 2. Substituting Eq. (4:5-12) into Eqs. (4:5-10) and (4:5-11), and evaluating x at either resonance point x_β, we obtain,

$$\mathrm{Re}\,\phi_{k,\omega}(x_\beta) = \sum_\alpha M_{\beta\alpha}\,\mathrm{Im}\,\phi_{k,\omega}(x_\alpha) \tag{4:5-13}$$

$$\mathrm{Im}\,\phi_{k,\omega}(x_\beta) = -\sum_\alpha M_{\beta\alpha}\,\mathrm{Re}\,\phi_{k,\omega}(x_\alpha)\ , \tag{4:5-14}$$

where

$$M_{\beta\alpha} = \frac{\pi\, k\, (d^2 V_E/dx_\alpha^2)}{|k(d V_E/dx_\alpha)|}\, G^c_{k,\omega}(x_\beta, x_\alpha) \tag{4:5-15}$$

To have nonvanishing $\phi_{k,\omega}(x)$, the coefficients of Eqs. (4:5-13) and (4:5-14) must satisfy the relation,

$$1 + (M_{11} + M_{22})^2 + (M_{11}M_{22} - M_{12}M_{21})^2 = 0 \qquad (4:5-16)$$

But this equality does not hold because $M_{\alpha\beta}$ is real. Therefore, the terms on both sides of Eqs. (4:5-7) and (4:5-8) must be equal to zero separately, and the inversion (Eqs. (4:5-10) and (4:5-11)) is not valid. Thus, the difficulty encountered in Eq. (4:5-16) is removed.

The terms on the right of Eqs. (4:5-10) and (4:5-11) can all vanish if and only if $d^2V_E/dx^2 = 0$, at all resonance points. This proves the theorem.

It is interesting to point out that the condition $d^2V_E/dx^2 = 0$ is also necessary for unstable solutions. Therefore, this theorem in fact proves that for any flow, the existence of inflection points is necessary for any solution of Rayleigh's equation to exist (flows with more than two resonance points must have at least one inflection point, therefore the above statement is valid for any flow).

Furthermore, since solutions are always associated with an inflection point, the solutions of

Rayleigh's equation are never singular. This suggests that Tollmein's[23] invicid solution, which are Frobenius expansions around the singular point, are not useful for Rayleigh's equation.

4.6 Theory of Mixing-Layer Turbulence

In this section, we want to investigate the evolution of the mixing-layer width with an assumption that the mixing layer evolves self-similarly. A quasi-linear model is used to show that the layer width indeed expands linearly in time as observed in experiments and computer simulations.

We start with a brief review on the linear theory, and then follow with an analysis of the renormalization scheme. Subsequently, we construct a quasi-linear equation, whose second moment equation determines the evolution of the layer width. Finally, a solution of this second moment equation is obtained, and a discussion of this result then follows.

a. Linear Analysis for a Mixing-Layer Flow

To gain some physical insights as to how flow perturbation varies, we begin this section with analyzing

an analytically tractable model mean flow profile (Fig. 4-4),

$$
V_E(x) = \begin{cases} V_o & , \ x > a \\ \dfrac{x}{a} V_o & , \ |x| \leq a \\ -V_o & , \ x < -a \end{cases} \qquad (4{:}6a\text{-}1)
$$

Since $d^2 V_E/dx^2 = 0$ everywhere except $x = \pm a$, the eigenfunction of Eq. (4:5-6) is simply

$$
\phi_{k,\omega}(x) = \begin{cases} e^{-k(x-a)} & , \ x > a \\ A_1 e^{-kx} + A_2 e^{+kx}, & |x| \leq a \\ A_3 e^{k(x+a)} & , \ x < a \end{cases}
$$

The coefficients A_1, A_2, and A_3 are determined by matching $\phi_{k,\omega}$ and $d\phi_{k,\omega}(x)/dx$, at $x = \pm a$. By this, the dispersion relation can also be determined.

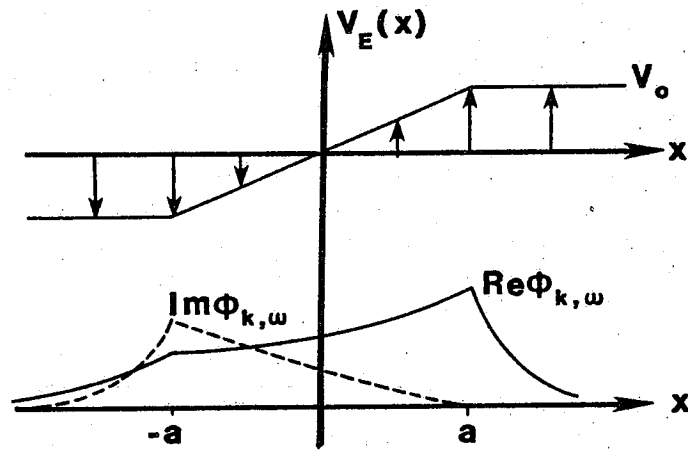A straightforward exercise shows that the eigenfunction is,

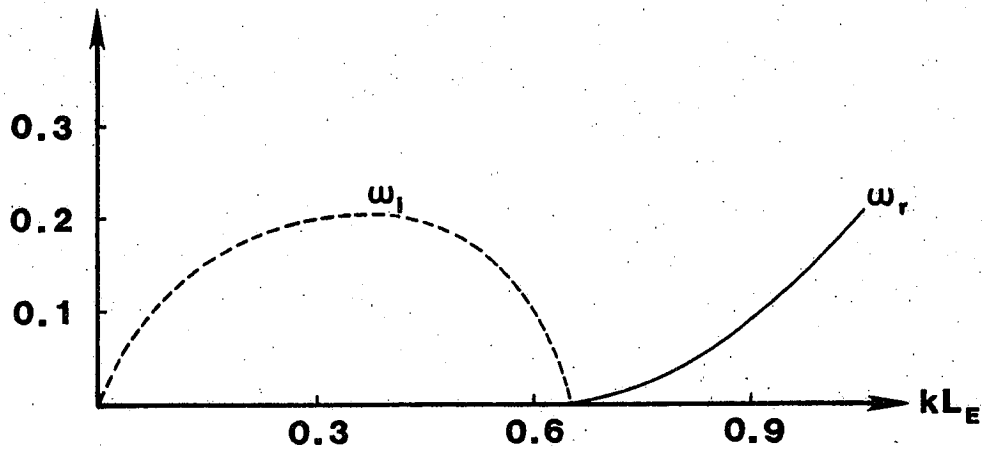Figure 4-4. Broken-line mean flow profile and linear eigenfunction of a typical mixing layer.

Figure 4-5. Dispersion relation for the mean flow profile in Figure 4-4.

$$\phi = \begin{cases} e^{-(k-a)}, & x > a \\ \\ \dfrac{1}{1 + [(2ka - 1) - \frac{2\omega a}{V_o}]} \left[\left[(2ka - 1 \right.\right. \\ \qquad \left.\left. - \dfrac{2\omega a}{V_o} \right] e^{-k(x-a)} + e^{k(x-a)} \right], & |x| \le a \\ \\ \dfrac{1}{1 + [(2ka - 1) - \frac{2\omega a}{V_o}]} \left[e^{-2ka} \right. \\ \qquad \left. + e^{2ka} \left[(2ka - 1) - \dfrac{2\omega a}{V_o} \right] \right] e^{k(x+a)}, & x < a \end{cases}$$

$$(4:6a-2)$$

And the dispersion relation Fig. (4-5) is

$$\omega^2 = \frac{V_o^2}{4a^2} \left[(2ka - 1)^2 - e^{-4ka} \right] \qquad (4:6a-3)$$

For $k \le 0.65/a$, modes are purely growing; the most unstable mode occurs at $k = 0.4/a$. For $k > 0.65/a$, modes are neutrally stable (satisfying our new theorem in the previous section), and the phase velocity $|\omega/k| \le V_o$. The stable solutions are real and asymmetric in x. At the marginally stable wavenumber, $k = 0.65/a$, the solution is symmetric with respect to the origin, $x = 0$. The unstable solutions are complex and asymmetric in x. However, the absolute value of the eigenfunction $|\phi_{k,\omega}|$ is

symmetric with respect to the origin. At vanishingly
small k, the growth rate approaches zero, and the solu-
tion becomes real and antisymmetric with respect to the
origin. A typical unstable mode is shown in Fig. (4-4).
It is mostly confined in the region, $|x| \leq a$.

b. Nonlinear Interactions
    and Renormalization

        In this subsection, we will briefly review the
method for renormalization of the nonlinear equation,
Eq. (4.5-5). The renormalization scheme that we adapt
here is an approximate Direct Interaction Approximation.
An even simpler version has been extensively used in the
previous chapters for ion-cyclotron turbulence. We will
not repeat the details in this section. However, in this
case, the global propagator $G_{k,\omega}$ for the field $\phi_{k,\omega}$ is
the basic quantity rather than the propagator for the
vorticity, $\nabla_{\perp}^2 G_{k,\omega}$. This is in sharp contrast to the case
of ion-cyclotron turbulence, where the local propagator
for particles, $i(\omega - k_{\parallel} v_{\parallel} - n\omega_c + \frac{i}{\tau})^{-1}$, is used. In the
previous treatments, we assumed that the field $\phi_{k,\omega}$ is
random and independent of the particle fluctuation $f_{k,\omega}$,
hence the response of $\phi_{k,\omega}$ to $f_{k,\omega}$ (and thus the shielding,

or self-binding, of $f_{k,\omega}$) have been totally ignored. In the present case, since the nonlocal propagator $G_{k,\omega}$ of the field $\phi_{k,\omega}$ is the fundamental quantity, the response of $\phi_{k,\omega}$ to vorticity fluctuations $\nabla_\perp^2 \phi_{k,\omega}$ can be taken into account.

Rearranging the nonlinear terms of Eq. (4:5-5), we have

$$
\left[-i\omega + ikV_E(x)\right]\nabla_\perp^2\phi_{k,\omega} + \frac{1}{2}\left[\frac{d}{dx}\sum_{\substack{k'\\\omega'}}\left[ik'\phi_{k',\omega'}\nabla_\perp^2\phi_{k'',\omega''}\right.\right.
$$

$$
\left.- (ik'')\phi_{k'',\omega''}\nabla_\perp^2\phi_{k',\omega'}\right]-ik\sum_{\substack{k'\\\omega'}}\left[\frac{d\phi_{k',\omega'}}{dx}\nabla_\perp^2\phi_{k'',\omega''}\right.
$$

$$
\left.\left.- \phi_{k'',\omega''}\frac{d\nabla_\perp^2\phi_{k',\omega'}}{dx}\right]\right] = ik\frac{d^2V_E}{dx^2}\phi_{k,\omega} \qquad (4:6b-1)
$$

This equation can be renormalized by substituting $\phi_{k'',\omega''}$ and $\nabla_\perp^2\phi_{k'',\omega''}$ for $\phi_{k'',\omega''}^{(2)}$ and $\nabla_\perp^2\phi_{k'',\omega''}^{(2)}$, respectively, where the latter quantities are driven by the direct beating of a test (k,ω) mode and background (k',ω') modes. (Detailed derivation of local and nonlocal renormalized terms, $D_{k,\omega}$ and $C_{k,\omega}$, respectively, is shown in Appendix E. In this analysis, we let R^2 in Eq. (E-3) equal to zero.)

In the present analysis, we shall neglect the nonlocal $C_{k,\omega}$ and retain only the more familiar $D_{k,\omega}$,

local operators of diffusion type, to model the effects of random convection by the turbulent velocity field. It is evident, from Eq. (E-4), that $D_{k,\omega}$ is composed of the diffusion of both vorticity $\nabla_\perp^2 \phi_{k,\omega}$ and field $\phi_{k,\omega}$ in the x and y directions. That is,

$$D_{k,\omega} = \left[\frac{d}{dx} D_x \frac{d}{dx} - k^2 D_y \right] \nabla_\perp^2 \phi_{k,\omega}$$

$$- \left[\frac{d}{dx} d_x \frac{d}{dx} - k^2 d_y \right] \phi_{k,\omega} \qquad (4:6b-2)$$

The linear convection together with diffusion of vorticity describe the perturbed orbit of a vorticity element, while the diffusion of the field describes modifications of the equilibrium profiles. As pointed out by Dupree, these two effects cancel in the total energy (not energy per mode) evolution equation.[43] In the present case of spatially inhomogeneous profiles, they combine to form a term of a total derivative with respect to x, representing the divergence of energy flux. Hence, these two groups of terms in $D_{k,\omega}$ account for the nonlinear spatial rearrangement of the kinetic energy.

In the region where $|\phi_{k,\omega}|^2$ is large, we have $|d^2/dx^2| \gg k^2$. Hence we retain only

$$\frac{d}{dx} D_x \frac{d}{dx} \nabla_\perp^2 \phi_{k,\omega}$$

to represent the locally renormalized nonlinearity. The nonlinear evolution equation for vorticity can thus be approximated by

$$\left[-i\omega + ikV_E - D\frac{d^2}{dx^2}\right]\nabla_\perp^2 \phi_{k,\omega} = ik\frac{d^2 V_E}{dx^2}\phi_{k,\omega} \qquad (4{:}6b{-}3)$$

c. The Second Moment Equation

In this subsection, we will derive an equation for the second moment of vorticity whose square-root is defined to be the width of the shear layer. In our strategy, we assume the mixing layer evolves self-similarly, hence at any instant the large-scale fluctuations are excited with nonlinear growth rates. Since the relaxation of the mean vorticity or shear layer depends on the fluctuation level, and since the latter depends on growth rates, and thus on the shear layer width, the fluctuation level and shear layer width are thus coupled and evolve together.

The mean vorticity, $\rho_o \equiv dV_E/dx$, satisfies the equation,

$$\frac{\partial \rho_o}{\partial t} = \frac{1}{(2\pi)^2} \frac{\partial}{\partial x} \sum_{\substack{k \\ \omega}} (ik) [\phi_{k,\omega}^* \rho_{k,\omega}], \qquad (4:6c-1)$$

where $\rho_{k,\omega} = \nabla_\perp^2 \phi_{k,\omega}$. Substituting $\rho_{k,\omega}$ from Eq. (4:6b-3), we obtain

$$\frac{\partial \rho_o}{\partial t} = \left(\frac{\partial}{\partial x} D \frac{\partial}{\partial x}\right) \rho_o, \qquad (4:6c-2)$$

where

$$D \simeq \sum_{\substack{k \\ \omega}} \frac{1}{(2\pi)^2} \frac{i}{\omega - kV_E(x) + i\frac{D}{a^2}} k^2 |\phi_{k,\omega}|^2 \qquad (4:6c-3)$$

In the denominator of the above expression of D, we have used the Markovian approximation for $D_{k,\omega}$ obtained earlier. Also, we have approximated the operator $\partial^2/\partial x^2$ associated with vorticity diffusion by $-1/a^2$. Because of the spectral sum, we assume that D is spatially uniform across the layer. Taking the second moment of Eq. (4:5c-2), we obtain

$$\frac{da^2}{dt} = 2D$$

$$= \frac{2}{(2\pi)^2} \sum_{\substack{k \\ \omega}} \text{Re} \left[\frac{1}{\gamma_k + ikV_E + \frac{D}{a^2}}\right] k^2 |\phi_{k,\omega}^{(0)}|^2$$

$$\cdot \exp[2\int dt \gamma_k(t)], \qquad (4:6c-4)$$

where a is the shear layer width, defined as

$$a^2(t) = \frac{\int x^2 \rho_O(x,t)dx}{\int \rho_O(x,t)dx} \quad , \tag{4:6c-5}$$

and $\rho_O \equiv dV_E/dx$, mean flow vorticity.

Note that the nonlinear growth rate is related to the linear growth rate γ_k^L by $\gamma_k = \gamma_k^L - D/a^2$, and the initial noise can be expressed as,

$$|\phi_k^{(0)}|^2 = \frac{1}{2\pi} \sum_\omega |\phi_{k,\omega}^{(0)}|^2,$$

it thus follows that:

$$\frac{da^2}{dt} = \frac{1}{\pi} \sum_k Re\left[\frac{1}{\gamma_k^L + ikV_E}\right] k^2 |\phi_k^{(0)}|^2$$

$$\cdot \exp 2\int dt(\gamma_k^L - \frac{D}{a^2}) \quad . \tag{4:6c-6}$$

The k sum in Eq. (4:6c-6) can be evaluated using the method of the steepest descent. The maximum of the integrand occurs approximately at the wavenumber of the fastest growing linear mode. Thus, the diffusion coefficient D becomes,

$$D \approx \frac{1}{\pi} \left[\frac{\gamma^L_{k_m} \Delta k_m}{(\gamma^L_{k_m})^2 + k_m^2 V_E^2} \right] k^2 |\phi^{(0)}_{k_m}|^2$$

$$\cdot \exp\left(2 \int dt \left[\gamma^L_{k_m}(t) - \frac{D}{a^2} \right] \right) \qquad (4:6c-7)$$

Here, k_m scales with the instantaneous layer width $a(t)$. We assume that the layer grows so slowly that the maximum growth rate γ^L_{km} and its wavenumber k_m scale with $a(t)$ in a same manner as in the initial phase. That is, $k_m = \sigma/a$, $\gamma^L_{km} = \beta V_0/a$, where σ and β are numbers determined by the specific profile chosen. Furthermore, we let the initial noise spectrum behave as

$$\frac{1}{2\pi} k^2 |\phi^{(0)}_k|^2 \cong (k/k_0)^\alpha \left[\frac{1}{2\pi} k_0^2 |\phi^{(0)}_{k_0}|^2 \right]$$

for low-k spectrum, where k_0 is the most unstable wavenumber for the initial layer width a. Finally, Δk_m can be evaluated from the width of the integrand, and scales with $a(t)$, i.e., $\Delta k_m = \xi/a(t)$. Notice also that, from Eq. (4:6c-4), we have $2Ddt = da^2$, hence the nonlinear correction to linear growth rate, in the exponential of Eq. (4:6c-6), can be expressed

$$\exp(-\int dt(2D/a^2)) = a(0)/a(t)$$

To express this second moment equation in a dimensionless form, we let $W(t) \equiv a(0)/a(t)$, $\tau \equiv 2\beta(V_o/a(0))t$, and $\overline{A} \equiv \xi(\beta^2 + \sigma^2)(k_o^2 |\phi_{k_o}^{(0)}|^2/(2\pi V_o a(0)))$, where V_o characterizes the magnitude of $V_E(x)$.

$$\frac{dW}{d\tau} = -\overline{A}W^{3+\alpha+2\mu} \exp\left[\int_0^\tau d\tau W(\tau)\right], \qquad (4:6c-8)$$

where we have introduced another dimensionless parameter μ to represent the nonlinear correction to the growth rate. That $\mu = 1$ corresponds to the expression in Eq. (4:6c-6) where the nonlinear correction is taken into account; while that $\mu = 0$ corresponds to neglecting D/a^2 in Eq. (4:6c-6).

d. Solutions

To solve Eq. (4:6c-8), we differentiate with respect to τ on both sides of the equality, and obtain

$$\frac{d^2W}{d\tau^2} = \frac{dW}{d\tau}\left[W + \left[\frac{3 + \alpha + 2\mu}{W}\right]\frac{dW}{d\tau}\right] \qquad (4:6d-1)$$

Notice that τ does not appear in Eq. (4:6d-1), hence we can use W as the independent variable and $dW/d\tau (\equiv P)$ as the dependent variable. This gives

$$\frac{dP}{dW} = (3 + \alpha + 2\mu)\frac{P}{W} + W \qquad\qquad (4{:}6d\text{-}2)$$

This is a first-order nonlinear ordinary differential equation, and can be integrated. After an integration factor $W^{-(3+\alpha+2\mu)}$ is introduced and an integration constant is appropriately determined from the initial condition, Eq. (4:6d-2) becomes

$$\frac{dW}{\frac{1}{3}W^2 - \left(\frac{1}{3} - A\right)W^{3+\alpha+2\mu}} = -d\tau \qquad\qquad (4{:}6d\text{-}3)$$

The appropriate solution satisfies $W = a(0)/a(t) \ll 1$ because the layer grows. If $3 + \alpha + 2\mu > 2$, then we can ignore the term $W^{3+\alpha+2\mu}$ in the denominator of Eq. (4:6d-3), i.e.,

$$\frac{3\,dW}{W^2} \cong -d\tau \qquad\qquad (4{:}6d\text{-}4)$$

$$W \cong \frac{3}{\tau} \quad .$$

That is,

$$\frac{a(t)}{a(0)} \cong \frac{2}{3} \cdot \frac{\beta V_o}{a(0)} \cdot t \qquad\qquad (4{:}6d\text{-}5)$$

Interestingly, this expression does not depend on the initial noise level, neither on the turbulent diffusion (characterized by μ), but only on the linear growth rate (characterized by β). The occurrence of the linear time dependence can be traced back to the term W on the right-hand side of Eq. (4:6d-2), and thus $\exp[2\int dt(\beta V_O/a(t))]$ of Eq. (4:6d-7). That is, the a dependence of $\gamma^L_{k_M}$, $\gamma^L_k \propto 1/a$, is essential to obtain this linear time dependence.

The total initial noise energy has to be finite, that is, the integral $\int dk k^2 |\phi_k^{(0)}|^2$ is convergent. This requires that $\alpha > -1$ at the low wavenumber end of spectrum, where α is defined as $k^\alpha \propto k^2 |\phi_k^{(0)}|^2$. Hence, the condition that $3 + \alpha + 2\mu > 2$ is always satisfied even when the eddy viscosity is ignored, i.e., $\mu = 0$. As a consequence of this analysis, we find that the linear time-dependent solution, Eq. (4:6d-5), is the only physical solution. This result is independent of the details of nonlinear interactions or initial noise, but dependent only on the assumption of the self-similar evolution.

For the mean flow profile,

$$V_{\bar{E}}(x) = V_O \tan h(x/L),$$

it follows that,

$$\gamma_k^L \cong 0.2 \ V_o/L_E \ .$$

From the definition of a, Eq. (4:6c-5), it follows that a $\cong$ 0.9 L_E and Eq. (4:6d-5) becomes,

$$\frac{a(t)}{a(0)} = 0.12 \ \frac{V_o}{a(0)} \ t \qquad\qquad (4:6d-6)$$

Using the hyperbolic tangent mean flow profile and the definition of a, Eq. (4:6c-5), we find that the expansion rate obtained from Aref's computer simulation and Brown's experiment are 0.072 $V_o/a(0)$ and 0.08 $V_o/a(0)$, respectively. They are approximately 40 percent smaller than our rate. A numerical factor on the order of this magnitude may very well be introduced from the method of the steepest descent used to evaluate the spectral k sum, or from the approximate mean flow profile used to evaluate the slope.

It is instructive to examine the energy of large-scale fluctuations and the energy loss of mean flows. Assuming a broken-line mean flow profile for the sake of simplicity we have

$$V_E(x) = \begin{cases} V_E = -V_o & x < -\sqrt{3}a \\[2mm] V_E = \dfrac{x}{\sqrt{3}a} V_o & -\sqrt{3}a < x < \sqrt{3}a \\[2mm] V_E = V_o & x > \sqrt{3}a \end{cases}$$

(4:6d-7)

where the coefficients are so chosen that " a " satisfies its definition, Eq. (4:6c-5). The energy loss of the mean flow is

$$\frac{1}{2} \left[\int_{-\sqrt{3}a}^{\sqrt{3}a} V_E^2(x)\,dx - \int_{-\sqrt{3}a_o}^{\sqrt{3}a_o} V_E^2(x)\,dx \right] = \frac{V_o^2}{\sqrt{3}} (a - a_o)$$

$$\cong \frac{V_o^2}{1.73} a(t) \qquad (4:6d-8)$$

Thus, the energy loss behaves linearly in time.

The fluctuation energy can be estimated as follows. The diffusion coefficient D is related to the fluctuation energy per mode,

$$\epsilon_k = \frac{1}{2} k^2 |\phi_k|^2 + \frac{1}{2} \left| \frac{d\phi_k}{dx} \right|^2 \cong \frac{|\phi_k|^2}{a^2} \cong \frac{k^2 |\phi_k|^2}{\sigma^2} \,,$$

by

$$D \cong \frac{1}{2\pi} \sum_k \frac{k^2 |\phi_k|^2}{(D/a)^2} = \left[2\sigma^2 a^2 \sum_k \frac{\epsilon_k}{2\pi} \right]^{1/2} \qquad (4:6d-9)$$

where σ is a numerical factor, less than unity, given by
the relation $k = \sigma/a$. From Eq. (4:6c-4), we have $D = ada/dt$, hence the fluctuation energy density inside the
mixing layer is,

$$\sum_k \frac{\epsilon_k}{2\pi} = \frac{1}{\sigma^2}\left(\frac{da}{dt}\right)^2 = \frac{4}{9}\frac{\beta V_o}{\sigma} \qquad (4:6d-10)$$

where the last equality has used Eq. (4:6d-5). The fluc-
tuation energy density is constant in time. Hence the
fluctuation energy inside the mixing layer increases
linearly in time,

$$\int_{-\sqrt{3}a}^{\sqrt{3}a} dx \sum_k \frac{\epsilon_k}{2\pi} = \frac{8}{3\sqrt{3}}\left(\frac{\beta}{\sigma}\right)^2 V_o^2 a(t)$$

$$\cong \frac{V_o^2}{2.1} a(t) \qquad (4:6d-11)$$

Comparing Eq. (4:6d-8) with Eq. (4:6d-11), we note that
the energy loss from the mean flow is greater than the
energy gain of the large-scale fluctuations. This energy
difference should be deposited to small fluctuations.

4.7 Small-scale Fluctuations of Two-
dimensional Free Shear Flow
Turbulence

In this section, we are specifically interested
in two-dimensional wake or jet turbulence which primarily

comprises small-scale nonwave fluctuations. Small-scale
nonwave fluctuations extract free energy from mean flows
in a fundamentally different way than do large-scale wave-
fluctuations. Generation of small-scale fluctuations is
due to the relaxation of mean flow vorticity from an un-
stable configuration toward a stable one. Mean flow
vorticity does not relax in an arbitrary way but is con-
strained by the conservation of vorticity along the
trajectories of vortex elements. That is, mean vorticity
relaxes by exchanging the locations of vortex tubes of
different vorticity (randomly rearranging vortex tubes
due to the convection of the turbulent velocity field),
thus small-scale vorticity granulations can be created.

Simultaneously, the turbulent velocity field
that relaxes mean vorticity can also tear a vorticity
clump apart. If the size of a clump is small enough
(smaller than the lengthscale of turbulence), every point
in it is convected by approximately the same velocity
field. Thus, the clump can preserve its structural in-
tegrity for a time longer than the average correlation
time. It is this type of turbulent "tidal force" that
balances the source (mean vorticity relaxation) of clump
generation to sustain stationary shear flow turbulence.

It is important to note that the possibility for vorticity clumps to exist depends not only on that the relative diffusion diminishes at a small separation, but also on the positivity of the driving source. If the source term is negative (and becomes a sink) somewhere in the flow, the small-scale clumps generated in some positive-source region may be absorbed in the sink region. In this case, whether stationary turbulence of the clump type exists or not becomes unclear.

In this section, we first briefly review the linear theory, then discuss the relative turbulent diffusion obtained by using a closure scheme for triplet correlation, and then we show the positivity of the source term for a wake or jet. Finally, the vorticity correlation at small separation and high-k vorticity spectrum are obtained.

a. Linear Analysis

In fully developed wake (or jet) turbulence, the linear modes may become irrelevant. Nonetheless, a linear propagator $G_{k,\omega}^{(0)}(x,x')$, which satisfies

$$\left[\frac{d^2}{dx^2} - k^2 + \frac{kd^2V_E/dx^2}{\omega - kV_E} \right] G^{(0)}_{k,\omega}(x,x') = \delta(x - x'),$$

$$(4:7a-1)$$

can usually be used to approximate a nonlinear propagator when only crude features of turbulence are required. As shown in the previous section, the propagator is so useful for our nonlinear calculation that it is worthwhile to examine the properties of a linear propagator. In particular, for the present case, if we treat the incoherent vorticity fluctuations as highly localized seed fluctuations to induce velocity field $\phi_{k,\omega}$, then $\phi_{k,\omega}$ will behave as the propagator does. That is, the velocity field fluctuations in vorticity-clump turbulence satisfy,

$$\left[\frac{d^2}{dx^2} - k^2 + \frac{kd^2V_E/dx^2}{\omega - kV_E} \right] \phi_{k,\omega}(x)$$

$$= \tilde{\rho}_{k,\omega}(x) \propto \delta(\omega - kV_E(x)).$$

$$(4:7a-2)$$

For these reasons, we shall adopt the following simple model profile that permits an analytical expression for $G^{(0)}_{k,\omega}$. We use a mean flow $V_E(x)$ Fig. (4-6a), where

$$V_E = \begin{cases} 0 & , \quad |x| > a \\ V_o(1 - x/a), & a > x > 0 \\ V_o(1 + x/a), & 0 > x > -a \ . \end{cases}$$
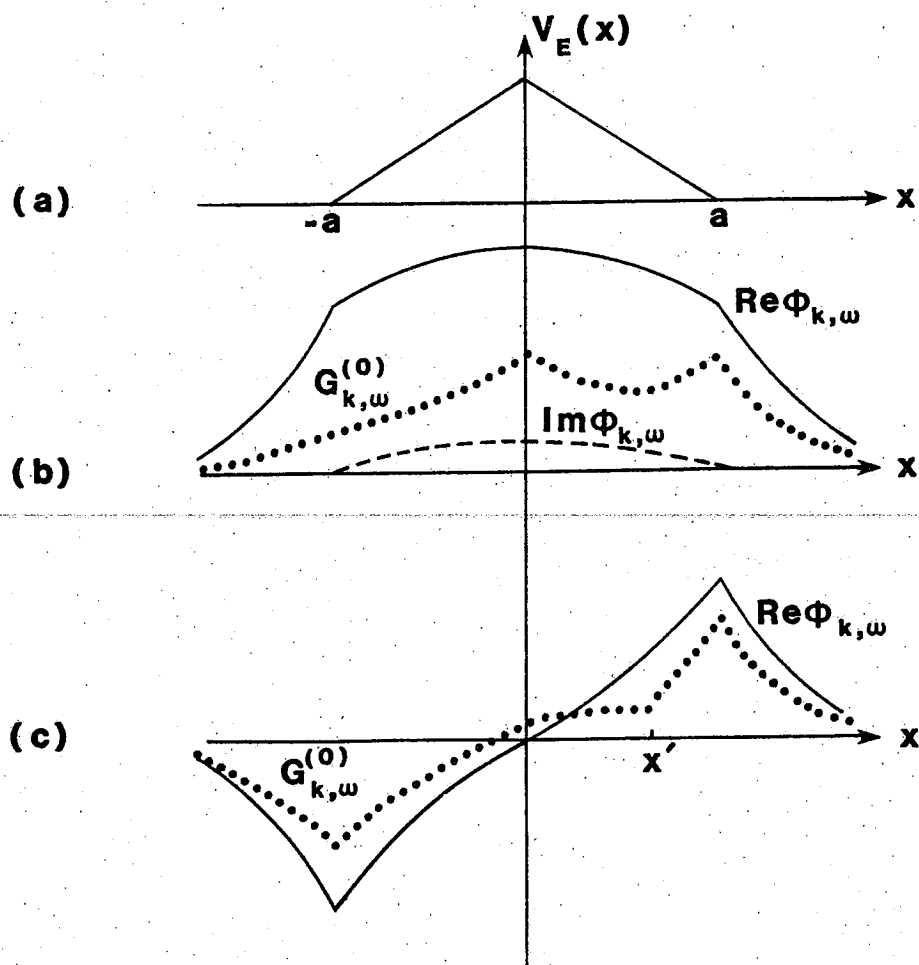
$$(4:7a-3)$$

Figure 4-6. Broken-line mean flow profile and linear
eigenfunction of a typical jet or wake.

Because of the reflectional symmetry of the mean flow, we let the source (δ-function) be located in the range, $0 < x < a$. A solution of Eq. (4:7a-1) can easily be solved for and expressed as,

$$G_{k,\omega}^{(0)} = \begin{cases} -e^{-kx}\left[\dfrac{A(F + e^{-2ka})G}{[F(1 + G) + (1 - G)e^{-2ka}][F + e^{-2ka}]} - \dfrac{\sin h(kx')}{k}\right], & x > a \\[4ex] -A\dfrac{[(G - 1)e^{-2ka} - F]e^{-kx} + [F(G + 1) + e^{-2ka}]e^{kx}}{[F(1 + G) + (1 - G)e^{-2ka}][F + e^{-2ka}]} \\ \quad + \dfrac{\sin h(k(x - x'))}{k}, & a > x > x' \\[4ex] -A\dfrac{[(G - 1)e^{-2ka} - F]e^{-kx} + [F(G + 1) + e^{-2ka}]e^{kx}}{[F(1 + G) + (1 - G)e^{-2ka}][F + e^{-2ka}]}, & x' > x > 0 \\[4ex] -A\dfrac{Ge^{-k(x+2a)} + FGe^{kx}}{[F(1 + G) + (1 - G)e^{-2ka}][F + e^{-2ka}]}, & 0 > x > -a \\[4ex] -A\dfrac{e^{kx}G(F + 1)}{[F(1 + G) + (1 - G)e^{-2ka}][F + e^{-2ka}]}, & -a > x \end{cases}$$

where

$$A = \frac{e^{ky}}{2k}\left[\frac{e^{-2ka}}{F} + e^{-2ky}\right], \quad G = \frac{\omega a}{V_o} - ka,$$

and

$$F = \frac{2\omega a}{V_o} - 1 \; .$$

Notice that the denominator in the expression of $G_{k,\omega}^{(0)}$ is exactly the linear dispersion. A typical $G_{k,\omega}^{(0)}$ near $F + e^{-2ka} = 0$ is shown in Fig. (4-6b). At this collective resonance, $G_{k,\omega}^{(0)}$ becomes a neutrally stable eigenfunction of odd parity. Near $F(1 + G) + (1 + G)e^{-2ka} = 0$, a typical $G_{k,\omega}^{(0)}$ is shown in Fig. (4-6c). At this collective resonance, $G_{k,\omega}^{(0)}$ becomes an eigenfunction of even parity. (These two dispersion relations are also shown in Fig. (4-7).)

Consequently, the velocity field fluctuation $\phi_{k,\omega}$ of vorticity clump turbulence, which has similar properties as $G_{k,\omega}^{(0)}$ at low turbulence fluctuation level, can be viewed as being induced by seed vorticity fluctuations and shielded by the collective response. At collective resonances, $\phi_{k,\omega}$ becomes a usual eigenmode. This picture is analogous to that of plasma clump turbulence, where electric field is induced by seed clumps (macroparticles) and shielded by the dielectric response.

For moderate turbulence fluctuation level, the collective resonances are broadened, and $\phi_{k,\omega}$ is
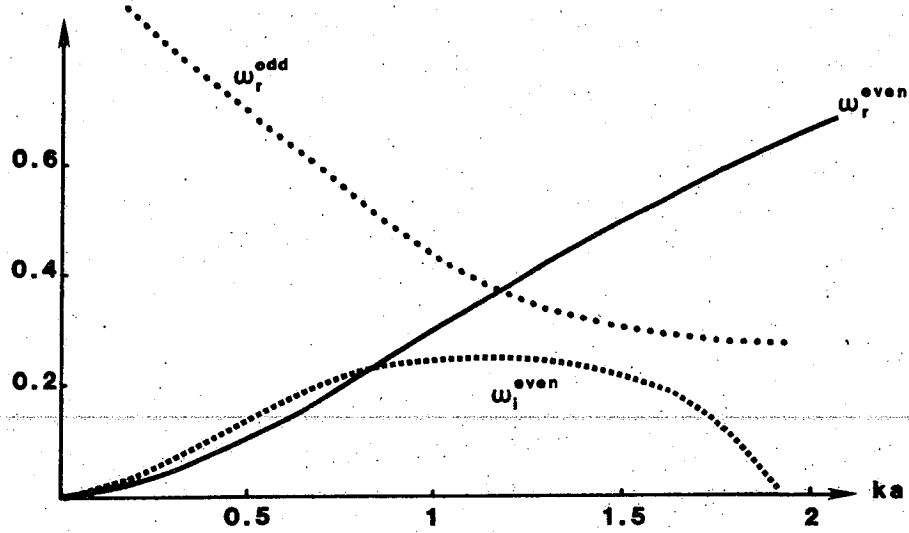
Figure 4-7. Dispersion relation for the mean flow profile in Figure 4-6.

accordingly modified. The collective resonance broadening can be estimated by substituting $\omega + i/\tau_c$ for ω in the dispersion relations, where τ_c is the turbulence correlation time and determined by turbulence level. In this regime, it corresponds to a fluid counterpart of Vlasov turbulence of the wave-clump type.

b. Two-Point Vorticity Correlation
    Equation--Triplets

The dynamics of slow time scale (nonlinear time scale) evolution can be described by a two-point, one-time vorticity correlation function. The enstrophy evolution equation is obtained by multiplying $\delta\rho(2)$ by $d\rho(1)/dt = 0$, $\delta\rho(1)$ by $d\rho(2)/dt = 0$, summing up these two equations, and then taking an ensemble average. It yields

$$\frac{1}{4\pi^2} \sum_{\substack{k \\ \omega}} \left[\frac{\partial}{\partial t} < \rho_{k,\omega}^{(1)} \rho_{k,\omega}^{*(2)} > + ik(V_E^{(1)} - V_E^{(2)}) < \rho_{k,\omega}^{(1)} \rho_{k,\omega}^{*(2)} > \right]$$

$$+ \frac{i}{4\pi^2} \sum_{\substack{k' \\ \omega'}} \left\{ \left[k' \frac{d\phi_{k'',\omega''}^{(1)}}{dx_1} \rho_{k',\omega'}^{(1)} \rho_{k,\omega}^{*(2)} \right. \right.$$

$$\left. \left. + k'' \frac{d\rho_{k',\omega'}^{(1)}}{dx_1} \phi_{k'',\omega''}^{(1)} \rho_{k,\omega}^{*(2)} \right] + \left[1 \longleftrightarrow 2 \right]^* \right\}$$

$$= -\frac{1}{4\pi^2} \sum_{\substack{k \\ \omega}} \left[k \frac{d^2 V_E(1)}{dx_1^2} <\phi_{k,\omega}(1)\rho^*_{k,\omega}(2)> \right.$$

$$\left. - k \frac{d^2 V_E(2)}{dx_2^2} <\phi^*_{k,\omega}(2)\rho_{k,\omega}(1)> \right] \qquad (4:7b-1)$$

where we have used the fact that the system is transla-
tional invariant in the y direction, and that the fast
timescale variations can be Fourier-transformed and the
slow ones are described by the time derivative. Also,
[1⟷2]* stands for terms with indices 1 and 2 exchanged,
and complex conjugate taken.

In the following, we will show that the triplet
correlation in Eq. (4:6-1) can be approximated by a rela-
tive diffusion of the vorticity correlation, and a term of
a total derivative with respect to x, serving as a non-
linear source for the vorticity correlation. The itera-
tion scheme used in the previous section is used to ob-
tain this result. The triplet terms can be expressed,
in terms of second order driven field and vorticity, as

$$i \sum_k \left[\left[k' \left< \frac{d\phi_{k''}^{(2)}(1)}{dx_1} \rho_{k'}(1)\rho^*_k(2) \right> \right. \right.$$

$$\left. \left. + k'' <\phi_{k''}^{(2)}(1) \frac{d\rho_{k'}(1)}{dx_1} \rho^*_k(2)> \right] \right]$$

$$
+ \left[k'' \left\langle \frac{d\phi_{k'}(1)}{dx_1} \, \rho_{k''}^{(2)}(1)\rho_{k}^{*}(2) \right\rangle \right.
$$

$$
+ k' \left\langle \phi_{k'}(1) \, \frac{d\rho_{k''}^{(2)}(1)}{dx_1} \, \rho_{k}^{*}(2) \right\rangle
$$

$$
+ k \left\langle \frac{d\phi_{k'}(1)}{dx_1} \, \rho_{k''}(1)\rho_{k}^{*(2)}(2) \right\rangle
$$

$$
\left. + k' \left\langle \phi_{k'}(1) \, \frac{d\rho_{k''}(1)}{dx_1} \, \rho_{k}^{*(2)}(2) \right\rangle \right]
$$

$$
+ \left[1 \longleftrightarrow 2 \right]^{*} \tag{4:7b-2}
$$

Here, each of $\phi(1)$, $\phi(2)$, $\rho(1)$ and $\rho(2)$ can be driven by other modes.

To avoid unnecessary complication associated with the spatial derivatives of driven modes ($d\phi^{(2)}/dx$ or $d\rho^{(2)}/dx$), we can absorb them into terms of total derivatives. That is, we let

$$
\frac{d\phi_{k''}^{(2)}(1)}{dx_1} \, \rho_{k'}(1)\rho_{k}^{*}(2) = \left[\frac{d}{dx_1} \left[\phi_{k''}^{(2)}(1)\rho_{k'}(1)\rho_{k}^{*}(2) \right] \right.
$$

$$
\left. + \phi_{k''}^{(2)}(1)\rho_{k'}(1) \, \frac{d\rho_{k}^{*}(2)}{dx_2} \right]
$$

$$
- \phi_{k''}^{(2)}(1)\rho_{k'}(1) \, \frac{d\rho_{k}^{*}(2)}{dx_2}
$$

and

$$\phi_{k'}(1)\,\frac{d\rho_{k''}^{(2)}(1)}{dx_1}\,\rho_k^*(2) = \left[\frac{d}{dx_1}\left[\phi_{k'}(1)\rho_{k''}^{(2)}(1)\rho_k^*(2)\right]\right.$$

$$+\;\phi_{k'}(1)\rho_{k''}^{(2)}(1)\,\frac{d\rho_k^*(2)}{dx_2}\Big]$$

$$-\;\phi_{k'}(1)\rho_{k''}^{(2)}(1)\,\frac{d\rho_k^*(2)}{dx_2}$$

After this rearrangements, it is straightforward to substitute $\phi^{(2)}$ and $\rho^{(2)}$ from Eqs. (E-2) and (E-1) of Appendix E into the triplet terms, which yields

Triplet

$$=\left[\frac{d}{dx_1}+\frac{d}{dx_2}\right]\sum_{\substack{k',\omega'\\k,\omega}}\int dx'\left[\left[\frac{i}{\omega''-k''V_E}\,G_{k'',\omega''}(1,x')\right]\right.$$

$$\cdot\,(k')^2\left[\langle\rho_{k',\omega'}(1)\rho_{k',\omega'}^*(x')\rangle\langle\frac{d\phi_{k,\omega}(x')}{dx'}\,\rho_{k,\omega}^*(2)\rangle\right.$$

$$-\;\langle\rho_{k',\omega'}(1)\phi_{k',\omega'}^*(x')\rangle\langle\frac{d\rho_{k,\omega}(x')}{dx'}\,\rho_{k,\omega}^*(2)\rangle\Big]$$

$$-\;\left[\frac{i}{\omega''-k''V_E}\,\nabla_\perp^2 G_{k'',\omega''}(1,x')\right]$$

$$\cdot\,(k')^2\left[\langle\phi_{k',\omega'}(1)\rho_{k',\omega'}^*(x')\rangle\langle\frac{d\phi_{k,\omega}(x')}{dx'}\,\rho_{k,\omega}^*(2)\rangle\right.$$

$$- \left\langle \phi_{k',\omega'}(1) \phi^*_{k',\omega'}(x') \right\rangle \left\langle \frac{d\rho_{k,\omega}(x')}{dx'} \, \rho^*_{k,\omega}(2) \right\rangle \Bigg] \Bigg]$$

$$- \sum_{\substack{k',\omega' \\ k,\omega}} \int dx \Bigg[k^2 \Bigg[\frac{i}{\omega'' - k''V_E} \nabla^2_\perp G_{k'',\omega''}(1,x') \Bigg] \cdot$$

$$\cdot \Bigg[\left\langle \frac{d\phi_{k',\omega'}(1)}{dx_1} \, \frac{d\phi^*_{k',\omega'}(x')}{dx'} \right\rangle \left\langle \rho_{k,\omega}(x') \rho^*_{k,\omega}(2) \right\rangle$$

$$- \left\langle \frac{d\phi_{k',\omega'}(1)}{dx_1} \, \frac{d\rho^*_{k',\omega'}(x')}{dx'} \right\rangle \left\langle \phi_{k,\omega}(x') \rho^*_{k,\omega}(2) \right\rangle \Bigg]$$

$$- (k'')^2 \Bigg[\frac{i}{\omega - kV_E} \nabla^2_\perp G^*_{k,\omega}(2,x') \Bigg]$$

$$\cdot \Bigg[\left\langle \frac{d\phi_{k',\omega'}(1)}{dx_1} \, \frac{d\phi^*_{k',\omega'}(x')}{dx'} \right\rangle \left\langle \rho^*_{k'',\omega''}(x') \rho_{k'',\omega''}(1) \right\rangle$$

$$- \left\langle \frac{d\phi_{k',\omega'}(1)}{dx_1} \, \frac{d\rho_{k',\omega'}(x')}{dx'} \right\rangle \left\langle \phi^*_{k'',\omega''}(x') \rho_{k'',\omega''}(1) \right\rangle \Bigg] \Bigg]$$

$$+ \sum_{\substack{k',\omega' \\ k,\omega}} \int dx' (k')^2 \Bigg[\Bigg[\frac{i}{\omega'' - k''V_E} \nabla^2_\perp G_{k'',\omega''}(1,x') \Bigg]$$

$$\cdot \Bigg[\left\langle \phi_{k',\omega'}(1) \rho^*_{k',\omega'}(x') \right\rangle \left\langle \frac{d\phi_{k,\omega}(x')}{dx'} \, \frac{d\rho^*_{k,\omega}(2)}{dx_2} \right\rangle$$

$$- \left\langle \phi_{k',\omega'}(1) \phi^*_{k',\omega'}(x') \right\rangle \left\langle \frac{d\rho_{k,\omega}(x')}{dx'} \, \frac{d\rho^*_{k,\omega}(2)}{dx_2} \right\rangle \Bigg]$$

$$- \Bigg[\frac{i}{\omega - kV_E} \nabla^2_\perp G^*_{k,\omega}(2,x') \Bigg]$$

$$\cdot \Bigg[\left\langle \phi_{k',\omega'}(1) \rho^*_{k',\omega'}(x') \right\rangle \left\langle \frac{d\phi^*_{k'',\omega''}(x')}{dx'} \, \frac{d\rho_{k'',\omega''}(1)}{dx_1} \right\rangle$$

structures, for terms that are smooth functions of $x_1 - x_2$ at a small separation, we shall evaluate x_2 at x_1. These "smooth" terms include those serving as a source, and those retained on the left of the equality but having integral operators operated on. This is because the singularity of $<\delta\rho(1)\delta\rho(2)>$ at $x_1 = x_2$ is not too strong (will be shown to be a logarithmic singularity), the terms mentioned above are "smooth" at a small separation. After this operation, the "smooth" terms on the left cancel among themselves, and those on the right almost cancel except a term that appears in a form of a total derivative. Hence the remaining terms on the left appear as either $<\rho(1)\rho(2)>$ or $\left\langle (d\rho(1)/dx_1)(d\rho(2)dx_2) \right\rangle$.

In other words, the above operation yields that $\left[B_3 \right]$ cancels, and $(d/dx_1 + d/dx_2)\left[A(1,2) \right]$ becomes $d/dx_1\left[A(1,1) \right]$, a total derivative serving as a nonlinear source, and that $\left[B_1 \right] + \left[B_2 \right]$ becomes

$$
\sum_{\substack{k',\omega' \\ k,\omega}} \left[k^2 \left[\frac{i}{\omega'' - k''V_E} \right] \left| \frac{d}{dx_1}\phi_{k',\omega'}(1) \right|^2 \left\langle \rho_{k,\omega}(1)\rho^*_{k,\omega}(2) \right\rangle \right.
$$

$$
- (k'')^2 \left[\frac{i}{\omega - kV_E} \right] \left\langle \frac{d\phi_{k',\omega'}(1)}{dx_1} \frac{d\phi^*_{k',\omega'}(2)}{dx_2} \right\rangle
$$

$$
\cdot <\rho^*_{k'',\omega''}(1)\rho_{k'',\omega''}(2)>
$$

$$+ \ (k')^2 \left[\frac{i}{\omega'' - k''V_E} \right] \left\langle |\phi_{k',\omega'}(1)|^2 \right\rangle$$

$$\cdot \ \left\langle \frac{d\rho_{k,\omega}(1)}{dx_1} \frac{d\rho^*_{k,\omega}(2)}{dx_2} \right\rangle$$

$$- \ (k')^2 \left[\frac{i}{\omega - kV_E} \right] <\phi_{k',\omega'}(1)\phi^*_{k',\omega'}(2)>^*$$

$$\cdot \ \left\langle \frac{d\rho^*_{k'',\omega''}(1)}{dx_1} \frac{d\rho_{k'',\omega''}(2)}{dx_2} \right\rangle \ \Bigg]$$

$$\cdot \ e^{-iky_-}$$

Now, we let $\left\langle (d\rho(1)/dx_1)(d\rho(2)/dx_2) \right\rangle$ be expressed as $-d^2/dx_-^2 \ <\rho(1)\rho(2)>$, and property change the dummy index k'' to k, by which a factor $e^{ik'y_-}$ will be introduced and attached to the coefficients $<d\phi(1)/dx_1 \ d\phi(2)/dx_2>$ and $<\phi(1)\phi(2)>$. Finally, we expand these two coefficients at $\underset{\sim}{x}_1 = \underset{\sim}{x}_2$, then $\left[B_1 \right] + \left[B_2 \right]$ can be expressed explicitly as

$$\left[(D_x k_o^2 y_-^2 + D_y k_o^2 x_-^2)\frac{\partial^2}{\partial x_-^2} + (D_y k_o^2 y_-^2 \right.$$

$$\left. + \ D_y'' x_-^2)\frac{\partial^2}{\partial y_-^2} \right] <\rho(1)\rho(2)>$$

where

$$
\begin{bmatrix} D_x \\ \\ D_y \\ \\ D''_y \end{bmatrix} = \frac{1}{2\pi} \sum_{\substack{k' \\ \omega'}} \frac{i}{\omega' - k'V_E} \begin{bmatrix} (k')^2 <\phi^2>_{k',\omega'} \\ \\ \left\langle \left| \frac{d\phi}{dx} \right| \right\rangle^2_{k,\omega} \\ \\ \left\langle \left| \frac{d^2\phi}{dx^2} \right| \right\rangle^2_{k,\omega} \end{bmatrix} \qquad (4:7b-4)
$$

and k_o is the spectrum averaged wavenumber. In the above expressions, a Markovian approximation has been used, where $i/(\omega'' - k''V_E)$ is replaced by $i/(\omega' - k'V_E)$. The approximation actually assumes a velocity field-vorticity resonance, $\omega - kV_E = 0$.

This result has the following meanings. Turbulent convection tends to tear vorticity granulations apart. At small separation, vortex elements are convected by approximately the same turbulent velocity field, so that they experience less relative diffusion. Simultaneously, due to the spatial inhomogeneity, nonlinear effects locally redistribute the linear source (due to the form of a total derivative w.r.t. x), thus yield a modified source.

c. Two-Point Vorticity Correlation
    Equation--Source

From Eq. (4:7b-1), the source, when evaluated
at the same point, is $<S>(1,1)$

$<S>(1,1)$

$$= -\mathrm{Re} \sum_{\substack{k \\ \omega}} \left[\frac{ik}{2\pi^2} \frac{d^2 V_E}{dx^2} <\phi^*_{k,\omega} \rho_{k,\omega}> \right] \qquad (4:7c-1)$$

Now, we separate the total vorticity fluctuation $\rho_{k,\omega}$
into $\rho^c_{k,\omega}$ and $\tilde{\rho}_{k,\omega}$, where $\rho^c_{k,\omega}$ is the coherent vorticity
fluctuation satisfying

$$\rho^c_{k,\omega} \approx -k \frac{d^2 V_E}{dx^2} \frac{\phi}{\omega - kV_E} \qquad (4:7c-2)$$

and $\tilde{\rho}$ is the incoherent vorticity fluctuation satisfying

$$-i(\omega - kV_E)\tilde{\rho}_{k,\omega} \cong 0 \qquad (4:7c-3)$$

To extend this formalism further, we note that the veloc-
ity field $\phi_{k,\omega}$ is induced by the seed incoherent fluctua-
tions $\tilde{\rho}_{k,\omega}$. Therefore, the one-point equation should be
expressed as

$$\nabla_{\perp}^2 \phi_{k,\omega} + k \frac{d^2 V_E}{dx^2} \frac{\phi_{k,\omega}}{\omega - kV_E} = \tilde{\rho}_{k,\omega} \qquad (4:7c\text{-}4)$$

In Eqs. (4:7c-2), (4:7c-3) and (4:7c-4), we have neglected the nonlinear corrections to these expressions. With these relations, we can now express $\phi_{k,\omega}$ in terms of the seed fluctuation $\tilde{\rho}_{k,\omega}$ and a propagator $G_{k,\omega}(x,x')$ of Rayleigh's equation. That is,

$$\phi_{k,\omega} = \int dx' \, G_{k,\omega}(x,x') \tilde{\rho}_{k,\omega}(x') \qquad (4:7c\text{-}5)$$

The source can now be given explicitly,

$$\langle S \rangle (1,1)$$

$$= \sum_{\substack{k \\ \omega \\ \alpha}} 2k^2 \left[\frac{d^2 V_E}{dx^2} \right]^2 \delta(\omega - kV_E) \left[\frac{A_k}{\left| k \frac{dV_o}{dx_\alpha} \right|} \left| G_{k,\omega}(x_\alpha, x_\alpha) \right|^2 \right]$$

$$- \sum_{\substack{k \\ \omega \\ \alpha}} \frac{2k}{\pi} \frac{d^2 V_E}{dx^2} \delta(\omega - kV_E) A_k \operatorname{Im} G_{k,\omega}(x_\alpha, x_\alpha) \qquad (4:7c\text{-}6)$$

where we have used the fact that the incoherent fluctuation $\rho_{k,\omega}$ peaks at the resonance point.

$$\omega - kV_E(x_\alpha) = 0 \; . \qquad (4:7c\text{-}7)$$

Hence $\langle\tilde{\rho}_{k,\omega}(1)\tilde{\rho}^*_{k,\omega}(2)\rangle$ peaks at small separation, and is modelled by

$$\langle\tilde{\rho}_{k,\omega}(1)\tilde{\rho}^*_{k,\omega}(2)\rangle = A_k[2\pi\delta(\omega - kV_E(x_1))\delta(x_1 - x_2)]$$

$$= \sum_\alpha A_k\left[\frac{2\pi\delta(x_1 - x_\alpha)\delta(x_1 - x_2)}{|k\,dV_E/dx_1|}\right] \qquad (4:7c-8)$$

Here, x_α stands for each resonance point, and A_k is a positive quantity, characterizing the fluctuation amplitude. Actually, we can show later (in Eqs. (4:7d-1) and (4:7d-5)) that the vorticity correlation function is indeed sharply peaked at small separation with an amplitude-dependent width. In Eq. (4:7c-6), the first term represents the diffusion of mean vorticity due to turbulent field, and is positive definite; the second term represents a "drift" of mean vorticity.

In the following analysis, we want to show that for a wake or jet, the drift term of Eq. (4:7c-6) is positive definite. From the expression of the drag force term, $\mathrm{Im}G_{k,\omega}(x_\alpha, x_\alpha)$ has to be determined explicitly. This can be achieved by the following manipulations. Separating the real and imaginary parts of the propagator equation, Eq. (4:7a-1), we have

$$\left[\nabla_\perp^2 + k\frac{d^2V_E}{dx^2}\frac{(\omega_r - kV_E)}{(\omega_r - kV_E)^2 + \omega_i^2}\right]\mathrm{Re}\,G_{k,\omega}(x,x_\beta)$$

$$= k\frac{d^2V_E}{dx^2}\frac{\omega_i}{(\omega_r - kV_E)^2 + \omega_i^2}\,\mathrm{Im}\,G_{k,\omega}(x,x_\beta)$$

$$+\ \delta(x - x_\beta) \tag{4:7c-9}$$

$$\left[\nabla_\perp^2 + k\frac{d^2V_E}{dx^2}\frac{(\omega_r - kV_E)}{(\omega_r - kV_E)^2 + \omega_i^2}\right]\mathrm{Im}\,G_{k,\omega}(x,x_\beta)$$

$$= -k\frac{d^2V_E}{dx^2}\frac{\omega_i}{(\omega_r - kV_K)^2 + \omega_i^2}\,\mathrm{Re}\,G_{k,\omega}(x,x_\beta) \tag{4:7c-10}$$

An important step in this calculation is to introduce another propagator $G_{k,\omega}^c(x,x')$ as we did in the previous section in proving the new theorem. $G_{k,\omega}^c(x,x')$ satisfies Eq. (4:5-9). If $\omega_i \ll \omega_r$, then

$$\frac{\omega_i}{(\omega_r - k_o V_E)^2 + \omega_i^2} = \sum_\alpha \frac{\pi\delta(x - x_\alpha)}{|k\ dV_E/dx|}$$

And,

$$\mathrm{Re}\,G_{k,\omega}(x,x_\beta) = \int dx'\,G_{k,\omega}^c(x,x')$$

$$\cdot\left[k\frac{d^2V_E}{d(x')^2}\left(\frac{\omega_i}{(\omega_r - kV_E)^2 + \omega_i^2}\right)\mathrm{Im}\,G_{k,\omega}(x',x_\beta)\right.$$

$$\left.+\ \delta(x' - x_\beta)\right].$$

$$= \sum_{\alpha} \pi k \frac{d^2 V_E}{dx_\alpha^2} \frac{G_{k,\omega}^c(x,x_\alpha)}{|k \ dV_E/dx_\alpha|} \ \mathrm{Im}G_{k,\omega}(x_\alpha,x_\beta)$$

$$+ \ G_{k,\omega}^c(x,x_\beta) \qquad\qquad\qquad (4:7c\text{-}11)$$

Similarly,

$$\mathrm{Im}G_{k,\omega}(x,x_\beta) = -\sum_{\alpha}$$

$$\pi k \frac{d^2 V_E}{dx_\alpha^2} \frac{G_{k,\omega}^c(x,x_\alpha)}{|k \ dV_E/dx_\alpha|} \ \mathrm{Re}G_{k,\omega}(x_\alpha,x_\beta) \qquad (4:7c\text{-}12)$$

Notice that this operation is almost identical to that
in the proof of the new theorem in the previous section.
Now, evaluating x at each resonance point, we obtain a
set of inhomogeneous equations.

For a wake or jet, there are only two resonance
points. A straightforward calculation shows that

$$\frac{\pi k(d^2 V_E/dx_1^2)}{|k(dV_E/dx_1)|} \ \mathrm{Im}G_{k,\omega}(x_1,x_1)$$

$$= \frac{-(M_{11}M_{22} - M_{12}M_{21})^2}{1 + (M_{11} + M_{22})^2 + (M_{11}M_{22} - M_{12}M_{21})^2} \quad (4:7c\text{-}13)$$

and

$$\frac{\pi k (d^2 V_E / dx_1^2)}{|k(dV_E/dx_1)|} \, \mathrm{Re}G_{k,\omega}(x_1, x_1)$$

$$= \frac{M_{22}(M_{11}M_{22} - M_{12}M_{21})}{1 + (M_{11} + M_{22})^2 + (M_{11}M_{22} - M_{12}M_{21})^2} \quad (4:7c\text{-}14)$$

where $M_{\alpha\beta}$ has been defined in Eq. (4:5-15).

Substituting $\mathrm{Im}G_{k,\omega}(x_\alpha, x_\alpha)$ and $\mathrm{Re}G_{k,\omega}(x_\alpha, x_\alpha)$ into Eq. (4:7c-6), it yields,

$$\left[\mathrm{Drift}\right] = \sum_{\substack{k \\ \omega}} \frac{2A_k}{\pi^2} \left[\, |k(dV_E/dx_1)| \right.$$

$$\left. + \, |k(dV_E/dx_2)| \, \right] \cdot \delta(\omega - kV_E)$$

$$\cdot \frac{(M_{11}M_{22} - M_{12}M_{21})^2}{1 + (M_{11} + M_{22})^2 + (M_{11}M_{22} - M_{12}M_{21})^2} \quad (4:7c\text{-}15)$$

and

$$\left[\mathrm{Diffusion}\right] = \sum_{\substack{k \\ \omega}} \frac{2A_k}{\pi^2} \left[\, |k(dV_E/dx_1)| \right.$$

$$\cdot \, [M_{22}^2 + (M_{11}M_{22} - M_{12}M_{21})^2]$$

$$\left. + \, |k(dV_E/dx_2)| \cdot [M_{11}^2 + (M_{11}M_{22} - M_{12}M_{21})^2] \right]$$

$$\cdot \, \delta(\omega - kV_E) \cdot \frac{(M_{11}M_{22} - M_{12}M_{21})^2}{[1 + (M_{11} + M_{22})^2 + (M_{11}M_{22} - M_{12}M_{21})^2]^2}$$

Both drift and diffusion terms are positive definite.

It is instructive to compare this result with that of a one-dimensional single-species plasma. The latter has a vanishing source term because of the local momentum conservation of Vlasov plasmas. In the fluid case, vortices do not have to obey any analogous conservation law, hence interactions between vortices can lead to relaxation of mean vorticity and thus drive local fluctuations.

Mathematically, the analogy between these two systems breaks down when Poisson's equation is compared with its counterpart in the shear-flow system. Poisson's equation can be expressed in an integral form as

$$\phi(z) = -(4\pi e)\int \nabla^{-2}(z,z')\delta f(z',v)dz'dv.$$

By contrast, its counterpart, velocity field-vorticity relation, is given by

$$\phi(x,y) = \int \nabla^{-2}(x,y;x',y')\delta\rho(x',y')dx'dy' \quad .$$

Notice the opposite sign between these two expressions.

It is the sign difference that leads to the completely different dynamics of discrete vortices (Biot-Savort's law) from that of discrete charged particles (Coulomb force). It is this sign difference that yields the nonvanishing vorticity fluctuation source as opposed to the vanishing particle density fluctuation source (this point will become transparent when the mean flow has a monotonic profile, where $\left[\text{Drift}\right] = \left[\text{Diffusion}\right]$).

We are now able to give explicitly an approximated evolution equation for the two-point, one-time vorticity correlation function:

$$\left[\frac{\partial}{\partial t} + V'_e x_- - \left[(D_x k_o^2 y_-^2 + D_y k_o^2 x_-^2)\frac{\partial^2}{\partial x_-^2}\right.\right.$$

$$\left.\left. + (D_y k_o^2 y_-^2 + D''_y x_-^2)\frac{\partial^2}{\partial y_-^2}\right]\right]$$

$$\cdot <\delta\rho(1)\delta\rho(2)>$$

$$= -\frac{d}{dx}\left\{\text{Re}\left[\sum_{\substack{k',\omega'\\k,\omega}}\int dx'\ \frac{2i}{\omega'' - k\ V_E}\ G_{k'',\omega''}(1,x')\right.\right.$$

$$\cdot (k')^2\left[<\rho_{k',\omega'}(1)\rho^*_{k',\omega'}(x')>\left\langle\frac{d\phi_{k,\omega}(x')}{dx'}\ \rho^*_{k,\omega}(1)\right\rangle\right.$$

$$\left.\left.\left. - <\rho_{k',\omega'}(1)\phi^*_{k',\omega'}(x')>\left\langle\frac{d\rho_{k,\omega}(x')}{dx'}\rho^*_{k,\omega}(1)\right\rangle\right]\right]\right\}$$

$$- \text{Re}\left[\sum_{\substack{k',\omega' \\ k,\omega}} \int dx' \frac{2i}{\omega'' - k''V_E} G_{k'',\omega''}(1,x')\right.$$

$$\cdot (k')^2 \left[<\phi_{k',\omega'}(1)\rho^*_{k',\omega'}(x')>\left\langle\frac{d\phi_{k,\omega}(x')}{dx'} \rho^*_{k,\omega}(1)\right\rangle\right.$$

$$\left.\left.- <\phi_{k',\omega'}(1)\phi_{k',\omega'}(x')>\left\langle\frac{d\rho_{k,\omega}(x')}{dx'} \rho^*_{k,\omega}(1)\right\rangle\right]\right]\right\}$$

$$+ \left[\left[\text{Drift}\right] + \left[\text{Diffusion}\right]\right]$$

$$= - \frac{d}{dx_1} A(1,1) + <S> \equiv <S>_T \qquad (4:7c-17)$$

d. Vorticity Clump Correlation
   Function and Its Spectrum

Now, we are in a position to seek a steady state
solution for Eq. (4:7c-17). Formally, we can invert the
left-hand-side operator and obtain

$$<\delta\rho(1)\delta\rho(2)> = \tau_{cl}(x\_,y\_)<S>_T \qquad (4:7d-1)$$

To evaluate the operator τ_{cl}, we first need to understand
what it means. τ_{cl} has a dimension of time; depends on
the separation of the two points; is singular at zero
separation because of vanishing diffusion coefficients
at this limit; and is small at large separation. Hence,

$\tau_{cl}(x_-, y_-)$ may be approximately interpreted as the time required for two points, initially separated by x_- and y_-, to separate by an average correlation length. This time can be evaluated by solving for the relative trajectory. In fact, the above argument and the method to be used in evaluating τ_{cl} are similar to those of the plasma clump theories.

The relative orbit obeys a Langevin equation of spatially varying-intensity noise. A set of second-moment equations, obtained from taking the second moments of a propagator equation described by the left-side operators of Eq. (4-7c-17), is given by

$$\frac{d\langle y_-^2\rangle}{dt} = 14k_o^2 D_y\langle y_-^2\rangle + 2D_y''\langle x_-^2\rangle + 2V_E'\langle x_-y_-\rangle$$

$$\frac{d\langle x_-y_-\rangle}{dt} = 6k_o^2 D_y\langle x_-y_-\rangle + V_E'\langle x_-^2\rangle$$

$$\frac{d\langle x_-^2\rangle}{dt} = 2k_o^2 D_x\langle y_-^2\rangle + 14k_o^2 D_y\langle x_-^2\rangle . \qquad (4:7d-2)$$

Note that vorticity fluctuation $\rho_{k,\omega}(\approx d^2\phi_{k,\omega}/dx^2)$ exhibits strong localization (i.e., strong gradient), hence $\langle|d_x^2\phi_{k,\omega}^{(1)}|^2\rangle (\propto \tau_{cl})$ is much larger than $k^2\langle|d\phi_{k,\omega}/dx|^2\rangle$ and $k^4\langle|\phi_{k,\omega}|^2\rangle$. That is, $D_y'' \gg k_o^2 D_y$

and $k_o^2 D_x$. On the other hand, $d\phi_{k,\omega}/dx$ and $\phi_{k,\omega}$ are smoothly varying functions (no singularities), hence we let $<|d\phi_{k,\omega}/dx|^2> \approx k^2 <|\phi_{k,\omega}|^2>$. That is, $D_y \approx D_x \equiv D$. Also, we let D_y'' be approximately $(k_o \Delta x)^{-2} k_o^2 D$, where the vorticity correlation length Δx can be self-consistently determined once the functional dependence of the vorticity correlation function is obtained. A laborious, but straightforward, calculation shows that the time asymptotic solution is

$$<y_-^2(t)> = \frac{1}{3} \exp \frac{-t}{\tau_c} \cdot \Big[<y_-^2(0)>$$

$$+ 2V_E'\tau_c <x_-(0)y_-(0)> + 2(V_E'\tau_c)^2 <x_-^2(0)> \Big] \qquad (4{:}7d{-}3)$$

where

$$\tau_c^{-1} = (12 k_o^2 D)^{1/3} (V_E')^{2/3} , \qquad (4{:}7d{-}4)$$

and $k_o^2 D/V_E' \ll 1$ has been assumed.

The clump lifetime $\tau_{cl}(x_-, y_-)$ is defined as, $k_o^2 y_-^2(t = \tau_{cl}) = 1$. Therefore,

$$\tau_{cl}(x_-, y_-) = -\tau_c \cdot \ln \Big[\frac{k_o^2}{3} \Big[y_-^2 + 2V_E'\tau_c x_- y_-$$

$$+ 2(V_E'\tau_c)^2 x_-^2 \Big] \Big] \qquad (4{:}7d{-}5)$$

Note that

$$\Delta x \approx (k_o \tau_c V_E')^{-1} = \left(\frac{12D}{k_o V_E'}\right)^{1/3} \qquad (4\!:\!7d\text{-}6)$$

One can substitute Eqs. (4:7d-4) and (4:7d-6) into the set of coupled equations, Eq. (4:7d-2), and easily find that this set of equations effectively reduces to

$$\frac{d\langle y_-^2\rangle}{dt} = 2V_E'\langle x_- y_-\rangle$$

$$\frac{d\langle x_- y_-\rangle}{dt} = V_E'\langle x_-^2\rangle \qquad (4\!:\!7d\text{-}7)$$

$$\frac{d\langle x_-^2\rangle}{dt} = 2k_o^2 D\langle y_-^2\rangle$$

These equations show that the relative streaming (characterized by V_E') plays a very significant role for the determination of the time-asymptotic relative orbit (when $V_E'\tau_c \gg 1$).

Because of Eq. (4:7d-1), the vorticity wave-number spectrum can then be determined by the Fourier transform of $\tau_{cl}(x_-, y_-)$. We find that

$$\langle \delta\rho\,\delta\rho\rangle_{\underset{\sim}{k}} = \frac{4\pi}{k_o^2\,|V_E'|\,p^2}\,[1 - J_o(P)]\langle S\rangle_T \;, \qquad (4\!:\!7d\text{-}8)$$

where

$$p^2 \equiv 2\left(\frac{k_x + k_y}{k_o}\right)^2 + \frac{k_x^2}{2k_o^2(V_E'\tau_c)^2}$$

$$= \frac{k^2}{k_o}\left[\left[2 + \frac{1}{4(V_E'\tau_c)^2} + \left[4\right.\right.\right.$$

$$\left.\left.+ \frac{1}{16(V_E'\tau_c)^4}\right]^{1/2}\right]\sin^2(\theta_k - \psi)$$

$$+ \left[2 + \frac{1}{4(V_E'\tau_c)^2} - \left[4\right.\right.$$

$$\left.\left.+ \frac{1}{16(V_E'\tau_c)^4}\right]^{1/2}\right]\cos^2(\theta_k - \psi)\right] \qquad (4{:}7\text{d-}9)$$

$$\tan \theta_k \equiv k_x/k_y,$$

and

$$\tan \psi \equiv \frac{-8(V_E'\tau_c)^2}{(1 + 64(V_E'\tau_c)^4)^{1/2} - 1} \qquad (4{:}7\text{d-}10)$$

Since $V_E'\tau_c \gg 1$, we can expand in the small parameter $(V_E'\tau_c)^{-2}$ and approximate p^2 by

$$p^2 \approx \frac{k^2}{k_o^2}\left[4 \sin^2(\theta_k + \frac{\pi}{4})\right.$$

$$\left.+ \frac{15}{64(V_E'\tau_c)^2} \cos^2(\theta_k + \frac{\pi}{4})\right] \qquad (4{:}7\text{d-}11)$$

The spectral contours (Fig. (4-8)) are elliptical, with the minor and major widths scaled with $k_0/2$ and $8k_0 |V_E \tau_c|/\sqrt{15}$, respectively, and tilted by an angle, $-45°$.

At the limit $\underset{\sim}{k}^2/k_0^2 \gg 1$ and thus $J_0'(p) \approx 0$, the vorticity wavenumber spectrum has a simple expression,

$$\left[|\underset{\sim}{k}| <\delta\rho\,\delta\rho>_k \right] \approx \frac{1}{|\underset{\sim}{k}|^{-1}} \left[4 \sin^2 \left(\theta_k + \frac{\pi}{4}\right) \right.$$

$$\left. + \frac{15}{64(V_E'\tau_c)^2} \cos^2 \left(\theta_k + \frac{\pi}{4}\right) \right]^{-1}$$

$$\cdot \left[\frac{4\pi}{|V_E'|} <S>_T \right] . \tag{4:7d-12}$$

The dependence,[45] $|\underset{\sim}{k}|^{-1}$, is exactly the same as that obtained by the Komogoroff's type enstrophy cascade arguments in two-dimensional fluids. The angular dependence is due to the shearing of the mean flow motion. However, this point is not totally transparent from Eqs. (4:7d-8), (4:7d-9) and (4:7d-10). By taking the limit, $V_E'\tau_c = 0$, one does not recover an isotropic spectrum. The reason is that in deriving these equations, we have made the approximation, $V_E'\tau_c \gg 1$, to obtain the relative trajectory, Eq. (4:7d-3). Thus, the limit, $V_E'\tau_c = 0$, is not legitimately taken, therefore a correct answer should not be expected.
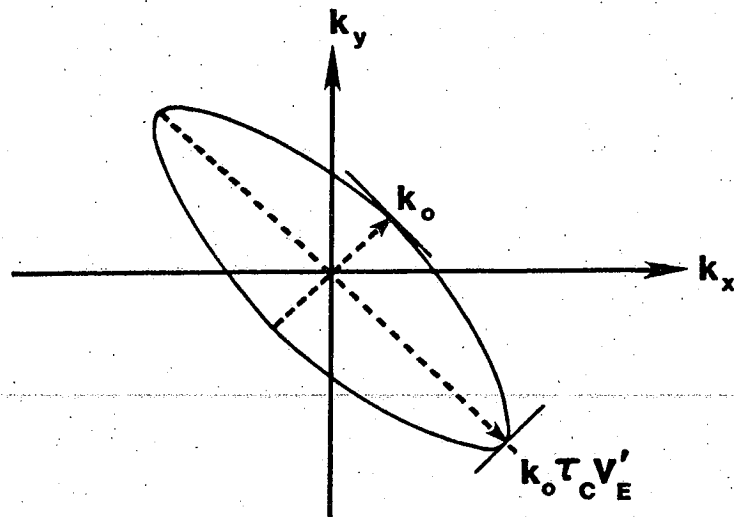
Figure 4-8. A contour of equivorticity spectrum in the wavenumber space.

Some physical insights can be gained from this
anisotropic spectrum. The small-scale vorticity clumps
discussed here are obviously different from the self-
similar eddies of the isotropic inertial range. The
vorticity clumps are large enough to experience the shear-
ing of the mean flow motion. However, the self-similar
eddies are too fine to sense the inhomogeneity of the
mean flow, hence their dynamics are governed by the inter-
actions among eddies of comparable sizes (eddy cascade).
Nevertheless, the vorticity clumps are still small enough
so that enstrophy received by a clump can immediately
be transferred to clumps of smaller sizes. As a result,
some sort of quasi-equilibrium is established and, thus
yields the $|\underset{\sim}{k}|^{-1}$ dependence of the high-k vorticity
spectrum. (Notice that this dependence actually arises
from the vanishing relative diffusion coefficient at zero
separation, that is, from the balance between the non-
linear diffusion and incoherent mode coupling of the
vorticity spectrum equation.)

As we have mentioned above, whether the vorticity
clumps exist crucially depends on the positivity of the
driving source. When fluctuation amplitudes are small
and thus nonlinear modifications (nonpositive definite)

of the linear source are negligible, we have shown that
the driving source is positive definite. Now, a question
arises: For a system with sufficient free energy to
drive fluctuations, what happens when the initially grow-
ing vorticity clumps exceed certain amplitudes so that
the source becomes nonpositive definite? If clump fluc-
tuations then disappear, where does fluctuation energy
go?

For the first question, we think that vorticity
clumps (small-scale fluctuations) will probably be damped
out as soon as the source becomes nonpositive in the
flow field. For the second question, we think that the
fluctuation energy of clumps may be transferred to other
types of fluctuations, namely, large-scale fluctuations.
Experimental observation of wake turbulence, within some
range of intermediate values of Reynolds numbers (e.g.,
Re $\approx$ 300) shows that small-scale and large-scale fluc-
tuations alternatively appear. We speculate that the
transition from small-scale fluctuations to large-scale
fluctuations may be related to the nonpositivity of the
driving source for small-scale fluctuations.

4.8 <u>Summary and Conclusion</u>

In this chapter, we have studied two types of turbulence in two-dimensional, incompressible fluids. Plasmas of uniform and strong magnetization are approximately dynamically equivalent to such a fluid, if fluctuations are low-frequency and electrostatic. The first type of turbulence consists of large-scale fluctuations, and is associated with the mixing-layer mean flow. The second type of turbulence is dominated by small-scale fluctuations, and is associated with the wake and jet mean flows.

For the first type of turbulence, our principal results are:

(a) Assuming that the mixing-layer flow evolves self-similarly, and that the dominant fluctuations are wave-like, thus nonwave fluctuations are ignored, we have shown that the mixing layer expands linearly in time. The expansion rate is consistent with those observed in computer simulations by Aref, et al., and experiments by Brown, et al.

(b) This result of the shear-flow expansion has little dependence on details of the quasi-linear model,

such as the initial noise spectrum, nonlinear modification of linear growth rate. Experimental observations show that the expansion rate is very weakly dependent on Reynolds numbers (comparing Fig. 4-2b with Fig. 4-2d) for $R_e \sim 10^4$. Our result depends on Reynolds number primarily through the maximum linear growth rate. For such high Reynolds numbers of the experiments, the maximum linear growth rate is very weakly dependent on R_e, thus so is the expansion rate.

(c) We have also shown that the mean flow loses kinetic energy linearly in time, and that the energy of large-scale fluctuations increases linearly in time, albeit at a slower rate.

For the type of small-scale turbulence of wakes and jets, our principal results are:

(a) We have shown that the small-scale fluctuations in wake or jet turbulence can be treated using the clump theory. To do so, we show that the relative diffusion of vorticity correlation is small when the separation of two vortex elements is small. More importantly, we show that the driving source for vorticity correlation is positive definite. It ensures the existence of vorticity clumps. This is because the presence of a

positive source can secularly drive the vorticity correlation function of zero separation (where relative diffusion vanishes), and yield a singularity.

(b) The vorticity correlation function and vorticity wavenumber spectrum of stationary turbulence are obtained. This correlation function has a logarithmic singularity at small separation, reflecting the strong correlation at this limit. The wavenumber spectrum has equi-vorticity contours of elliptical shape, with major axis (tilted at an angle, $-45°$, from the x direction) scaled with $k_o \tau_c V_E'$ and minor axis with k_o. For $|\underset{\sim}{k}| \gg k_o$, the wavenumber spectrum can be separated into a function dependent on $|\underset{\sim}{k}|$ multiplied by another function dependent on the angle, i.e., k_x/k_y. The former is $|\underset{\sim}{k}|^{-2}$, which can also be obtained by using the Komogoroff's cascade argument.

In addition to these results of nonlinear theory for shear flow turbulence, we also show that the necessary condition for existence of a solution of Rayleigh's equation is that inflection points of mean flow velocity must exist.

Since the model for the mixing-layer evolution is very crude, it is instructive to examine this model

with more care. Previously, we have assumed that the
fluctuation energy is concentrated on modes of large
scale, hence these modes interact not only with the mean
flow but also with themselves. Thus, we eliminate the
direct interaction between the large-scale and small-
scale fluctuations, whereby the small-scale fluctuations
do not explicitly appear in our analysis. Small-scale
fluctuations implicitly serve as a perfect absorber (sink
without feedback) in this model.

The result of an energy balance calculation
shows that both energy released from the mixing-layer
mean flow and energy absorbed by the large-scale fluctua-
tions increase linearly in time. However, the latter has
a slower rate (20% slower for the model profile). This
is consistent with our assumption that most of the energy
loss from the mean flow is absorbed by the large-scale
fluctuations, and some small portion of energy is trans-
ferred to the small-scale fluctuations.

For small-scale turbulence, our analysis re-
lies heavily on the existence of resonances of fluctua-
tion phase velocity with the shear flow velocity, i.e.,
$\omega/k = V_E(x)$. This resonance is so important that we
have been partly motivated by it to pursue the vorticity
clump theory. The reasons are elaborated on below.

Consider a vorticity correlation function at a small separation. Using Rayleigh's equation, we obtain

$$< \rho_{k,\omega}(1) \rho^*_{k,\omega}(2) >$$

$$\propto \left(\frac{d^2 V_E}{dx^2} \right) \frac{1}{(\omega/k - V_E(1))(\omega/k - V_E(2))^*} \qquad (4:8\text{-}1)$$

At $1 = 2$, the correlation function has not only a second order singularity at $\omega/k = V_E$, but an irremovable essential singularity due to pole pinching. That is, two first order singularities, $\omega/k = V_E(1)$ and $\omega/k = V_E(2)$, approach each other from either side of the real axis as 1 approaches 2. Note that a first order singularity can always be circumvented by making a detour around the singularity. In the case of pole pinching, any detour is impossible to remove the singularity because the contour has to pass in between the two poles.

This singularity indicates that there are localized fluctuations to be accounted for. In the two-point correlation evolution equation, this singularity is properly accounted for by the vanishing relative diffusion at a zero separation.

Furthermore, the validity of the approximation that

$$\text{Re} \left[\frac{i}{\omega - kV_E} \right] = \pi \delta(\omega - kV_E)$$

also depend on the existence of fluctuation spectrum with a broad phase-velocity range. For example, in mixing-layer turbulence, most of the fluctuation energy is contained in large-scale fluctuations, which have zero phase velocity, or a narrow range (for asymmetric mixing layers) thereof. The vorticity clump theory breaks down in this type of flow. For wake turbulence, the normal mode has a wide range of phase velocity which persists in a later stage of fully developed turbulence. Hence, the vorticity clump theory is applicable.

Besides these conditions for the existence of vorticity clumps, the driving source must also be positive everywhere in the flow field. At small fluctuation amplitude, the source is indeed positive definite. Also the nonlinear modification, resulting from the triplet correlation, does not alter the global dynamics of the flow. This finding is because the nonlinear term has a form of a total derivative in x, and vanishes upon an integration over the system size when it is performed.

When fluctuations are driven, grow and become sufficiently large (turbulent velocity fluctuations

larger than those of mixing-length level) so that the
total source is not everywhere positive definite, the
small-scale fluctuations will be damped. In this case,
it is speculated that the fluctuation energy is trans-
ferred to large-scale fluctuations. This may be related
to the reappearance of large-scale fluctuations observed
in experiments.

For two-dimensional systems which do not have
mean flow inflection points, we have shown that there is
no linear (unstable) eigensolution. However the linearized
form of a nonlinear equation is only valid for a finite
time (depending on the noise level). It is interesting
to ask whether this type of flow is nonlinearly unstable.
The method for investigation of this type of instability
is similar to that of one-dimensional plasmas. However,
the present case is technically more complex because not
only does one have to solve an integral equation, but
also simultaneously one must solve for the propagator,
$G_{k,\omega}$, to evaluate the coefficients of the integral equa-
tion.

Extensive study in this direction is too in-
volved to be included in this dissertation. However, it
is of great interest, and will be a worthwhile project
for future investigation.

C H A P T E R   V

EFFECTS OF A RADIAL ELECTRIC FIELD

ON TOKAMAK EDGE TURBULENCE

5.1 Introduction

Recent measurements of turbulence in the edge
region of tokamaks indicate the existence of a time-
independent radial electric field.[47,48] This field is
large (50 volt/cm), has a very steep gradient ($L_E \approx 1$ cm)
and reverses sign near the limiter. Its scale length is
$L_E/\rho_i \approx 10$. Fluctuation measurements in the region of
maximum gradient show an isotropic spectrum with widths
in frequency and wavenumber which exceed by a factor of
two the anisotropic spectra measured away from the maxi-
mum (Fig. 5-1).[47] These measurements are corroborated
by flow visualizations, assembled from probe array data
which suggest the presence of vortex-like motion in this
region.

The radial variation of the electric field im-
plies rotation in the ion diamagnetic direction outside
the limiter and rotation in the electron direction
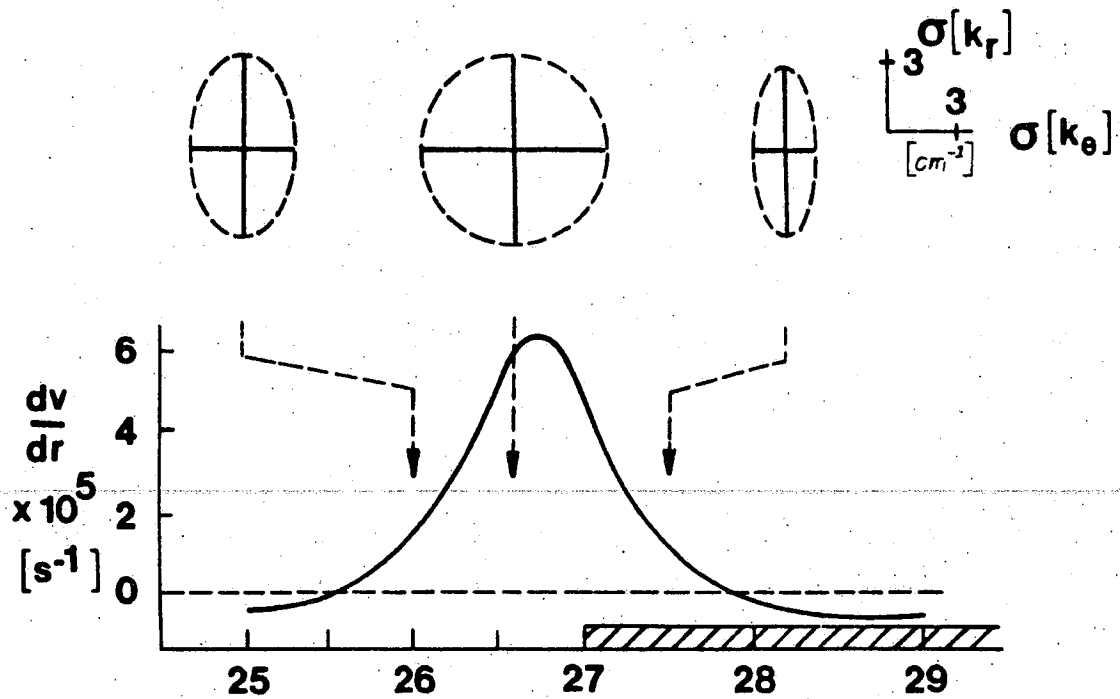further in (radially). It is thus possible, on the

Figure 5-1. Radial profile of vorticity and fluctuation
spectra measured by Ritz, et al., (C. P.
Ritz, et al., Phys. Fluids 27, 2956) (1984)).
The standard deviations of the measured
spectra, $\sigma(k_r)$ and $\sigma(k_\theta)$, indicate the change
of turbulence characteristics, from an iso-
tropic spectrum at high velocity shear to
anisotropic spectra at low velocity shear
(Figure used with permission).

basis of an electric field dependent Doppler shift in frequency, to reconcile theories which predict phase velocities in the electron direction,[50,51] with measurements made at the extreme edge which indicate phase velocities in the ion direction.[52,53] However it also becomes necessary to determine the effects of a radial electric field on turbulence in the edge region. The fact that broadened spectra are observed both away from and near a strong vorticity maximum and have a character which changes noticeably near the maximum suggest that both "standard" density or temperature-gradient-driven turbulence and electric-field-gradient-driven turbulence play a role in determining edge turbulence spectra. Furthermore, nonambipolar transport processes have recently been proposed [54,55] as relevant to understanding the separatrix region of diverted H-mode discharges. The shear flow stability properties of plasmas, which support the electric fields that result, is therefore also important for understanding H-mode profiles and confinement.

In this study we explore the effects of a radial electric field on edge turbulence models. A sheared radial electric field is included in a two-point theory

of density-gradient-driven turbulence developed pre-
viously. It is found that the correlation decay rate
due to (velocity) shear induced relative drift is greater
than that due to the ambient turbulence. The extent to
which this enhanced decay affects the scale size is cal-
culated quantitatively using the theory of two-point cor-
relation.[51] On the basis of these results, we conclude
that the electric field shear alone is strong enough to
determine the radial density correlation length at the
maximum (velocity) shear region. Thus, the strength of
the shear suggests that its role as a free energy source
for instability should also be examined.

For turbulence driven by the gradient of the
radial electric field, we study the shear flow (Rayleigh)
instability and consider additional (stabilizing) effect
of magnetic shear. The linear growth rate and eigen-
function structure are obtained using the reduced MHD
equations in the electrostatic limit, and an approxi-
mate radial electric field profile. In the limit of
vanishing magnetic shear, this instability reduces to the
familiar Rayleigh instability, where flow shear relaxes
by an interchange of vortex tubes around a vorticity maxi-
mum, in which case restoring forces vanish. Moreover,

as the linear mode structure is broad and has approximately the same length scales in the radial and poloidal directions, an isotropic spectrum is expected.

Two possible nonlinear saturation mechanisms are proposed, and the saturation level corresponding to each is estimated. The strength of the magnetic shear damping relative to that of the destabilizing source determines which mechanism is operative. When magnetic shear is weak, saturation of unstable modes relies on an enstrophy cascade which transfers mode energy from unstable modes to high k stable modes. When magnetic shear is moderate or strong, fewer modes are destabilized. For those remaining unstable, saturation results from nonlinear mode broadening (Fig. 5-6) which effectively transfers energy from the source (vorticity gradient) to the sink. For parameters consistent with the TEXT tokamak, magnetic shear damping is moderately strong in the edge, and the latter mechanism is expected to determine saturation.

For a model shear-flow profile, $V_E(x) = V_0 \tan h(x/L_E)$, the saturation level of the root-mean-square potential fluctuations is

$$\frac{e\Phi_{rms}}{T_e} \sim \frac{1}{4\sqrt{3}(k_0 L_E)} \left[\frac{V_0}{\rho_s C_s k_{MIN}}\right] ,$$

in the case where saturation arises from a cascade process. This result is easily recognized as the familiar mixing-length fluctuation level. At such levels, the coupling to the higher k stable modes is equal to input from the gradient source. For saturation due to nonlinear broadening of mode structure, the rms potential fluctuation level at saturation is

$$\frac{e\Phi_{rms}}{T_e} \sim \left[\frac{1}{k_0 L_E R^2}\right]^{15/16} \left[\frac{V_0 L_E}{C_s \rho_s}\right]$$

where k_0 and k_{MIN} are the average and minimum wavenumbers, respectively. C_s is sound speed, ρ_s is the ion gyroradius with electron temperature, and

$$R^2 = \frac{4\pi V_A^2}{C^2} \cdot \frac{L_E^3}{\eta V_0 L_s^2}$$

characterizing the strength of magnetic shear, V_A is Alfven speed, η is the resistivity and L_s is the magnetic shear length. At such levels, convection to dissipation at finite $\underline{k} \cdot \underline{B}_0$ equals input from the gradient source. We find that when $R = 2.6(k_{MIN}L_E)^{1/2}$, transition from one regime to the other occurs.

We also estimate the density and magnetic field fluctuation levels. In an incompressible fluid, density fluctuations arise from the convection of fluid elements along the density gradient by the fluctuating velocity field; magnetic field fluctuations result from the coupling of the electric and magnetic fields via Ohm's law. When the cascade process is responsible for saturation, the saturated density and magnetic field fluctuations are

$$\frac{\delta n_{rms}}{n_0} \sim \frac{L_E}{L_n}$$

$$\frac{\tilde{B}_{rms}}{B_0} \sim \frac{\pi}{\sqrt{3}} \cdot \left(\frac{L_E V_0}{\eta L_s k_{MIN} c^2} \right)$$

When the mechanism of nonlinear mode-structures broadening dominates saturation, they are

$$\frac{\delta n_{rms}}{n_0} \sim \frac{L_E}{L_n} \left[\frac{1}{k_0 L_E R^2} \right]^{15/16}$$

$$\frac{\tilde{B}_{rms}}{B_0} \sim \left[\frac{V_0^2 L_S}{V_A^2 L_E} \right] \left[\frac{1}{k_0 L_E R^2} \right]^{9/16}$$

where L_n is the density scale length.

For the parameters in the tokamak edge of TEXT, $T_e \cong 20 eV$, $n_0 \sim 2 \times 10^{12} cm^{-3}$, $Z_{eff} \cong 3 \sim 4$ $B_0 \cong 0.7 \times 10^4$ Gauss, $V_0 \cong 3 \times 10^5$ cm/sec, $L_E \cong 0.5$ cm, $L_n \cong 1.5$ cm, $L_s \cong 200 \sim 400$ cm, we estimate $R \cong 2$ for $L_s \cong 300$ cm, and the root-mean-square fluctuation levels at saturations are

$$\frac{e\Phi_{rms}}{T_e} \sim 0.42, \quad \frac{\delta n_{rms}}{n_0} \sim 0.35, \quad \text{and}$$

$$\frac{B_{rms}}{B_0} \sim 5 \times 10^{-5}.$$

The values for $e\Phi/T_e$ and $\delta n/n_0$ are consistent with those measured.

The remainder of this chapter is organized as follows: In Section 5.2 we extend the previous study of density-gradient driven turbulence to incorporate the inhomogeneous radial electric field and examine the consequences. In Section 5.3, we make a preliminary linear analysis of the fluctuations driven by the radial electric field gradient. This analysis reveals a key point for nonlinear saturation, discussed later. In Section 5.4, we outline the renormalization scheme, and propose two competing saturation mechanisms characterized by the

strength of magnetic shear. Subsequently, various
relevant quantities are estimated in Section 5.5 and
compared with those obtained from experiments. Finally,
conclusions are discussed in Section 5.6.

5.2 Effect of an Electric Field on the Density Fluctuation Correlation Function

a. We first study density gradient-driven turbu-
lence and consider the fluid equations for dissipative
drift waves in a torus. Since the electron temperature
is sufficiently low at the tokamak edge, the electron-
ion collision frequency ν_{ei} exceeds the inverse transit
time (time for electrons to travel around the toroidal
device), i.e., $\nu_{ei} > u_{Te}/Rq$, where R is the major radius
and q is the safety factor. Electrons have short mean
free path for thermalization, thus temperature fluctua-
tions can be ignored. Furthermore, the frequency of
fluctuation ω, Doppler-shifted by the radial electric
field-induced poloidal flow, is smaller than ν_{ei}, hence
electron inertia can be neglected. Thus, the electron
fluid equations are:

$$\frac{\partial}{\partial t} \delta n + \nabla \cdot [(n_0 + \delta n) \underset{\sim}{v}_{\perp e}] + \nabla_{\parallel} v_{\parallel e} = 0 \qquad (5:2-1)$$

$$\nu_{ei} v_{\parallel e} = v_{Te}^2 \nabla_{\parallel}\left[\frac{e\Phi}{T_e} - \delta n\right] , \qquad\qquad (5:2\text{-}2)$$

where "$\parallel$" and "$\perp$" refer to the direction of the local magnetic field line $\hat{b}$, and $\underset{\sim}{v}_{\perp e}$ is the $E \times B$ drift, i.e., $C/B_o(\underset{\sim}{E}_o \times \nabla\Phi) \times \hat{b}$. These two equations describe the electron density and parallel dynamics, respectively.

We substitute $\underset{\sim}{v}_{\perp e}$ and Eq. (5:2-2) into Eq. (4:5-21). Noting that

$$\nabla \cdot [(n_o + \delta n)\underset{\sim}{v}_{\perp e}] = \frac{CT_e}{eB_o}\left(\frac{d}{dr} \ell n \ n_o\right) \cdot \frac{1}{r} \frac{d}{d\theta}\left(\frac{e\Phi}{T_e}\right)$$

$$+ \frac{C}{B_o} (\underset{\sim}{E}_o - \nabla\Phi) \times \hat{b} \cdot \nabla\delta n,$$

We can now express the nonadiabatic electron density evolution equation as:

$$\left(\frac{\partial}{\partial t} + \frac{v_{Te}^2}{\nu_{ei}} \nabla_{\parallel}^2 + \frac{C}{B_o}(\underset{\sim}{E}_o - \nabla\Phi) \times \hat{b} \cdot \nabla\right)H$$

$$= \frac{-e}{T_e}\left[\frac{\partial\Phi}{\partial t} + (V_E + v_D) \cdot \frac{1}{r} \frac{\partial}{\partial\theta} \Phi\right] \qquad\qquad (5:2\text{-}3)$$

where $H = \delta n - e\Phi/T_e$, the nonadiabatic electron density,

$$v_D = \frac{CT_e}{eB} \frac{d}{dr} \ell n \ n_o ,$$

the electron diamagnetic drift, and $V_E = C/B_o E_o$, electric field-induced poloidal flow.

We consider toroidal geometry and apply the ballooning transformation,

$$\begin{bmatrix} \Phi \\ \\ H \end{bmatrix} = \sum_n \exp(in\phi)\sum_m \exp(-im\theta)\int d\eta \exp[i[m - mq(r)]\eta]$$

$$\cdot \begin{bmatrix} \Phi_n(\eta) \\ \\ H_n(\eta) \end{bmatrix} \qquad\qquad (5:2-4)$$

where ϕ is the toroidal angle, θ is the poloidal angle, and η is the coordinate along a field line. Using this and a temporal-Fourier transformation, Eq. (5:2-3) is obtained explicitly,

$$-i(\omega - \omega_E)H_{n,\omega} - \frac{v_{Te}^2}{\nu_{ei}(Rq)^2} \frac{\partial^2}{\partial\eta^2} H_{n,\omega} + N_{n,\omega}$$

$$= \frac{ie}{T_e} (\omega - \omega_E - \omega_{*e})\Phi_{n,\omega} \qquad (5:2-5)$$

where $\omega_E = nqV_E/r$, $\omega_{*e} = nqv_D/r$, diamagnetic drift frequency, and $N_{m,\omega}$ is the E $\times$ B nonlinearity explicitly given by

$$N_n^\omega = \sum_{n'} \sum_m \frac{c}{B_o} k_\theta k'_\theta (2\pi m \hat{s}) \exp[2\pi i(n'$$

$$- q(r)m)] \hat{\phi}_{-n'}^{-\omega'} (\eta + 2\pi m) H_{n+n'}^{\omega+\omega'}(\eta) \qquad (5:2-6)$$

Eq. (5:2-5) contains a convection due to the radial electric field-induced poloidal flow, parallel viscous diffusion, the E × B mixing and a density gradient source term.

It is important to note that Eq. (5:2-5) is applicable to the regime where

$$k_\parallel^2 v_{Te}^2 / v_{ei}\omega \geq 1. \qquad (5:2-7)$$

The density response is significant, and electrons behave quasi-adiabatically. This condition is generally true for edge plasma parameters typical of TEXT, Pretext and the Caltech tokamak, where $\omega_{*e} \approx 10^5$ rad/sec $\ll \omega_E$ 10^6 rad/sec thus $\omega \approx \omega_E$. However, inequality (5:2-7) may be invalid for fluid-like modes located near the region of the maximum poloidal-flow shear. This will be discussed in the next section. In that case, reduced MHD is the plasma model used, and density evolution, Eq. (5:2-1), is neglected.

For the values of ω_{*e} and ω_E given in the above, ω_E exceeds ω_{*e} by an order of magnitude except in the close vicinity of the electric field null point. This implies that measured phase velocities of edge fluctuations are primarily determined by the electric field, with a shift due to ω_{*e}. Hence, the phase velocities can be in the direction opposite to the electron drift.

Similar linear properties of Eq. (5:2-5) are discussed in references 49 and 57, and we will not repeat here. In the following discussion, we will study the effects of the electric field-induced flow on the density correlation function.

b.   To determine the effect of the radial electric field on density correlations in the turbulent flow, we study the two-point density correlation $<H(1)H(2)>$. The equation for two-point density correlation is readily derived from the one-point equation. Standard renormalization procedures may be applied to the nonlinearity to obtain an equation with diffusion in the relative variables,

$$(y_-, n_-, r_1) = 1/2 \; (y_1 - y_2, \eta_1 - \eta_2, r_1 - r_2).$$

$$\left[\frac{\partial}{\partial t} - \frac{c}{B_0} r \frac{E_0}{L_E} \frac{\partial}{\partial y_-} - \frac{v_{Te}^2}{(Rq)^2 \nu_{ei}} \frac{\partial^2}{\partial \eta_-^2} \right.$$

$$\left. - D_-(y_-,\eta_-,r_-) \cdot \frac{\partial^2}{\partial y_-^2} \right] \langle H(1)H(2) \rangle$$

$$= S = \sum_{\substack{k' \\ \omega'}} \frac{i|e|}{T_e} (e^{ik'y_-})(\omega' - \omega_E'$$

$$- \omega_{*e}') \langle H(1)\Phi(2) \rangle_{k',\omega'} \qquad (5:2-8)$$

where $D_-(y_-,\eta_-,r_-)$ is the renormalized turbulent diffusion coefficient for the predominant (y_-) diffusion, and $k = nq/r$. According to Eq. (5:2-8), the two-point density correlation is governed by the competition of the driving source on the right-hand side with the decay processes of relative diffusion and drift on the left-hand side. The driving source is fed by the density gradient and is homogeneous in the relative coordinate. It is the inhomogeneities associated with the decay which determine the spatial dependence of the correlation function. The decay processes are (1) the relative drift between fluid elements at different points on the drift velocity profile $V_E(r) = c/B_0$, $E_r(r) \approx cE_0/B_0 \, r/L_E$, (2) the relative parallel diffusion due to collisional viscosity and (3) the inhomogeneous relative diffusion due to the turbulent

E × B mixing. Note that while the E × B diffusion vanishes as the relative separation goes to zero (a consequence of correlation in the scattering field at short separation), the parallel collisional diffusion does not. Because of this property the density correlation peaks at small scale, but is finite at zero relative separation.

For small relative separation the turbulent diffusion is given approximately as

$$D_- = D(k_0^2 y_-^2 + \eta_-^2/\Delta\eta^2 + k_0^2 \hat{s}^2 r_-^2), \qquad (5:2-)$$

where

$$\phi(r) = \sum_m e^{imy} \sum_n e^{i(n-mq)\eta} \int d\eta\, \phi(\eta),$$

and

$$D = \frac{C^2}{B_0^2} \sum_{k'} k'^2 \hat{s}^2 \mathrm{Re} \left[\omega' - \omega_E' - \frac{v_{Te}^2 \frac{\partial^2}{\partial\eta^2}}{im_e \nu_{ei}} \right]^{-1} \sum_m (2\pi m)^2 <\phi(\eta + 2\pi m)^2>_k .$$

The quantities k_0^{-2}, $(Rq\Delta\eta)^2$ and $(k_0 \hat{s})^{-2}$ are the poloidal

($k = nq/r$), parallel and radial scales on which the relative diffusion begins to decrease from its asymptotic value D. The poloidal scale corresponds to a typical wavenumber in the spectrum. The parallel scale is determined by the toroidicity-induced eigenmode structure. The relation $\Delta r = (k\hat{s})^{-1}$ is a consequence of ballooning representation.

The spatial dependence of the steady state solution of Eq. (5:2-8) is obtained by the inversion of the operator on the left-hand side of Eq. (5:2-8) which yields $\tau_{cl}(y_-,\eta_-,r_-)$, the two-point correlation time. The correlation time is calculated by taking moments of the L.H.S. of Eq. (5:2-8), which yields differential equations governing the evolution of neighboring fluid element positions. For the operator in Eq. (5:2-8) the correlation time is

$$\tau_{cl}(y_-,\eta_-,r_-) = (k_0^2 D)^{-1} \ln\left[\left[k_0^2 (y_-^2 + \eta_-^2/\Delta\eta^2 k_0^2 \right. \right.$$
$$\left. \left. + \frac{R_e^{-1}}{k_0^2} + \left[\hat{s}^2 + \frac{1}{2} \frac{c^2 E_0^2}{B_0^2 L_E^2} \frac{1}{k_0^4 D^2} \right] r_-^2 \right]^{-1} \right] \qquad (5:2-10)$$

where $R_e = D k_0^2 (Rq)^2 \Delta\eta^2 \nu_{ei}/v_{Te}^2$ is the Reynolds number and parameterizes the relative strengths of the linear (parallel collisional viscosity) and nonlinear (E × B diffusion)

processes. For Reynolds numbers exceeding order unity,
Eq. (5:2-10) exhibits logarithmic peaking inside the
correlation scale. The correlation scales are determined
by the coefficients of the relative coordinates. The
scale of radial correlation is thus

$$\Delta r = \left[\hat{s}^2 + \frac{1}{2} \frac{c^2 E_0^2}{B_0^2 L_E^2} \frac{1}{k_0^4 D^2} \right]^{1/2} k_0^{-1}$$

$$= \left[\hat{s}^2 + \left(\frac{\tau_c}{\tau_E} \right)^{2} \right]^{1/2} k_0^{-1} , \qquad (5:2-11)$$

where $\tau_c = 1/k_0^2 D$, the correlation time, and $\tau_E = \sqrt{2} B_0 L_E / c E_0$, the dynamical time scale of the poloidal flow.
For parameters consistent with the edge plasmas already
referred to,[47,52,53] τ_E is comparable to τ_c and the cor-
relation scale determined from Eq. (5:2-11) is of the
order of 1 cm. For $k_0^{-1} \sim 10 \rho_s$ this is qualitative agree-
ment with the radial correlation scale measured in the
TEXT and Caltech tokamak.[47] However, at the region of
maximum flow shear,

$$\tau_c / \tau_E > \hat{s} \approx 1 .$$

This observation that τ_E is the shortest dynamically

relevant time-scale suggests that effects of the electric field gradient on edge turbulence may be more involved than a simple Doppler shift. Thus, in the next section, we shall thus examine the electric field gradient as a driving mechanism for turbulence.

5.3 Radial-Electric-Field-Driven Turbulence: Basic Analysis

We now examine electric-field driven fluctuations. In a magnetized plasma, the radial electric field, $-\nabla_r \Phi(r)$, causes a poloidal drift $V_E = (C/B_0^2)\underline{B}_0 \times \nabla_r \Phi$. Since this radial electric field has spatial dependence, the resulting plasma flow is a source of free energy and can potentially drive instabilities. In the case of strong toroidal magnetic fields, plasma motion is quasi-two-dimensional, the electric potential Φ can be looked upon as the flow stream function, and $\nabla_\perp^2 \Phi$ as the vorticity. Suitable equations for description of the vorticity evolution in the tokamak edge are the reduced MHD equations,[22]

$$\rho \frac{d}{dt} \nabla_\perp^2 \phi = B_0 \nabla_\parallel J_\parallel + \nabla_\perp A_\parallel \times \hat{b} \cdot \nabla_\perp J_\parallel \qquad (5:3\text{-}1)$$

$$\frac{d}{dt} A_\parallel = \frac{B_0}{C^2} \nabla_\parallel \phi + \eta J_\parallel$$

where $\phi \equiv \Phi c^2/B_0$, $\hat{b} \equiv \underline{B}_0^{(r)}/B_0^{(r)}$, and $A_\parallel$ and $J_\parallel$ are the vector potential and current along the field line, respectively.

Here, the dynamical time and length scales are approximately determined by the shear flow, i.e., $|d/dt| \sim V_0/L_E$, and $|\nabla_\perp| \sim 1/L_E$. When comparing the electromagnetic piece, $dA_\parallel/dt$, with the current piece, $\eta J_\parallel (= \eta c^2/4\pi \ \nabla_\perp^2 A_\parallel)$, of the parallel Ohm's law, Eq. (5:3-2), we find $\eta c^2/4\pi V_0 L_E \gg 1$, and the electromagnetic piece, $dA_\parallel/dt$, can be dropped. Hence, using the electrostatic limit of Ohm's law, reduced MHD yields the vorticity equation,

$$\rho \ \frac{d}{dt} \ \nabla_\perp^2 \phi = \frac{B_0^2}{\eta c^2} \ \nabla_\parallel^2 \phi \ .$$ (5:3-3)

In the limit of vanishing magnetic shear $(\nabla_\parallel = 0)$, Eq. (5:3-3) gives

$$\frac{d}{dt} \ \nabla_\perp^2 \phi = 0,$$

which is a statement of conservation of vorticity. It is well-established that a necessary condition for instability in this equation is the existence of a vorticity maximum at the point of inflection of the equilibrium

flow $V_E(r)$.[23,41] In view of this criterion, the profiles of Ritz et al. clearly point to the possibility of shear flow driven turbulence in the tokamak edge.

Shear flow instability is associated with the interchange of vortex tubes at the vorticity maximum, where the restoring force vanishes. Any localized perturbed motion around this point cannot be stopped, thus instability arises.

When magnetic shear is considered, free energy provided by the vorticity gradient can be dissipated by the resistive dissipation. Thus instability can be effectively suppressed unless the vorticity maximum coincides with the location of the magnetic resonance surface. There, the dissipation associated with $\nabla_\parallel J_\parallel$ is minimized, and instability can be locally excited for the longest wavelength modes. To simplify the analysis, we will use slab geometry, with x and y representing the radial and poloidal directions, respectively. We then Fourier transform Eq. (5:3-3) with respect to y and the parallel variable and obtain

$$\left[\frac{\partial}{\partial t} + ikV_E(x)\right]\nabla_\perp^2 \phi_k - ik \frac{d^2 V_E}{dx^2} \phi_k - k^2 R^2 (x - x_0)^2 \phi_k$$

$$= i \sum_{k'} \left[k' \nabla_\perp^2 \phi_{k'} \frac{d\phi_{k''}}{dx} - k' \phi_{k'} \frac{d}{dx} \nabla_\perp^2 \phi_{k''} \right], \quad (5:3-4)$$

where $k \equiv k_y$, velocity, length and time variables are nor-
malized to the characteristic shear flow velocity V_0,
the width of shear flow L_E and their ratio L_E/V_0, re-
spectively, and ϕ is normalized to $L_E V_0$. In addition, we
have used $k_\parallel^2 - k^2(x - x_0)^2/L_s^2$ to account for the magnetic
shear, hence $R^2 = 4\pi V_A^2 L_E^2/\eta V_0 C^2 L_s^2$, where V_A is the Alfven
speed. Note that the magnitude of the sink term rela-
tive to that of the source term is kR^2. This defines a
length $L_E/(kR^2)^{1/2}$ for the dissipation-free region where
the source is much stronger than the sink.

Linearly unstable modes can be locally excited
within the dissipation-free region if the energy source
(with a width of the shear layer L_E) decouple from the
linear dissipation. Stability is crucially dependent on
the degree of overlap between the energy source and dis-
sipation region. Long wavelength modes have a larger
dissipation-free region, and thus are easier to excite.
In the limit of large R, the unstable wavenumber k must
be sufficiently small in order for the energy source to
overcome dissipation. Consequently, kR^2 for the unstable
modes will approach a constant of order unity, as R be-
comes much larger than unity. Further increase in R can
force the wavenumber k to be smaller than the system
allows, k_{MIN}, and yields stability.

In order to discuss stability and describe turbulence properties, it is necessary to specify profiles for $V_E(x)$. $V_E(x)$ is measured in TEXT and appears to be essentially linear in the region of interest. Outside the linear region, the velocity profile is flat. For simplicity, we model this observed profile with a hyperbolic tangent,

$$V_E(x) = V_0 \tan h\left(\frac{x}{L_E}\right).$$

We solve the linearized eigenvalue problem of Eq. (5:3-6) numerically to determine the frequency. The eigenfunctions, which are purely growing and excited around the central region, are shown in Fig. 5-2 it is noted that the length scale of a linear mode in the dissipation-free region is different from that of the dissipation region. The former can be estimated by comparing the linear convective term with the gradient source and is approximately,

$$\Delta_i^L \approx L_E ; \tag{5:3-5}$$

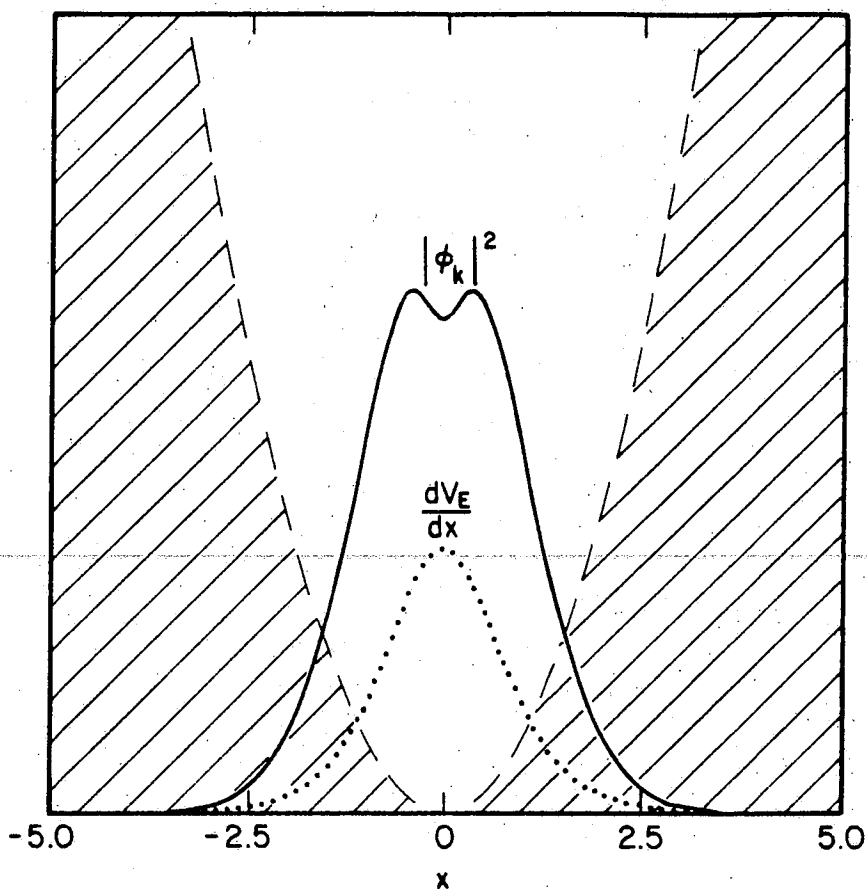the latter by balancing the inertia term with the sink and is approximately,

Figure 5-2. Linearly unstable eigenfunction, and loca-
tions of the (shear flow) driving source and
(resistive) sink. The driving source is
centered at the minimum of the magnetic
shear of R = 2, thus avoids dissipation.
The localized eigenvunction ϕ_k of k = 0.0i
is excited. The source vorticity is indi-
cated by the dotted line, the sink is in the
shaded region; and the eigenfunction $|\phi_k|^2$
is indicated by the solid line.

$$\Delta_0^L \approx \frac{L_E}{(2kR^2)^{1/4}} \tag{5:3-6}$$

The relevance of these two length scales will be discussed in the next section.

In Fig. 5-3, we show the growth rate γ_k versus the wavenumber k for various values of R. In the above, we have chosen $x_0 = 0$, i.e., the vorticity maximum is centered at the $\underline{k} \cdot \underline{B}_0$ surface. As R increasing, unstable modes are confined to those of increasingly longer wavelengths. The maximum growth rates decrease. When the vorticity maximum is not centered at the $\underline{k} \cdot \underline{B}_0 = 0$ surface, $x_0 \neq 0$, the modes become more stable, as shown in Fig. 5-4 because greater overlap occurs between the energy source and the dissipation region (Fig. 5-5). This damping is a sort of dissipative line-tying. In the more unstable $x_0 = 0$ case, we find that kR^2 for the most unstable modes asymptotically approaches 0.5 from below, as R becomes very large

For TEXT parameters, R is of order unity, hence magnetic shear, though significant, is not sufficient to suppress the hydrodynamic shear-flow instability. To study turbulence caused by this instability, a nonlinear analysis is then necessary.
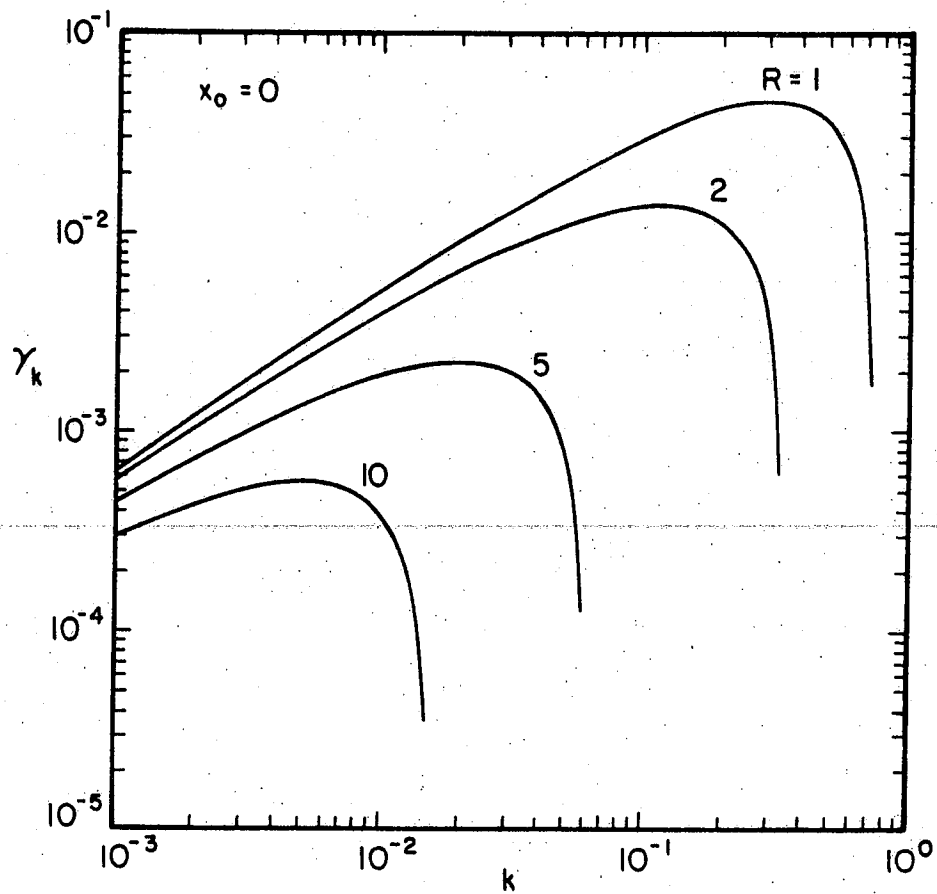
Figure 5-3. Growth rate γ_k vs. wavenumber k, with $x_0 = 0$, i.e., the driving source centered at the minimum of magnetic shear. Modes of intermediate values of k have the greatest growth rates. As magnetic shear R increases, γ_k is reduced.
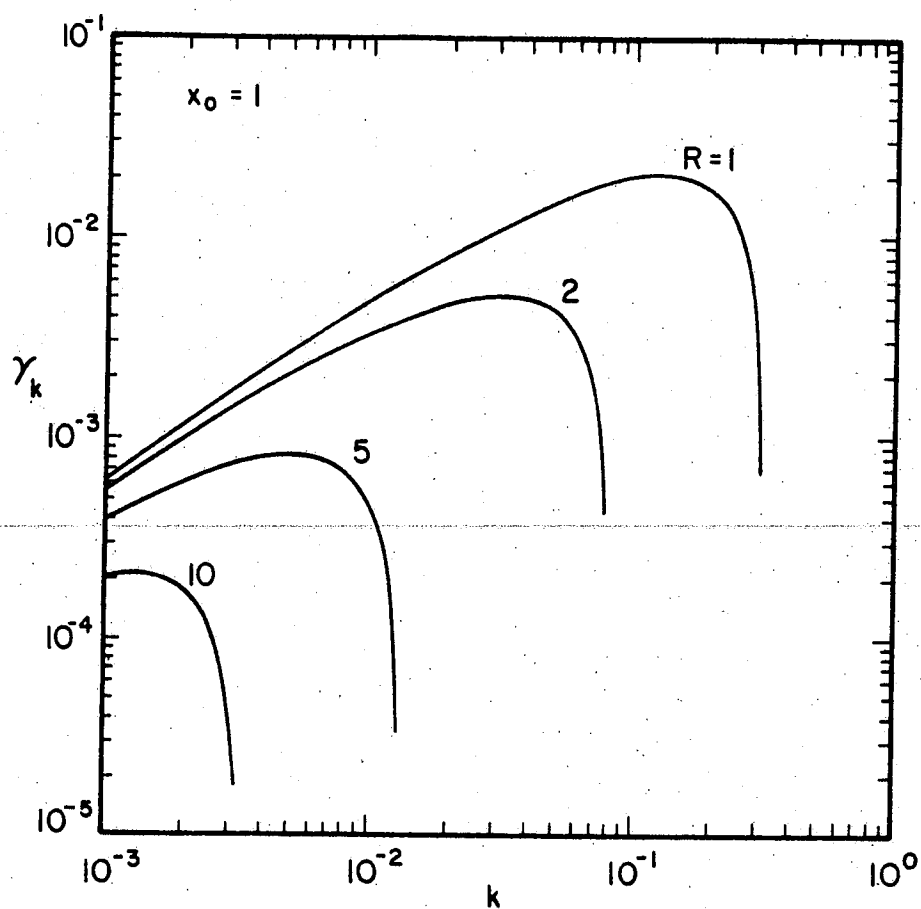
Figure 5-4.   Growth rate γ_k vs. wavenumber k, with
$x_0 = 1$, i.e., the driving source having a
large portion overlapped with the sink.
When compared with Figure 3, the growth rates
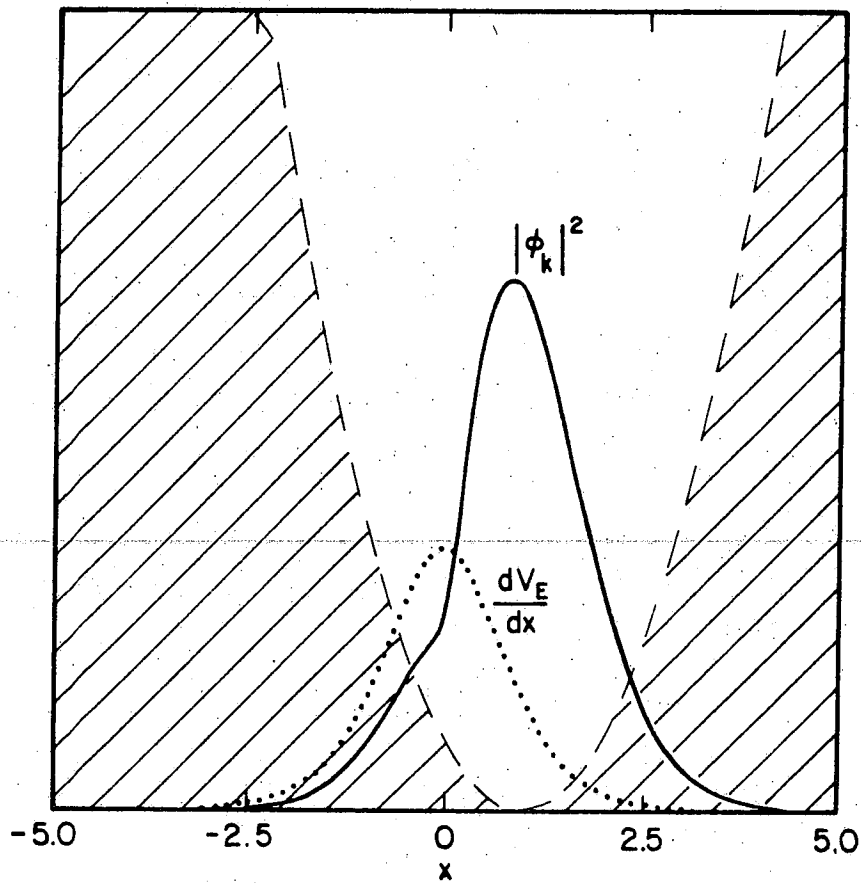are significantly reduced.

Figure 5-5. Linearly stable eigenfunction, and locations of the (shear flow) driving source and (resistive) sink. The driving source is not centered at the minimum of the magnetic shear of R = 2, hence leads to a large region of overlap. The eigenfunction ϕ_k of k = 0.08 is therefore stabilized. The source vorticity is indicated by the dotted line, the sink is in the shaded region; and the eigenfunction $|\phi_k|^2$ is indicated by the solid line.

5.4 Nonlinear Analysis and Saturation Mechanisms

In this section, we investigate possible saturation mechanisms. In the present case, two processes compete to drain wave energy from the unstable modes. Both rely on parallel dissipation and turbulent diffusion; however, the role of turbulent diffusion in each of these two processes is distinct. In the first process, turbulent diffusion nonlinearly couples different modes, permitting energy flow in k space which reaches the high-k energy sink. In the second process, turbulent diffusion broadens the mode structures, allowing energy to reach regions in x space with strong dissipation (Fig. 5-6).

To renormalize Eq. (5:3-4), a standard iterative method is used to approximate its convective nonlinearity. This has been shown in the previous chapter and in Appendix E. In the region where $|\phi_{k,\omega}|^2$ is large, we have $|d^2/dx^2| \gg k^2$. Hence we retain only

$$\frac{d}{dx} \, D_x \, \frac{d}{dx} \, \nabla_\perp^2 \phi_{k,\omega}$$

to represent the locally renormalized nonlinearity. The nonlinear evolution equation for vorticity can thus be approximated by

$$\left[\frac{\partial}{\partial t} + ikV_E - D\frac{d^2}{dx^2}\right]\nabla_\perp^2 \phi_k = \left[ik\frac{d^2V_E}{dx^2} + k^2R^2X^2\right]\phi_k \ ,$$

$$(5:4\text{-}1)$$

and that of the vorticity spectrum by

$$\int dx\left[\frac{\partial}{\partial t} \ |\nabla_\perp^2 \phi_k|^2 + 2D \ |\frac{d}{dx}\nabla_\perp^2 \phi_k|^2\right.$$

$$\left. - 2(\sum_{k'} \ |\frac{d}{dx}\nabla_\perp^2 \phi_{k'}|^2)D_k\right]$$

$$= 2\int dx(-k\frac{d^2V_E}{dx^2} \ \mathrm{Im}<\phi_k\nabla_\perp^2 \phi_k^*>$$

$$+ k^2R^2X^2\mathrm{Re}<\phi_k\nabla_\perp^2 \phi_k^*>) \qquad\qquad (5:4\text{-}2)$$

where the third term on the left of Eq. (5:4-2) is the nonlinear incoherent source. Together with the diffusion term, these two nonlinear terms are responsible for enstrophy cascade. Here, D is given explicitly by

$$D = \sum_k D_k \qquad\qquad (5:4\text{-}3)$$

and

$$D_k \cong \frac{k^2 |\phi_k|^2}{\omega + ikV_E(x) + D\frac{d^2}{dx^2}} \qquad\qquad (5:4\text{-}4)$$

In the remainder of this section, we separately present the details of the two nonlinear saturation processes previously mentioned. As the parameter R effectively determines which of the processes dominates, we consider the limits $R \ll 1$ and $R \cong O(1)$, respectively.

a. $\underline{R \ll 1}$

In this regime, the linear sink is very weak for a broad range of low-k modes. The dissipation region is spatially remote from the region where unstable modes are located, because the width of the dissipation-free region scales as $L_E (kR^2)^{-1/2}$. Thus, the linearly unstable modes do not sense the magnetic shear. Only those modes with sufficiently large wavenumbers experience appreciable linear dissipation. As a result, the only significant way available for the removal of wave energy from unstable modes is by a nonlinear coupling between low-k and high-k modes. This coupling allows an energy flow in k space toward the high-k dissipation range exactly as in the conventional picture of cascading. In the renormalized theory this nonlinear coupling is represented by turbulent diffusion which removes energy from the low-k linearly unstable modes.

Ignoring magnetic shear, we have an equation for low-k linearly unstable modes,

$$\left[-i\omega + ikV_E - D\frac{d^2}{dx^2} \right] \nabla_\perp^2 \phi_{k,\omega} = ik \frac{d^2 V_E}{dx^2} \phi_{k,\omega} \quad . \quad (5:4-5)$$

This is the Orr-Sommerfeld equation, and the stability boundary has been tabulated. For the hyperbolic-tangent flow profile, the longest wavelength modes are always unstable in spite of a large value of D. Hence the complete stabilization of all modes must rely on the existence of a lower bound of k, which may be imposed by finite system size or by other effects not contained in this model. For small kL_E, the Reynolds number, $R_e = V_0 L_E/D$, satisfies

$$R_e \cong 4\sqrt{3} \ kL_E \qquad\qquad (5:4-6)$$

at the stability boundary. Thus the diffusion coefficient is approximately

$$D \cong \frac{V_0 L_E}{4\sqrt{3} \ k_{MIN} L_E} \qquad\qquad (5:4-7)$$

at saturation, where k_{MIN} is the lower bound of the range of wavenumbers.

B. $R \sim 0(1)$

In this regime, magnetic shear very effec-
tively governs the stability of low-k modes. The stabil-
ity is determined by the competition of vortex interchange
and magnetic shear. Spatially, the dissipation region
lies in close proximity to the free energy source (Fig.
5-2), thus stability is crucially dependent on the de-
gree to which these two regions overlap. Nonlinearly,
it is more effective for the linear sink to couple to the
source, through real space by spatial broadening, than
through k space as in the previous case. Here, turbu-
lent diffusion creates a mode structure which extends
into the dissipative region (Fig. 5-6), through which
energy flows to parallel resistive sink. Thus, turbu-
lent diffusion nonlinearly couples source and sink.

Let Δ_i and Δ_0 be the characteristic lengths of
the nonlinearly broadened mode in the inner (source) and
outer (sink) regions, respectively. To determine them at
saturation, one can use Eq. (5:4-1) and balance the dif-
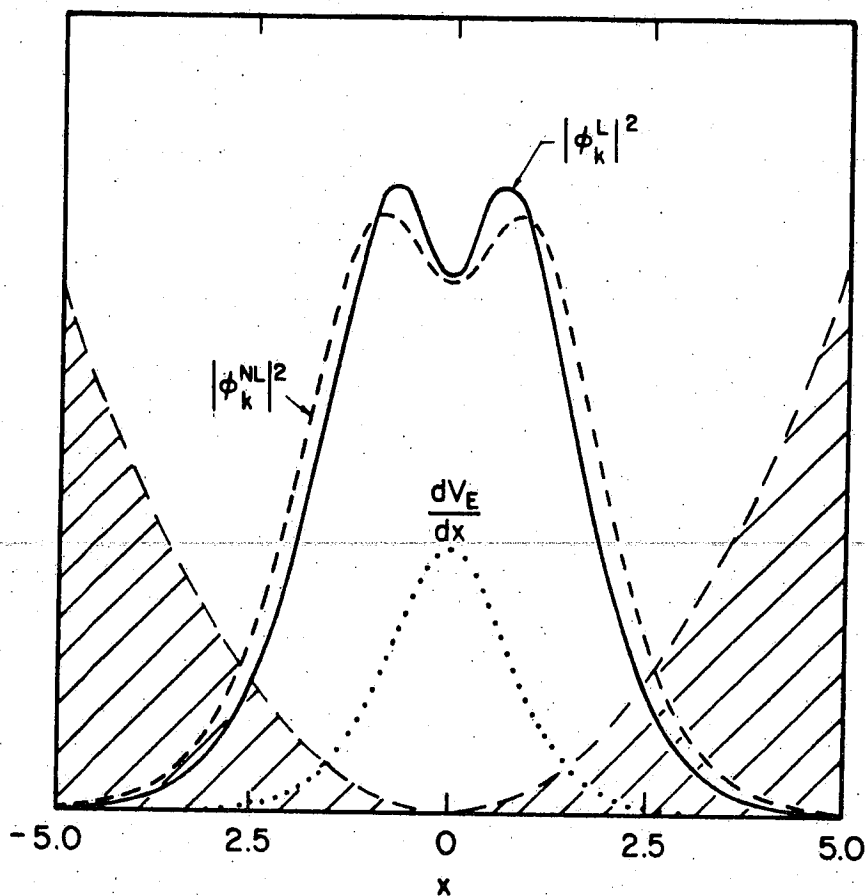fusion of vorticity with the source in the inner region,

Figure 5-6. A comparison of linear and nonlinear eigenfunctions. The nonlinear mode $|\phi_k^{NL}|^2$ is broader and extends into the dissipation region. Here, R = 2 and k = 0.02. The source vorticity is indicated by the dotted line, the sink is in the shaded region, the linear eigenfunction $|\phi_k|^2$ is indicated by the solid line; and the nonlinear eigenfunction is indicated by the dash line.

and the sink in the outer region, respectively. That is,

$$\frac{D}{\triangle_i^4} \; \phi_k \; \cong \; \left| k \left\langle \frac{d^2 V_E}{dx^2} \right\rangle \right| \phi_k \; = \; k \; \frac{V_0}{L_E^2} \; \phi_k$$

$$\frac{D}{\triangle_0^4} \; \phi_k \; \cong \; k^2 R^2 \triangle_0^2 \phi_k$$

Here, we have ignored the convection in the presence of diffusion of vorticity. In addition, we have approximated the averaged $d^2 V_E/dx^2$ in the inner region with a value V_0/L_E^2. Hence it follows that

$$\triangle_i \; \cong \; \left(\frac{D}{k} \right)^{1/4} \tag{5:4-8}$$

$$\triangle_0 \; \cong \; \left(\frac{D}{k^2 R^2} \right)^{1/6} \tag{5:4-9}$$

To determine D, we need to use Eq. (5:4-2), the vorticity spectrum equation. At steady state,

$$\int dx \; \frac{\partial}{\partial t} \; |\nabla_\perp^2 \phi_k|^2 \; = \; 0,$$

and the remaining pieces of Eq. (5:4-2) are the nonlinear enstrophy coupling terms on the left-hand side and the competition between driving and dissipation terms on the

right. In this regime, nonlinear cascade of enstrophy is less effective and can be neglected. Saturation occurs when the source balances the linear sink. Substituting $\nabla_\perp^2 \phi_k$ from Eq. (5:4-1) in Eq. (5:4-2), one obtains

$$0 = \int \frac{dx}{k^2 V_E^2 + \left[D \, \dfrac{d^2}{dx^2} \right]^2} \left[k^2 \left[\frac{d^2 V_E}{dx^2} \right]^2 \left[D \, \frac{d^2}{dx^2} \right] \right.$$

$$\left. + k^4 R^4 x^4 \left[D \, \frac{d^2}{dx^2} \right] \right] |\phi_k|^2 = 0.$$

where $d \, d^2/dx^2$ operates only on ϕ_k. Since ϕ_k is a localized function in x (Fig. 5-2), peaked at the inner region and evanescent in the dissipation region, $d^2/dx^2 \cong -1/\Delta^2$ for the source term and $d^2/dx^2 \cong 1/\Delta_0^2$ for the sink term. As a result, it follows that

$$\frac{1}{4} \Delta_i^2 \cong k^2 R^4 \Delta_0^7 \qquad\qquad (5:4-10)$$

where the convection term in the denominator has been ignored, and $|d^2 V_E/dx^2| \sim V_0/L_E^2$ has been used. In addition, the integral $\int dx$ has been evaluated with the values L_E (because of the localization of the source, $d^2 V_E/dx^2$) in the inner regions, and Δ_0 in the outer region.

D, Δ_i and Δ_0 can now be straightforwardly determined using Eqs. (5:4-8), (5:4-9) and (5:4-10). Thus,

$$\Delta_i = \left[\frac{1}{kR^2}\right]^{5/16} L_E \tag{5:4-11}$$

$$\Delta_0 = \left[\frac{1}{kR^2}\right]^{3/8} L_E \tag{5:4-12}$$

$$D = \frac{V_0 L_E}{(kR^2)^{1/4} R^2} \tag{5:4-13}$$

Comparing the nonlinear scale lengths (Eqs. (5:4-11) and (5:4-12)) with the linear ones (Eqs. (5:3-5) and (5:3-6)), we find that the nonlinear scale lengths are broadened $(kR^2 \leq 1)$.

5.5 Estimate of Fluctuation Levels at Saturation

Having obtained the vorticity diffusion coefficients D for both saturation mechanisms, we are now able to estimate several relevant quantities for comparison with experiments. The quantities include the root-mean-square potential, density and magnetic field fluctuations. These quantities will be estimated separately, for each saturation mechanism.

At steady-state, the vorticity diffusion coefficient D, arising from the random convection of velocity field, can be expressed as

$$D = \sum_k \frac{k^2 |\phi_k|^2}{ikV_E(x) - D\frac{d^2}{dx^2}} \cong \frac{1}{\left(\frac{D}{\Delta_i^2}\right)} \sum_k k^2 |\phi_k|^2$$

$$\cong \frac{k_0^2 <\phi^2> \Delta_i^2}{D} , \qquad\qquad (5:5\text{-}1)$$

hence the rms potential fluctuation level is approximately

$$\frac{e\Phi_{rms}}{T_e} \cong \frac{D}{\rho_s C_s} \frac{1}{k_0 \Delta_i} , \qquad\qquad (5:5\text{-}2)$$

where C_s is the ion sound speed and ρ_s is the ion gyro-radius with electron temperature. In the above expression (and hereafter), the original unit of Φ as the electric potential has been (and will be) retained.

The magnetic field fluctuation is related to the current fluctuation $J_\parallel$ by Ampere's law,

$$[\nabla \times \underset{\sim}{B}]_\parallel = \frac{4\pi}{C} J_\parallel ,$$

and the current fluctuation couples to the electric

potential fluctuation through the electrostatic Ohm's law, $-\nabla_{\parallel}\Phi = \eta J_{\parallel}$. Hence the rms magnetic field is approximately

$$\frac{\tilde{B}_{rms}}{B_0} = \left[\frac{4\pi\, k_0 \Delta_i^2}{\eta L_s \omega_{c_i}}\right]\left[\frac{c_s^2}{c^2}\right]\left[\frac{e\Phi_{rms}}{T_e}\right] \qquad (5:5-3)$$

To estimate the density fluctuation, it is noted that in this model of electric-field-driven turbulence the density gradient has been ignored, and so has the density fluctuation. Obviously, density gradient effects and density fluctuations significantly complicate this simple model, making analysis difficult. However, because the density gradient is smaller than that of the equilibrium flow in the region of interest, the effects of density gradient and density fluctuations on the evolution of vorticity are probably small in this case. We can estimate the saturation level of density fluctuations by consideration of a model, where density evolves by convection of the velocity field as a passive scalar. That is,

$$\frac{dn}{dt} = 0. \qquad (5:5-4)$$

Fourier-transforming Eq. (5:5-4) in the y-direction and renormalizing its nonlinear terms, we have

$$\left[\frac{\partial}{\partial t} + ikV_E(x) - D\frac{d^2}{dx^2}\right]\delta n_k = ik\Phi_k\left[\frac{c}{B_0}\right] \cdot \frac{dn_0}{dx} \,.$$

$$(5:5-5)$$

At saturation, we again neglect the convection of density fluctuations by the equilibrium flow in comparison with the diffusion term. Balancing the latter with the density fluctuation caused by fluctuating velocity fields randomly oscillating across the density gradient, we then obtain the rms density fluctuation level

$$\frac{\delta n}{n_0} \cong \frac{\Delta_i}{L_n} \qquad\qquad (5:5-6)$$

Substituting Δ_i, Δ_0 and D from Eqs. (5:3-5), (5:3-6), and (5:4-7) into Eqs. (5:5-2), (5:5-3), and (5:5-6), we obtain the fluctuation levels at saturation due to the nonlinear cascade process,

$$\frac{e\Phi_{rms}}{T_e} \cong \frac{1}{4\sqrt{3}\,k_0 L_E}\left[\frac{V_0}{\rho_s C_s k_{MIN}}\right] \qquad (5:5-7)$$

$$\frac{\tilde{B}_{rms}}{B_0} \cong \frac{\pi}{\sqrt{3}}\left[\frac{L_E V_0}{\eta L_s k_{MIN} c^2}\right] \qquad (5:5-8)$$

$$\frac{\delta n_{rms}}{n_0} \cong \frac{L_E}{L_n} \quad . \tag{5:5-9}$$

Substituting Δ_i, Δ_0 and D from Eqs. (5:4-11), (5:4-12) and (5:4-13) into Eqs. (5:5-2), (5:5-3) and (5:5-6), we obtain the fluctuation levels due to the nonlinearly broadened-mode-structure mechanism,

$$\frac{e\Phi_{rms}}{T_e} \cong \left[\frac{1}{k_0 L_E R^2}\right]^{15/16} \left[\frac{V_0 L_E}{\rho_s C_s}\right] \tag{5:5-10}$$

$$\cong \frac{e}{T_e} \cdot \left[\frac{\eta L_s^2 M_i n_0}{k_0 L_E}\right]^{15/16} \frac{c}{B_0}^{7/8} V_0^{31/16} L_E^{-29/16} \tag{5:5-10a}$$

$$\frac{B_{rms}}{B_0} \cong \left[\frac{1}{k_0 L_E R^2}\right]^{9/16} \left[\frac{V_0^2 L_s}{V_A^2 L_E}\right] \tag{5:5-11}$$

$$\cong \left[\frac{\eta c^2}{4\pi k_0 L_E}\right]^{9/16} V_0^{41/16} L_s^{17/8} V_A^{-25/8} L_E^{-13/14} \tag{5:5-11a}$$

and

$$\frac{\delta n_{rms}}{n_0} \cong \frac{L_E}{L_n} \left[\frac{1}{k_0 L_E R^2}\right]^{5/16} \tag{5:5-12}$$

$$\cong \frac{1}{L_n} \left[\frac{\eta V_0 L_s^2 c^2}{4\pi k_0 L_E V_A^2}\right]^{5/16} L_E^{1/16} \tag{5:5-12a}$$

Notice that for R much greater than unity, $k_0 L_E$ is forced to be small, and asymptotically approaches the

value 1/2R from below. Hence the expressions Eqs. (5:5-10),
(5:5-11) and (5:5-12) should be used to determine scal-
ings. For R not too much greater than unity, $k_0 L_E$ is rela-
tively insensitive to the value of R and the expressions
Eqs. (5:5-10a), and (5:5-11a) and (5:5-12a) should be
used for scaling laws. In the large R limit, we also
notice that $\Delta_i \rightarrow L_E$, provided that k_{MIN} is small enough
so that there is a range of small k satisfying this
asymptotic limit.

As R decreases from unity the results pre-
dicted by the broadened-mode-structure processed do not
approach those of the cascade processes. The reason is
obvious, for they correspond to two different, compet-
ing physical processes. The critical value of R at
which transition from one process to the other occurs
can be estimated in the following way. Intuitively one
expects that the saturation levels for the cascade pro-
cess should be greater than those of the broadened-
mode-structure processes, since the latter involves coup-
pling to linear damping that can directly draw energy from
the source and inhibit large fluctuation amplitudes. In
this case, the critical value of R occurs when the dif-
fusion coefficients of both processes are equal. That
is, $R_{crit} \cong 2.6 (k_{MIN} L_E)^{1/2}$.

For parameters consistent with those of the
TEXT tokamak in the edge, $R \cong 2$ and $R_{crit} \cong 0.4$, hence
the broadened-mode-structure mechanism prevails. The
estimated saturation levels are

$$\frac{e\,\phi_{rms}}{T_e} \cong 0.42$$

$$\frac{\delta n_{rms}}{n_0} \cong 0.35$$

$$\frac{\tilde{B}_{rms}}{B_0} \cong 5 \times 10^{-5}.$$

These values of fluctuation levels do not dramatically
differ from those of density-gradient-driven turbulence.
This is because the correlation time scales of both types
of turbulence (Eq. (5:2-11)) are comparable for the param-
eters of TEXT experiments, hence comparable spectral
amplitudes are expected.

5.6 Summary and Conclusion

An analytical theory is developed to describe
tokamak edge turbulence associated with the presence of a
sheared radial electric field. Turbulence in this region

can be driven by the density gradient and radial-electric-field gradient. Near the region where the maximum velocity shear of the equilibrium $E_0 \times B_0$ poloidal flow is located, the flow shear alone is strong enough to drive fluctuation. In the linear phase, energy provided by sources is partially dissipated by the sink, i.e., electron collisionality along field lines; the remainder is used to excite fluctuations. If the coupling of the sink to the source is made very effective through nonlinear modifications of the basic modes, fluctuations can be stabilized. For steady-state turbulence, energy provided by the source is then totally absorbed by the sink.

In this study, we have separately studied turbulence driven by the density gradient in the presence of radial electric field and that by the electric field gradient. For the former, effects of radial electric field do not drastically change the basic characteristics of turbulence, but simply modify them. Results of this study on the modifications of density-gradient-driven turbulence in the presence of the radial electric field can be summarized as follows:

tokamak edge, the mode structures are spatially broad;
the length scales in the poloidal and radial directions
are comparable. This indicates that the fluctuation
spectrum of electric-field-gradient-driven turbulence is
nearly isotropic.

(2) Linear growth rates have been obtained.
They indicate that instabilities are dependent sensitively
on the degree of overlap between the regions of the energy
source (vorticity gradient) and sink (parallel resistive
dissipation). Furthermore, it is found that the long
wavelength linear modes can be unstable due to a lack
of sufficient overlap.

(3) Nonlinearity is approximated by turbulent
diffusion of vorticity for linearly unstable modes. Two
types of nonlinear processes are simultaneously present
governing the evolution of turbulence. They are the non-
linear cascade and nonlinear broadening of mode struc-
ture. The former process produces coupling between modes
of different wavenumbers, whereby wave energy of unstable
modes can be extracted by the short-wavelength, linearly
stable modes. The latter process radially broadens mode
structures, which permits the sink to directly extract
energy from the source and stabilize linear instabilities.

A dimensionless quantity R, characterizing the strength
of magnetic shear, determines which of these two mechanisms
is dominant. When R << 1, the region of magnetic shear
damping is separated from that of energy input. The lat-
ter mechanism is not effective and the nonlinear cascade
then provides saturation. When $R \cong O(1)$, the location of
the sink is not far from that of the source and slight
broadening of mode width can effectively yield saturation.

(4) Diffusion coefficients and the rms poten-
tial, magnetic field and density fluctuations at satura-
tion have separately been estimated for each regime. For
parameters of the TEXT tokamak in the edge, we have esti-
mated $R \cong 2$, hence turbulence is governed by the mechanism
of nonlinear broadening of mode structure. The satura-
tion levels of potential, density and magnetic field
fluctuations estimated by this theory are consistent with
those observed in experiments.

It is interesting to note that, in the limit
of small R, the long wavelength modes cannot be saturated
by finite turbulent diffusion, and hence the complete
saturation necessitates a lower bound for wavenumbers,
i.e., k_{MIN}, which is usually determined by system sizes.
The inability of turbulent diffusion to saturate the low-k

modes actually lies in the fact that there is no charac-
teristic length in the region away from the shear layer,
thus the spatial derivatives d/dx scales as k^{-1}. Hence
the rate of decorrelation ($|D\ d^2/dx^2| \cong k^2 D$) can only
offset the growth rate ($\gamma_k \propto k$) if $\dot{D} \propto k^{-1}$ (thus $D \to \infty$
as $k \to 0$). By contrast, saturation mechanism in the
strong magnetic shear limit introduces another length
scale $L_E/(2kR^2)^{1/2}$ in addition to the length scale of L_E
of the source. This extra degree of freedom allows tur-
bulent diffusion to regulate the mode width so as to de-
feat the linear growth rate to a considerable extent
($D \propto k^{-1/4}$).

Saturation mechanisms of this type represent a
departure from the conventional   mixing length theory.
It is instructive to contrast this theory with mixing-
length theory and speculate as to its generality. In
this model, instead of using the width and e-folding time
of linear modes as the correlation length and decorrela-
tion time, the latter quantities have been self-
consistently determined. Moreover, as the sink (parallel
dissipation) is located at a certain distance from the
source, an additional length scale is introduced. This
extra degree of freedom allows turbulent diffusion to

adjust and yields a completely different correlation length and time from those of linear theory.

This type of nonlinear mechanism may have a wide range of generality, particularly for turbulence in the vicinity of single-helicity magnetic resonance surface, $\underline{k} \cdot \underline{B}_0 = 0$. For the case where magnetic field fluctuations are as important as electric field fluctuations (see Section 5.3), i.e., $\eta c^2/4\pi V_0 L_E \sim 1$, shear-flow-driven magnetic reconnection may occur. We expect that a similar, but more involved, analysis should apply.

In summary, this chapter has explored possible mechanisms responsible for the turbulence observed in the vicinity of the equilibrium vorticity maximum in the tokamak edge. The idea of the nonlinearly broadened mode structures, developed here and elsewhere, is seen to play an important role in the characterization of steady-state turbulence and should prove to be useful in other contexts.

CHAPTER VI

SUMMARY AND CONCLUSION

In this dissertation, several aspects of mag-
netized plasma turbulence have been examined. They in-
clude current-driven ion-cyclotron turbulence and electro-
static MHD shear-flow turbulence. The results provide
reasonable explanations for the substantial ion heating
observed in auroral plasma, the dynamics of large-scale
and small-scale fluctuations in two-dimensional shear
flows, and some of the observed characteristics of tokamak
edge fluctuations. Furthermore, the theories developed
here have stimulated some related new research, and can
be applied to other similar systems. Hence, these studies
not only lead us to a better understanding of the natures
of several turbulence related phenomena, but also open
a few doors for future turbulence research.

In Chapters II and III, we studied ion-cyclotron
turbulence in a weak collective dissipation regime. The
nature of turbulence consists of both waves and clumps.
Clumps behave as macroparticles, and thus emit waves when
travelling in a plasma. A state of stationary turbulence

232

requires the waves to be overdamped in order to balance clump noise emission. We derived a relation relating the overdamping of waves to the necessary condition for stationary turbulence. This is a collective Vlasov analogy of the test-particle model fluctuation-dissipation theorem. At vanishing fluctuation amplitude limit, the threshold current for nonlinear instability was determined by this necessary condition, and is (up to 7 percent) lower than the linear threshold current. Moreover, the growth rate near the marginal stability point was derived.

In stationary ion-cyclotron turbulence, the ion clump amplitude is much smaller than the electron clump amplitude because of finite ion Larmor radius effects. Furthermore, the fluctuation level and anomalous transport were also obtained. The potential fluctuation level is moderate, $(e\phi/T_e)_{rms} \leq 0.1$. Anomalous resistivity can sizably deviate from that predicted by conventional wave theories--particularly in the regime where $(m_e/M_i)^{1/2}T^i/T_e > 0.01$. Ion perpendicular heating was predicted to be the dominant mechanism for extracting the electron current energy. This is in marked contrast to the purely wave theories, which do not predict this result.

We also used a similar method to examine ion-acoustic turbulence of the wave-clump regime, and found that the clump effects were much more significant (up to 40 percent threshold current reduction for nonlinear instability).

Finally, this study concluded that to explain the large anomalous resistivity observed in auroral plasma, a theory of ion-cyclotron turbulence for the clump regime was necessary. This is also consistent with the large ion-electron temperature ratio ($T^i/T_e > 10$) observed, which thus leads to strong collective dissipation. We also suggested that a study of turbulence in this regime may have to include ion-acoustic fluctuations, because the large current required for ion-cyclotron nonlinear instability may exceed that for ion-acoustic nonlinear instability.

In Chapter IV, we studied two-dimensional shear flow fluid turbulence, which is dynamically equivalent to strongly magnetized (but weak magnetic shear) MHD turbulence. Two types of turbulence characterized by the mean flow profiles were examined. For mixing-layer mean flows, turbulence is dominated by large-scale fluctuations. We assumed that turbulence evolved self-similarly.

Using quasi-linear model, we were able to show that the mean-flow shear layer expanded linearly in time, and that the expansion rate was consistent with those observed in computer simulations by Aref, et al., and experiments by Brown, et al. Also, the energy contents of different components of the flow were examined. Both energy loss from the mean flow and energy gain of the large-scale fluctuations increase linearly in time. But the latter occurs at a slower rate, indicating that the excess energy from the mean flow is transferred to small-scale fluctuations.

For the other type of mean flow (wakes or jets), small-scale fluctuations dominate the turbulence. We recognized the similarity of this system to the one-dimensional Vlasov plasma, and attempted to develop a statistical theory describing the evolution of small-scale vortices. A singular vorticity correlation function at a small separation is a manifestation of the vanishing relative turbulent convection at this limit, and the presence of a positive driving source. We succeeded in showing the positivity of the source term, and in approximating the triplet correlation, with the property of the relative turbulent convection preserved.

Moreover, vorticity correlation function and wavenumber

spectrum were obtained. The spectrum is anisotropic and

of elliptic shape in the wavenumber space. The major

axis, tilted at an angle $-45°$ from the x direction,

scales with $k_o \tau_c V_E'$, and the minor axis with k_o.

With the understanding of the local vorticity

structures in shear flow turbulence, we suggested that

nonlinear instability, similar to that of a Vlasov plasma,

might occur. A project in this direction can be pursued

via an investigation of the global (integrating out the

relative coordinates) evolution of the vorticity correla-

tion function. The global evolution equation is a linear

integro-differential equation for fluctuation spectrum.

Nonlinear instability may occur when the gradient of mean

vorticity (free energy source), $|d^2 V_E/dx^2|$, exceeds a

certain magnitude.

In Chapter V, we extended the analysis of

Chapter IV to a situation where stabilizing magnetic

shear is present, and the mean flow profile is fixed dur-

ing the course of turbulence evolution. This configura-

tion corresponds to what is observed in the tokamak edge,

where a sheared poloidal flow is present, due to the $E \times B$

drift induced by a D.C. radial electric field near the

wall or limiter. The observed turbulence characteristics
change at the region of the maximum flow shear, from an
isotropic spectrum to an anisotropic one, at points away
from this region.

Away from the maximum flow shear, turbulence
driven by the density gradient was examined. Velocity
shear Doppler-shifts the frequency and modifies (reduces)
the radial density correlation length.

At the region of maximum flow shear, the shear
flow can drive instability, and thus turbulence. The
linearly unstable modes are not singular, hence the tur-
bulence is expected to be weakly anisotropic. Two satura-
tion mechanisms were proposed. In the case of weak mag-
netic shear,

$$R^2 \equiv \frac{4\pi V_A^3 L_E^3}{\eta V_o^2 L_s^2 c^2} \ll 1 ,$$

saturation occurs through an enstrophy cascade process
which couples regions of driving source and dissipation
in wavenumber space. For stronger magnetic shear, $R^2 \sim 1$,
such that the resistive layer is comparable to the radial
electric field scale-length, saturation occurs through
nonlinear broadening of the mode structure, which pushes
enstrophy into the region of dissipation.

We self-consistently determined the turbulence correlation lengths and times for both mechanisms. Using this information, the saturated fluctuation levels were obtained. Scalings of the potential, density and magnetic field fluctuation levels were determined. For TEXT tokamak parameters ($R \cong 2$), the mode-broadening mechanism prevails. Our estimates are consistent with the experimental results.

We indicated that the idea of the mode-broadening mechanism for saturation was useful in other contexts --in particular, for turbulence in the vicinity of single-helicity magnetic resonance surface, $\underset{\sim}{k} \cdot \underset{\sim}{B}_0 = 0$. To be specific, for the case when magnetic field fluctuations are as important as electric field fluctuations, i.e., $\eta c^2 / 4\pi V_0 L_E \leq 1$, shear-flow driven electromagnetic turbulence may occur. The mechanism of nonlinear saturation developed here may be applicable to this problem.

Several astrophysical and space phenomena are intrinsically related to shear flow (differential rotation) turbulence. An extention of the present analysis to these areas is worthwhile and feasible. Continued work in the immediate future will be focused on a quasi-two-dimensional model of shear-flow driven electromagnetic turbulence. Applications of this future

project include anomalous viscosity in accretion disks,[59],[60] magnetic field diffusion around a neutron star,[61] and electron acceleration mechanisms near the earth's neutral sheet, where a sunward plasma flow[62] may serve as a driving source.

APPENDICES

240

Appendix (A) Linear Analysis of ICW

The linear dielectric function in a current-carrying, magnetized plasma with anisotropic-Maxwellian velocity distributions can be expressed as (Stix, 1962),

$$\varepsilon = 1 - \sum_{\sigma=i,e} \sum_{n=-\infty}^{\infty} \frac{\Lambda_n(k^2\rho_\sigma^2)}{|\underset{\sim}{k}|^2\lambda_{D_\sigma}^2} \left\{ \frac{T_\perp^\sigma}{T_\parallel^\sigma} + \left[\frac{(\omega-\kappa v_{D\sigma}-n\omega_{c\sigma})T_\perp^\sigma + n\omega_{c\sigma}T_\parallel^\sigma}{\kappa T_\parallel^\sigma v_{t\parallel}^\sigma} \right] \right.$$

$$\left. \cdot Z\left(\frac{\omega-\kappa v_{D\sigma}-n\omega_{c\sigma}}{\kappa v_{t\parallel\sigma}} \right) \right\}$$

where the various quantities are defined as follows:

the perpendicular thermal speed

$$v_{t\perp\sigma} = \left(\frac{2T_\perp^\sigma}{M_\sigma} \right)^{1/2} ,$$

the parallel thermal speed

$$v_{t\parallel\sigma} = \left(\frac{2T_\parallel^\sigma}{M_\sigma} \right)^{1/2} ,$$

the perpendicular Debye length

$$\lambda_{D_\sigma} = \frac{v_{t\perp\sigma}}{\sqrt{2}\ \omega_{p_\sigma}} ,$$

the thermal gyroradius

$$\rho_\sigma = \frac{v_{t\perp\sigma}}{\sqrt{2}\,\omega_{c\sigma}} \;,$$

$$\Lambda_n(k^2\rho_\sigma^2) = I_n(k^2\rho_\sigma^2)\,e^{-k^2\rho_\sigma^2} \;.$$

Z is the plasma dispersion function and σ stands for species.

For fluctuations in the ion–cyclotron regime, where $k\rho_i \sim 1$, $k \gg \kappa$ and $\omega-\kappa v_D/\kappa v_{te} \ll 1$, the dielectric can be simplified as

$$\varepsilon_{\underline{k},\omega} \approx 1 + \frac{1}{2|\underline{k}|^2\lambda_{De}^2}\,Z'\Big(\frac{\omega-\kappa v_D}{\kappa v_{te}}\Big) - \sum_n \frac{\Lambda_n(k^2\rho_i^2)}{(|\underline{k}|^2\lambda_{Di}^2)}$$

$$\Big(\frac{T_\perp^i}{T_\parallel^i} + \frac{(\omega-n\omega_{ci})\big(\frac{T_\perp^i}{T_\parallel^i}\big)+n\omega_{ci}}{\kappa v_{t\parallel i}}\;Z\big(\frac{\omega-n\omega_{ci}}{\kappa v_{t\parallel i}}\big)\Big) \tag{A-1}$$

or

$$\approx \frac{-1}{|\underline{k}|^2\lambda_{De}^2}\Big[1 + i\sqrt{\pi}\,\big(\frac{\omega-\kappa v_D}{\kappa v_{te}}\big)\Big] - \sum_n \frac{\Lambda_n(k^2\rho_i^2)}{|\underline{k}|^2\lambda_{Di}^2}$$

$$\cdot\Big(\frac{T_\perp^i}{T_\parallel^i} + \frac{(\omega-n\omega_{ci})\big(\frac{T_\perp^i}{T_\parallel^i}\big)+n\omega_{ci}}{\kappa v_{t\parallel i}}\;Z\big(\frac{\omega-n\omega_{ci}}{\kappa v_{t\parallel i}}\big)\Big)\;. \tag{A-2}$$

Here, we have assumed that the electrons have an isotropic-velocity distribution. Since the magnitude of $|\mathrm{Re}\,\varepsilon_{\underline{k},\omega}|$ is larger than the magnitude of $|\mathrm{Im}\,\varepsilon_{\underline{k},\omega}|$, except near $\mathrm{Re}\,\varepsilon_{\underline{k},\omega}=0$, the zeros of $\varepsilon_{\underline{k},\omega}$ will be located near

$\mathrm{Re}\varepsilon_{\underset{\sim}{k},\omega} = 0$. Hence $\mathrm{Re}\varepsilon_{\underset{\sim}{k},\omega} = 0$ will determine the real part of the frequency ω, and $\mathrm{Im}\varepsilon$ will determine the imaginary part.

The analytical expression for the fundamental mode $\omega \approx \omega_{ci}$ is particularly simple, where $\mathrm{Re}\varepsilon_{\underset{\sim}{k},\omega} = 0$ can be expressed as

$$\frac{\omega}{\kappa v_{t_{\parallel i}}} \, \mathrm{Re}Z\left(\frac{\omega-\omega_c}{\kappa v_{t_{\parallel i}}}\right) \cong \frac{1 + \dfrac{T^i_\perp}{T^e_\parallel} - \dfrac{1-\Lambda_o(k^2\rho^2_i)}{k^2\rho^2_i}}{\Lambda_1(k^2\rho^2_i)} \, , \tag{A-3}$$

and the marginal stability, $\mathrm{Im}\varepsilon_{\underset{\sim}{k},\omega} = 0$, yields

$$\frac{v_D}{v_{t_{\parallel i}}} = -\left[\frac{1 + \dfrac{T^i_\perp}{T^e_\parallel} - \dfrac{1-\Lambda_o}{k^2\rho^2_i}}{\Lambda_1}\right]$$

$$\cdot \frac{1 + \left(\dfrac{T^i_\parallel}{T^i_\perp}\right)\left(\dfrac{T^e_\parallel}{T^i_\parallel}\right)^{3/2}\left(\dfrac{M_i}{m_e}\right)^{1/2} \Lambda_1 \, e^{\dfrac{-(\omega-\omega_{ci})^2}{\kappa^2 v^2_{t_{\parallel i}}}}}{\mathrm{Re}Z\left(\dfrac{\omega-\omega_{ci}}{\kappa v_{t_{\parallel i}}}\right)} \, , \tag{A-4}$$

the threshold-drift velocity for exciting the mode $\varphi_{\underset{\sim}{k},\omega}$.

The minimal threshold velocity[16] to excite ion-cyclotron wave can be obtained by minimizing $v_D/v_{t_{\parallel i}}$ with respect to $\omega-\omega_c/\kappa v_{t_{\parallel i}}$ and $k^2\rho^2_i$. The latter takes a value $k^2\rho^2_i \sim 2$ to yield the minimal threshold-drift velocity, and the value of $\omega-\omega_{ci}/\kappa v_{t_{\parallel i}}$ will be dependent on $T^i_\perp/T^i_\parallel$, $T^i_\parallel/T^e_\parallel$ and M_i/m_e. When $T^e_\parallel/T^i_\perp \sim 1$, Eqs. (A-3) and (A-4) can be simplied further,

$$\omega \approx \omega_{ci} \left[1 + \cfrac{\Lambda_1}{1 + \left(\cfrac{T^i_\perp}{T^e_\parallel}\right) - \Lambda_1 - \cfrac{1-\Lambda_o}{k^2\rho_i^2}}\right] \tag{A-5}$$

$$\frac{v_D}{v_{t_{\parallel i}}} \approx \frac{\omega}{\kappa v_{t_{\parallel i}}} \left[1 + \left(\frac{T^i_\parallel}{T^i_\perp}\right)\left(\frac{T^e_\parallel}{T^i_\parallel}\right)^{3/2}\left(\frac{M_i}{m_e}\right)^{1/2}\Lambda_1(k^2\rho_i^2)\ e^{\frac{-(\omega-\omega_c)^2}{\kappa^2 v^2_{t_{\parallel i}}}}\right] \ , \tag{A-6}$$

and the minimal threshold drift is,

$$\frac{v^{thr}}{v_{t_{\parallel i}}} = \left(\cfrac{1 + \cfrac{T^i_\perp}{T^e_\parallel} - \cfrac{1-\Lambda_o}{k^2\rho_i^2}}{1 + \cfrac{T^i_\perp}{T^e_\parallel} - \cfrac{1-\Lambda_o}{k^2\rho_i^2} - \Lambda_1}\right) \left\{\ln\left[2\left(\frac{T^i_\parallel}{T^i_\perp}\right)\left(\frac{T^e_\parallel}{T^i_\parallel}\right)^{3/2}\left(\frac{M_i}{m_e}\right)^{1/2}\Lambda_1\right]\right\}^{1/2}$$

Appendix (B) Calculation of the Source Term of ICW

$$\langle S \rangle = -\frac{q}{M} \left[\langle \underline{E}(1)\delta f(2) \rangle \cdot \frac{\partial \langle f \rangle}{\partial \underline{v}_1} + \langle \underline{E}(2)\delta f(1) \rangle \cdot \frac{\partial \langle f \rangle}{\partial \underline{v}_2} \right]$$

$$= \frac{iq}{M} \sum_{\substack{k \\ \omega}} \frac{e^{i\underline{k}\cdot\underline{R}}}{(2\pi)^4} \left\{ \left\langle \Phi_{\underline{k},\omega}(1) \; f_{\underline{k},\omega}^*(2) \left[\cos(\vartheta_1 - \psi_k)k \frac{\partial \langle f \rangle}{\partial V_1} + \kappa \frac{\partial \langle f \rangle}{\partial U_1} \right] \right\rangle \right.$$

$$\left. + \left\langle \Phi_{\underline{k},\omega}^*(2) \; f_{\underline{k},\omega}(1) \left[\cos(\vartheta_2 - \psi_k)k \frac{\partial \langle f \rangle}{\partial V_2} + \kappa \frac{\partial \langle f \rangle}{\partial U_2} \right] \right\rangle \right\} \; . \tag{B-1}$$

The fluctuation $f_{\underline{k},\omega}$ can be divided into a coherent part and an incoherent part, thus we have

$$\langle \Phi_{\underline{k},\omega}(1) f_{\underline{k},\omega}^*(2) \rangle = \frac{\varepsilon_{\underline{k},\omega}^*}{|\varepsilon|^2} \left[\langle \tilde{\Phi}_{\underline{k},\omega}(1) \tilde{f}_{\underline{k},\omega}^*(2) \rangle + \langle \tilde{\Phi}_{\underline{k},\omega} f_{\underline{k},\omega}^{c*}(2) \rangle \right] \; . \tag{B-2}$$

But

$$\tilde{\Phi}_{\underline{k},\omega}(1) = \sum_n J_n(1) \; e^{in(\vartheta_1 - \psi_k)} \tilde{\varphi}_{\underline{k},\omega}$$

$$\tilde{\Phi}_{\underline{k},\omega}\cos(\vartheta_1 - \psi_k) = \sum_n \frac{nJ_n(1)}{x_1} e^{in(\vartheta_1 - \psi_k)} \tilde{\varphi}_{\underline{k},\omega}$$

$$f_{\underline{k},\omega}^c = \frac{iq}{M} \sum_n e^{in(\vartheta - \psi_k)} G_{\underline{k},\omega,n} \varphi_{\underline{k},\omega} J_n \left[\frac{nk}{x} \frac{\partial \langle f \rangle}{\partial V} + \kappa \frac{\partial \langle f \rangle}{\partial U} \right] \; ,$$

where $x_1 \equiv kV_1/\omega_c$, $J_n(1) \equiv J_n(x_1)$ and $\cos\vartheta = \hat{x}\cdot\underline{V}_\perp/V$. Therefore,

$$\langle \Phi_{\underline{k},\omega}(1) f_{\underline{k},\omega}^{c*}(2) \rangle = \frac{-iq}{M} \sum_n e^{in(\vartheta_1 - \vartheta_2)} G_{\underline{k},\omega,n}^* J_n(1) J_n(2) \langle |\varphi_{\underline{k},\omega}|^2 \rangle \left[\frac{nk}{x_2} \frac{\partial \langle f \rangle}{\partial V_2} + \kappa \frac{\partial \langle f \rangle}{\partial U_2} \right]$$

and

$$\langle \Phi_{\underline{k},\omega}(1) f^{c*}_{\underline{k},\omega}(2)\, \cos(\vartheta_1 - \psi_k)\rangle = -\frac{iq}{M} \sum_n e^{in(\vartheta_1 - \vartheta_2)} G^*_{\underline{k},\omega,n}\left(\frac{n}{x_1}\right) J_n(1) J_n(2) \langle |\varphi_{\underline{k},\omega}|^2\rangle$$

$$\cdot \left[\frac{nk}{x_2}\frac{\partial \langle f\rangle}{\partial V_2} + \kappa\frac{\partial \langle f\rangle}{\partial U_2}\right].$$

Also, we have a term

$$\langle \tilde{\Phi}_{\underline{k},\omega}(1) \tilde{f}^*_{\underline{k},\omega}(1)\rangle = \sum_n e^{in(\vartheta_1 - \vartheta_2)} \langle \tilde{\Phi}_{\underline{k},\omega}(1)\tilde{f}^*_{\underline{k},\omega}(2)\rangle_n$$

$$= \sum_n e^{in(\vartheta_1 - \vartheta_2)} (2G^*_{\underline{k},\omega,n}) \langle \tilde{\Phi}_{\underline{k}}(1)\tilde{f}^*_{\underline{k}}(2)\rangle_n$$

$$= 2\sum_n e^{in(\vartheta_1 - \vartheta_2)} G^*_{\underline{k},\omega,n} J_n(1) J_n(2)\, \langle \tilde{\varphi}_{\underline{k}}\delta\tilde{f}^*_{\underline{k}}\rangle$$

where the second equality assumes that the dominant time-dependence of $\langle \tilde{\Phi}_{\underline{k}}(1,t_1)\tilde{f}^*_{\underline{k}}(2,t_2)\rangle_n$ is due to the Doppler-shifted ballistic propagation, i.e., $\omega - n\omega_c = \kappa v_{\parallel}$. Similarly, the term

$$\langle \tilde{\Phi}_{\underline{k},\omega}(1)\tilde{f}^*_{\underline{k},\omega}(2)\cos(\vartheta_1 - \psi_k)\rangle = 2\sum_n e^{in(\vartheta_1 - \vartheta_2)} \frac{n}{x_2} J_n(2) J_n(1) G^*_{\underline{k},\omega,n}(2) \langle \tilde{\varphi}_{\underline{k}}\delta\tilde{f}^*_{\underline{k}}\rangle.$$

Hence, the source term of the ions becomes

$$\langle S(1,1)\rangle^i = \frac{2q}{M}\sum_{\substack{\underline{k}\\\omega\\n}} \frac{J_n^2 G^*_{\underline{k},\omega,n}}{(2\pi)^2 |\varepsilon_{\underline{k},\omega}|^2} \left\{\frac{q}{M}\left[|\tilde{\varphi}^e_{\underline{k},\omega}|^2 + |\tilde{\varphi}^i_{\underline{k},\omega}|^2\right]\left(\frac{nk}{x}\frac{\partial\langle f\rangle}{\partial V} + \kappa\frac{\partial\langle f\rangle}{\partial U}\right)^2\right.$$

$$\left. - 2\left[\mathrm{Im}\chi^e_{\underline{k},\omega} + \mathrm{Im}\chi^i_{\underline{k},\omega}\right]\langle\delta\tilde{f}\tilde{\varphi}\rangle^i_{\underline{k}}\left(\frac{nk}{x}\frac{\partial\langle f\rangle}{\partial V} + \kappa\frac{\partial\langle f\rangle}{\partial U}\right)\right\}^i \tag{B-3}$$

where we have let

$$|\varphi_{\underset{\sim}{k},\omega}|^2 = \frac{|\tilde{\varphi}_{\underset{\sim}{k},\omega}|^2}{|\varepsilon_{\underset{\sim}{k},\omega}|^2} = \frac{|\tilde{\varphi}_{\underset{\sim}{k},\omega}^i|^2 + |\tilde{\varphi}_{\underset{\sim}{k},\omega}^e|^2}{|\varepsilon_{\underset{\sim}{k},\omega}|^2} \ .$$

Furthermore, we will assume that

$$<\delta\tilde{f}\tilde{\varphi}>_{\underset{\sim}{k}}^{\sigma} = N_{\sigma}(\underset{\sim}{k})<f>^{\sigma}\ \frac{4\pi q^{\sigma}}{k^2} \tag{B-4}$$

and $<f>^{\sigma}$ is a Maxwellian distribution. This yields

$$<|\tilde{\varphi}_{\underset{\sim}{k},\omega}^i|^2> = \frac{4\pi n_o q}{k^2}\ \sum_n \int d\underset{\sim}{V}(2G_{\underset{\sim}{k},\omega,n}^i)<\delta\tilde{f}\tilde{\varphi}>_{\underset{\sim}{k}}^i$$

$$= \frac{(8\pi^2 n_o q)^2}{2\pi n_o k^4}\ N_i \sum_n \wedge_n\ e^{-\frac{(\omega - n\omega_{ci})^2}{\kappa^2 v_{t_{\parallel i}}^2}}\ \left(\frac{1}{\sqrt{\pi}\ \kappa v_{t_{\parallel i}}}\right) \tag{B-5}$$

and

$$<|\tilde{\varphi}_{\underset{\sim}{k},\omega}^e|^2> = \frac{(8\pi^2 n_o e)^2}{2\pi n_o k^4}\ N_e\ e^{-\frac{(\omega - \kappa v_D)^2}{\kappa^2 v_{te}^2}}\ \left(\frac{1}{\sqrt{\pi}\kappa v_{te}}\right)\ . \tag{B-6}$$

Hence, Eq. (B-3) can be reduced to

$$<S(1,1)>^i = \frac{2q}{M}\ \sum_{\substack{\underset{\sim}{k}\\\underset{\sim}{\omega}\\n}}\ \frac{J_n^2 G_{\underset{\sim}{k},\omega,n}^* (\frac{4\pi e}{k^2})}{(2\pi)^4 |\varepsilon_{\underset{\sim}{k},\omega}|^2}\ \left(\ \frac{2\omega_{pi}^2}{k^2}\ \left[N_i(\underset{\sim}{k}) \sum_m \wedge_m\ \frac{e^{-\frac{(\omega - m\omega_c)^2}{\kappa^2 v_{t_{\parallel i}}^2}}}{v_{t_{\parallel i}}}\right.\right.$$

$$+ \frac{N_e(\underline{k})}{v_{te}} e^{-\frac{(\omega-\kappa v_D)^2}{\kappa^2 v_{te}^2}}] \; (\frac{\sqrt{\pi}}{\kappa}) \cdot (n\omega_{ci}+(\frac{T_\perp^i}{T_\parallel^i})\kappa U) \; <f_i>^2 \cdot (\frac{4}{v_{t_{\perp i}}^4})$$

$$+ 2[\mathrm{Im}\chi_{\underline{k},\omega}^e + \mathrm{Im}\chi_{\underline{k},\omega}^i] N_i(\underline{k}) <f_i>^2 (n\omega_{ci}+(\frac{T_\perp^i}{T_\parallel^i})\kappa U)(\frac{2}{v_{t_{\perp i}}^2}) \;) \Big|_{U = \frac{\omega-n\omega_c}{\kappa}} \cdot$$

Rearranging

$$(n\omega_c+(\frac{T_\perp^i}{T_\parallel^i})\kappa U)\Big|_{u = \frac{\omega-n\omega_c}{\kappa}} = \omega + (\omega-m\omega_c)(\frac{T_\perp^i}{T_\parallel^i} - 1) + (m-n)\omega_c(\frac{T_\perp^i}{T_\parallel^i} - 1)$$

the ion source becomes

$$<S(1,1)>^i = \frac{2q}{M_i} \sum_{\substack{\underline{k}\\ \omega\\ n}} \frac{J_n^2 G_{\underline{k},\omega,n}^*}{(2\pi)^4 |\varepsilon_{\underline{k},\omega}|^2} \frac{4\pi e}{k^2} \{ (N_i(\underline{k}) (\frac{2\omega_{pi}^2}{k^2 v_{t_{\perp i}}^2})$$

$$\sum_m [\frac{\omega}{\kappa} + \frac{(\omega-m\omega_c)}{\kappa} (\frac{T_\perp^i}{T_\parallel^i} - 1)]\Lambda_m \frac{e^{-\frac{(\omega-m\omega_c)^2}{\kappa^2 v_{t_{\parallel i}}^2}}}{v_{t_{\parallel i}}} \sqrt{\pi}$$

$$\cdot (n\omega_{ci} + (\frac{T_\perp^i}{T_\parallel^i})\kappa U)(\frac{2}{v_{t_{\perp i}}^2})<f^i>^2 + \frac{4\omega_{pi}^2 \sqrt{\pi}}{k^2 v_{t_{\perp i}}^4 \kappa} N_e(\underline{k}) \frac{e^{-\frac{(\omega-\kappa v_D)^2}{\kappa^2 v_{te}^2}}}{v_{te}}$$

$$(n\omega_{ci}+ (\frac{T_\perp^i}{T_\parallel^i})\kappa U)^2 <f^i>^2) + \{2[\mathrm{Im}\chi_{\underline{k},\omega}^e + \mathrm{Im}\chi_{\underline{k},\omega}^i] N_i(\underline{k})$$

$$\cdot \left(n\omega_{ci} + \left(\frac{T_\perp^i}{T_\parallel^i}\right)\kappa U\right)\left(\frac{2}{v_{t_{\perp i}}^2}\right)<f^i>^2\right) \left. \right) \Big|_{U = \frac{\omega - n\omega_c}{\kappa}}$$

$$+ \frac{2q}{M_i} \sum_{\substack{\underline{k} \\ \omega \\ n}} \frac{J_n^2 G_{\underline{k},\omega,n}^*}{(2\pi)^4 |\varepsilon_{\underline{k},\omega}|^2} \frac{4\pi e}{k^2} \left\{ N_i(\underline{k})\left(\frac{4\omega_{pi}^2}{k^2 v_{t_{\perp i}}^2}\right) \sum_m (m-n)\omega_c\left(\frac{T_\perp^i}{T_\parallel^i} - 1\right) \wedge_m \right.$$

$$\cdot \frac{e^{-\frac{(\omega-m\omega_c)^2}{\kappa^2 v_{t_{\parallel i}}^2}}}{v_{t_{\parallel i}}} \sqrt{\pi} \cdot \left(n\omega_{ci} + \left(\frac{T_\perp^i}{T_\parallel^i}\right)\kappa U\right)\left(\frac{2}{v_{t_{\perp i}}^2}\right)<f^i>^2\right) \Big|_{U = \frac{\omega - n\omega_c}{\kappa}} \tag{B-7}$$

where terms in the first spectral sum are the diffusion and drag, and those in the second spectral sum accounts for relaxation of anisotropy of the average-distribution function. The ion-ion diffusion will cancel the ion-ion drag. The remainder in the first bracket is the interactions between different species.

Finally, we can express source terms in terms of the electric field $<|\tilde{\varphi}_{\underline{k},\omega}^\sigma|^2>$, using Eqs. (B-5) and (B-6),

$$<S>^i \sim \frac{1}{(4\pi n_0 q)^2} \sum_{\underline{k}} \frac{J_{n_\omega}^2 <f^i>_\perp^2}{(2\pi)^3 |\varepsilon_{\underline{k},\omega}|^2} \left(\frac{2k^4\kappa^2}{\wedge_{n_\omega}^2 \pi^2}\right)\left\{ (Im\chi_{\underline{k},\omega}^i)^2 <|\tilde{\varphi}_{\underline{k},\omega}^e|^2> \right.$$

$$\left. + Im\chi_{\underline{k},\omega}^i Im\chi_{\underline{k},\omega}^e <|\tilde{\varphi}_{\underline{k},\omega}^i|^2> \right\} \Big|_{\omega = n_\omega \omega_c + \kappa U_i} \tag{B-8}$$

$$\langle S \rangle^e \sim \frac{1}{(4\pi n_o e)^2} \sum_{\underline{k}} \frac{\langle f^e \rangle_\perp^2}{(2\pi)^3 |\varepsilon_{\underline{k},\omega}|^2} \left(\frac{2k^4 \kappa^2}{\pi^2}\right) \{ (Im\chi^e_{\underline{k},\omega})^2 \langle |\tilde{\varphi}^i_{\underline{k},\omega}|^2 \rangle$$

$$+ Im\chi^i_{\underline{k},\omega} \, Im\chi^e_{\underline{k},\omega} \langle |\tilde{\varphi}^e_{\underline{k},\omega}|^2 \rangle \} \Big|_{\omega = \kappa U_e} \, , \tag{B-9}$$

where we have assumed, in Eq. (B-8), that only one harmonic n_ω is dominant for a given frequency ω.

Appendix (C)

For situations where the magnitude of $\text{Re}\varepsilon$ is not neccessarily larger than that of $\text{Im}\varepsilon$, we can evaluate the k' integral in Eqs. (3:1-12) and (3:1-13) in a slightly different way. First, we again assume that the k' integral is determined by the peak of $|\varepsilon_{k',\omega'}|^{-2}$. For a given value of ω', the integral $\int dk^3/|\varepsilon|^2$ can be evaluated by $\Delta k^3/|\varepsilon|^2$, where Δk^3 is the wavenumber "volume" contained in the peak of $|\varepsilon|^{-2}$. Since the functional dependence of ε on ω, k and v_D is known, hence Δk^3 can be expressed by ω and v_D.

Second, a set of coupled equations similar to Eqs. (3:1-14) and (3:1-15) can immediately be obtained, and thus the neccessary condition for stationary turbulence can now be expressed as

$$\frac{|\varepsilon_{k,\omega}|^2}{\Delta k^3} = \frac{(a^i + a^e)}{\kappa k^2} \ \text{Im} \ \chi^e_{k,\omega} \text{Im} \chi^i_{k,\omega} \ . \tag{C-1}$$

Notice that the terms on both sides of the equality are functions of ω, k and v_D; however, these are not free parameters. They must satisfy a relation so as to minimize the drift velocity, yielding the threshold drift velocity v^{thr} for clump instability. When v_D exceeds v^{thr}, ω should be replaced by $\omega + i/\tau_c$, reflecting the fluctuation amplitude dependence of nonlinear saturation.

Appendix (D)

In the wave–clump regime of one–dimensional ion–acoustic turbulence, we can use Eq. (3:1–16) to determine the threshold drift velocity v^{thr} for clump instability. For this case, the reduction of threshold drift from that of the linear theory is substantial, in marked contrast to the ion–cyclotron case. This can be explained as follows.

The threshold drift v^{thr} is determined by

(a) $Re\,\varepsilon=0$,

(b) $Im\,\varepsilon=(a^e+a^i)\underline{k}^2\lambda_D^2 Im\chi^e Im\chi^i$,

(c) Minimization of v_D with respect to ω and $\underline{k}$.

For ion–acoustic fluctuations, the dielectric is

$$\varepsilon_{\underline{k},\omega} = \frac{1}{\underline{k}^2\lambda_D^2} \left[Z'\left(\frac{\omega}{\kappa v_{te}} - \frac{v_D}{v_{te}}\right) + \frac{T^e}{T^i} Z'\left(\frac{\omega}{\kappa v_{ti}}\right)\right] \tag{D-1}$$

There are only two independent variables in $\varepsilon_{\underline{k},\omega}$, i.e. ω/κ and v_D, hence relation (a) and (b) are sufficient to determine v^{thr}. Relation (c) is of no use for this case. However, in the case of the ion–cyclotron fluctuations, ω, k and v_D are independent variables, thus relation (c) has to be used. In fact, it is this minimization of v_D that results in the slight reduction for ion–cyclotron threshold drift.

A straightforward numerical method shows that the threshold reduction of ion–acoustic fluctuations is enhanced monotonically as T^i/T^e increases (Fig. D-1). When $T^i/T^e \geq 0.5$, relations (a) and (b) yield unphysical complex values for v_D, indicating that the expansion around $Re\,\varepsilon=0$ fails. The ion–acoustic

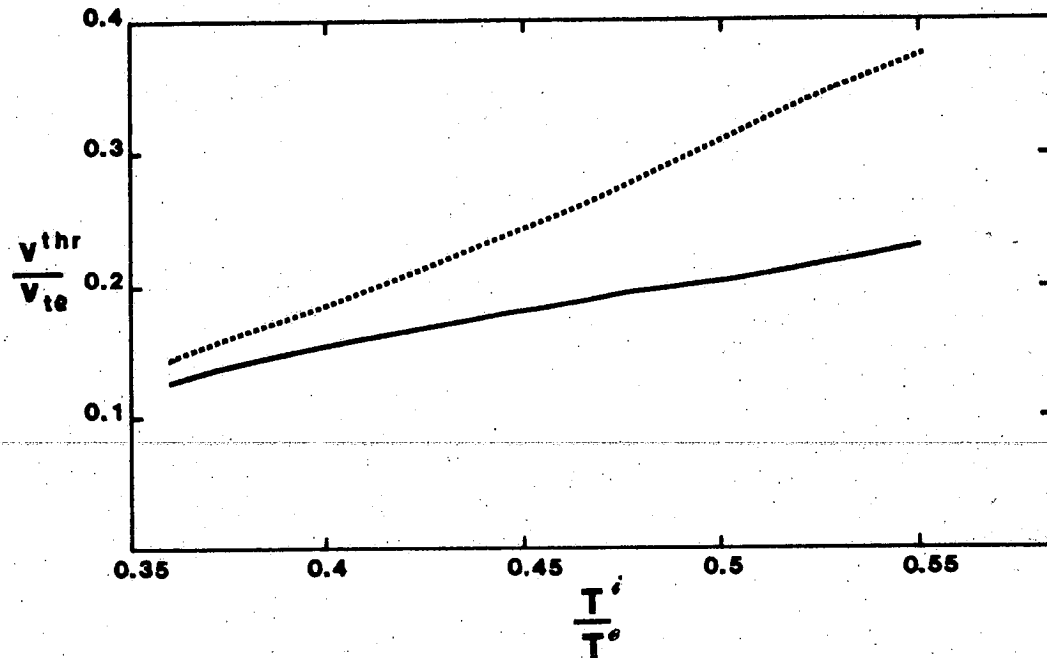Figure D-1. Threshold drift velocity for one-dimensional
             ion-acoustic turbulence of wave-clump type
             as a function T^i/T^e, with $M_i/m_e = 100$.
             Nonlinear and linear results are shown by
             the solid and dash lines, respectively.

turbulence becomes of clump type, and the method described in Appendix C or numerical integration for Eqs. (3:1-12) and (3:1-13) should be used.

With mass ratio, $M_i/m_e = 100$ and temperature ratio, $T^i/T^e = 0.5$, we find that the threshold reduction $\Delta v^{thr}/v^{thr} \approx 40\%$. We expect that with $T^i/T^e = 1$, the threshold reduction should exceed 40%. This is consistent with that observed in a recent particle simulation by Berman et al.[18]

Appendix (E)

Here we give the detailed derivation of renomalization for Eqs. (4:6b-1) and (5:3-4). The nonlinear terms can be renormalized by substituting $\varphi_{k'',\omega''}$ and $\nabla_\perp^2\varphi_{k'',\omega''}$ for $\varphi_{k'',\omega''}^{(2)}$ and $\nabla_\perp^2\varphi_{k'',\omega''}^{(2)}$ respectively, where the latter quantities are driven by the direct beating of a test (k,ω) mode and background (k',ω') modes. These driven modes satisfy

$$\nabla_\perp^2\varphi_{k'',\omega''}^{(2)} \cong \int dx' \left[\frac{-i\nabla_\perp^2 G_{k'',\omega''}(x,x')}{\omega''-k''V_E(x')}\right]\left[ik'\nabla_\perp^2\varphi_{k',\omega'}^* \frac{d\varphi_{k,\omega}}{dx'} - ik'\varphi_{k',\omega'}^*\right.$$

$$\left.\cdot \frac{d}{dx'}\nabla_\perp^2\varphi_{k,\omega} - ik\nabla_\perp^2\varphi_{k,\omega}\frac{d\varphi_{k',\omega'}^*}{dx'} + ik\varphi_{k,\omega}\frac{d}{dx'}\nabla_\perp^2\varphi_{k',\omega'}^*\right] \qquad (E-1)$$

$$\varphi_{k'',\omega''}^{(2)} \cong \int dx'\left[\frac{-iG_{k'',\omega''}(x,x')}{\omega''-k''V_E(x')}\right]\left[ik'\nabla_\perp^2\varphi_{k',\omega'}^*\frac{d\varphi_{k,\omega}}{dx'} - ik'\varphi_{k',\omega'}^*\right.$$

$$\left.\cdot \frac{d}{dx'}\nabla_\perp^2\varphi_{k,\omega} - ik\nabla_\perp^2\varphi_{k,\omega}\frac{d\varphi_{k',\omega'}^*}{dx'} + ik\varphi_{k,\omega}\frac{d}{dx'}\nabla_\perp^2\varphi_{k',\omega'}^*\right] , \qquad (E-2)$$

where $G_{k'',\omega''}(x,x')$ is a linear propagator satisfying

$$\nabla_\perp^2 G_{k'',\omega''}(x,x') = \frac{-1}{\omega''-k''V_E(x)}\left[k''\frac{d^2V_E}{dx^2} - ik''^2R^2x^2\right]G_{k'',\omega''}(x,x')+\delta(x-x')$$

$$\equiv L_{k'',\omega''}(x)\ G_{k'',\omega''}(x,x') + \delta(x-x') . \qquad (E-3)$$

Together with Eqs. (E-1), (E-2) and (E-3), nonlinear terms become

$$[NL]_{k,\omega}$$

$$\cong \sum_{\substack{k' \\ \omega'}} \left\{ \left(\frac{d}{dx} \left\{ \left(\frac{i}{\omega'' - k'' V_E} \right) (k')^2 \left[\langle \varphi_{k',\omega'} \nabla_\perp^2 \varphi_{k',\omega'}^* \rangle \frac{d\varphi_{k,\omega}}{dx} \right. \right. \right. \right.$$

$$\left. \left. - \langle |\varphi_{k',\omega'}|^2 \rangle \frac{d}{dx} \nabla_\perp^2 \varphi_{k,\omega} \right] \right\})$$

$$-k^2 \left\{ \left(\frac{i}{\omega'' - k'' V_E} \right) \left[\langle \frac{d\varphi_{k',\omega'}}{dx} \frac{d}{dx} \nabla_\perp^2 \varphi_{k',\omega'}^* \rangle \varphi_{k,\omega} - \langle |\frac{d\varphi_{k',\omega'}}{dx}|^2 \rangle \nabla_\perp^2 \varphi_{k,\omega} \right] \right\} \right)$$

$$+ \sum_{\substack{k' \\ \omega'}} \int dx' \left(\frac{i}{\omega'' - k'' V_E(x')} \right)$$

$$\left\{ (k')^2 \frac{d}{dx} \left\{ \left[L_{k'',\omega''}(x) G_{k'',\omega''}(x,x') \langle \varphi_{k',\omega'}(x) \nabla_\perp^2 \varphi_{k',\omega'}^*(x') \rangle \right. \right. \right.$$

$$\left. - G_{k'',\omega''}(x,x') \cdot \langle \nabla_\perp^2 \varphi_{k',\omega'}(x) \nabla_\perp^2 \varphi_{k',\omega'}^*(x') \rangle \right] \frac{d\varphi_{k,\omega}}{dx'}$$

$$- \left[L_{k'',\omega''}(x) G_{k'',\omega''}(x,x') \langle \varphi_{k',\omega'}(x) \varphi_{k',\omega'}^*(x') \rangle \right.$$

$$\left. - G_{k'',\omega''}(x,x') \cdot \langle \nabla_\perp^2 \varphi_{k',\omega'}(x) \varphi_{k',\omega'}^*(x') \rangle \right] \frac{d\nabla_\perp^2 \varphi_{k,\omega}}{dx'} \right\}$$

$$- k^2 \{ [L_{k'',\omega''}(x) G_{k'',\omega''}(x,x') < \frac{d\varphi_{k',\omega'}}{dx} \frac{d\nabla_\perp^2 \varphi_{k',\omega'}^*}{dx'} >$$

$$- G_{k'',\omega''}(x,x') < \frac{d\nabla_\perp^2 \varphi_{k',\omega'}}{dx} \frac{d\nabla_\perp^2 \varphi_{k',\omega'}^*}{dx'} >] \varphi_{k,\omega}(x')$$

$$- [L_{k'',\omega''}(x) G_{k'',\omega''}(x,x') < \frac{d\varphi_{k',\omega'}}{dx} \frac{d\varphi_{k',\omega'}^*}{dx'} >$$

$$- G_{k'',\omega''}(x,x') < \frac{d\nabla_\perp^2 \varphi_{k',\omega'}}{dx} \frac{d\varphi_{k',\omega'}^*}{dx'} >] \nabla_\perp^2 \varphi_{k,\omega}(x') \} \} \equiv D_{k,\omega} + C_{k,\omega} \quad \text{(E-4)}$$

Terms in the first spectral sum, $D_{k,\omega}$, arise from the local response ($\delta(x-x')$ of Eq. (E-3)) of the driven vorticity $\nabla_\perp^2 \varphi_{k'',\omega''}^{(2)}$. Terms in the second spectral sum $C_{k,\omega}$, are due to both the nonlocal response ($L_{k'',\omega''} G_{k'',\omega''}$ of Eq. (E-3)) of the driven vorticity $\nabla_\perp^2 \varphi_{k'',\omega''}^{(2)}$ and driven field $\varphi_{k'',\omega''}^{(2)}$.

R E F E R E N C E S

258

R E F E R E N C E S

1. M. Yamada and H. W. Hendel, Phys. Fluids 21, 1555 (1978).

2. H. Bohmer and S. Fornaca, J. Geophys. Res. 84, 5234 (1979).

3. D. R. Dakin, T. Tajima, G. Benford and N. Rynn, J. Plasma Phys. 15, 175 (1976).

4. F. S. Mozer, C. W. Carlson, M. K. Hudson, R. B. Torbert, B. Parady, J. Yatteau and M. C. Kelly, Phys. Rev. Lett. 38, 292 (1977).

5. R. L. Lysak, H. K. Hudson and M. Temerin, J. Geophys. Res. 85, 678 (1980).

6. H. Okuda, C. Z. Cheng and W. W. Lee, Phys. Fluids 24, 1060 (1981).

7. C. T. Dum and T. H. Dupree, Phys. Fluids 13, 2064 (1970).

8. S. P. Hirshman and K. Molvig, Phys. Rev. Lett. 42, 648 (1979).

9. T. H. Dupree, Phys. Fluids 9, 1733 (1966).

10. T. Boutros-Ghali and T. H. Dupree, Phys. Fluids 24, 1839 (1981).

11. T. Boutros-Ghali and T. H. Dupree, Phys. Fluids 25, 874 (1982).

12. D. J. Tetreault, Phys. Fluids 26, 3247 (1983).

13. R. H. Berman, D. J. Tetreault, and T. H. Dupree, Phys. Fluids 28, 155 (1985).

14. P. W. Terry and P. H. Diamond, in Statistical Physics and Chaos in Fusion Plasmas, W. Horton and L. Reichl, Eds., John Wiley and Sons, 1984, p. 335.

15. P. W. Terry and P. H. Diamond, Institute for Fusion Studies Report No. 114, 1984, to be published in Phys. Fluids.

16. K. F. Lee, J. Plasma Phys. 8, 379 (1972).

17. R. H. Berman, J. N. Leboeuf, T. Chiueh, and P. H. Diamond, Bull. Amer. Phys. Soc. 29, 1409 (1984).

18. R. H. Berman, R. H. Dupree, and D. J. Tetreault, Bull. Amer. Phys. Soc. 29, 1240 (1984).

19. T. H. Dupree, Phys. Fluids 15, 334 (1972).

20. T. H. Stix, The Theory of Plasma Waves, McGraw-Hill, 1962.

21. M. Wakatani, and A. Hasegawa, Phys. Fluids 27, 611 (1984).

22. H. R. Strauss, Phys. Fluids 20, 1354 (1977).

23. C. C. Lin, The Theory of Hydrodynamic Stability, Cambridge University Press, 1955.

24. S. A. Orszag, and A. T. Petera, in Chaotic Behavior of Deterministic Systems, ed. by G. Iooss, R. H. G. Helleman and R. Stora, North-Holland Publishing Co., 1983.

25. A. A. Townsend, The Structure of Turbulent Shear Flow, Cambridge University Press, 1976.

26. G. L. Brown, and A. Roshko, J. Fluid Mech. 64, 775 (1974); and A. Roshko, AIAA Journal, 14, 1349 (1976).

27. H. Aref, and E. D. Siggia, J. Fluid Mech. 100, 705 (1980).

28. M. Van Dyke, An Album of Fluid Motion, The Parabolic Press, 1982.

29. S. Taneda, J. Phys. Soc. Japan 14, 843 (1959).

30. P. E. Dimotakis and G. L. Brown, Tech. Rept. CIT-7-PU Project SQUID, 1975; and J. Fluid Mech. 78, 535 (1976).

31. P. R. Bandyopadhyay and A. K. M. F. Hussain, Phys. Fluids 27, 2221 (1984).

32. N. J. Zabusky, and G. S. Deem, J. Fluid Mech. 47, 353 (1971).

33. J. T. C. Liu, and L. Merkine, Proc. R. Soc. Lond. A. 352, 213 (1976).

34. T. B. Gatski, and J. T. C. Liu, Proc. R. Soc. Lond. A. 393, 473 (1980).

35. R. H. Kraichnan, Phys. Rev. 113, 1181.

36. A. N. Kolmogoroff, J. Fluid Mech. 13, 82 (1967).

37. J. T. C. Liu, Phys. Fluids 14, 2251 (1971).

38. G. K. Bachelor, Homogeneous Turbulence, Cambridge University Press, 1960.

39. L. D. Landau, and E. M. Lifshitz, Fluid Mechanics, Pergamon Press.

40. A. S. Monin, and A. M. Yaglom, Statistical Fluid Mechanics, vol. 1, MIT Press, 1971.

41. P. G. Drazin, and L. N. Howard, in Advances in Applied Mechanics, vol. 7, ed. G. Kuerti, Academic Press, 1966.

42. R. H. Kraichnan, Phys. Rev. 113, 1181 (1966).

43. T. H. Dupree, and D. J. Tetreault, Phys. Fluids 21, 425 (1978).

44. A. Michalke, J. Fluid Mech. 19, 543 (1964).

45. R. H. Kraichnan, J. Fluid Mech. 67, 155 (1975).

46. H. L. Grant, J. Fluid Mech. 4, 149 (1958).

47. C. P. Ritz, R. D. Bengtson, S. J. Levinson and E. J. Powers, Phys. Fluids 27, 2956 (1984).

48. S. J. Zweben, private communication.

49. S. J. Zweben, accepted by and to appear in Phys. Fluids.

50. A. Hasegawa and M. Wakatani, Phys. Rev. Lett. 48, 1828 (1982).

51. P. W. Terry and P. H. Diamond, Institute for Fusion Studies Report No. 114 (1984), accepted by and to appear in Phys. Fluids.

52. S. J. Zweben and R. W. Gould, Nucl. Fusion 23, 1625 (1983).

53. S. J. Levinson, J. M. Beall, E. J. Powers and R. D. Bengtson, Nucl. Fusion 24, 527 (1984).

54. F. L. Hinton, et al., Proc. 10th Int. Conf. on Plasma Phys. and Contr. Nucl. Fusion, London (1984).

55. F. Wagner, et al., Phys. Rev. Lett. 53, 1453 (1984).

56. S. J. Zweben and R. W. Gould, Bull. Amer. Phys. Soc. 28, 1204 (1983).

57. L. Chen, M. S. Chance and C. Z. Cheng, Nucl. Fusion 22, 293 (1983).

58. L. Garcia, P. H. Diamond, B. A. Careeras, and J. D. Callen, IFS Report No. 146, 1984.

59. D. M. Eardley and A. P. Lightman, Ap. J. 200, 187 (1975).

60. F. V. Coroniti, Ap. J. 200, 187 (1981).

61. P. Ghosh and F. K. Lamb, Ap. J. 232, 259 (1979).

62. W. I. Axford, Rev. Geophys. Space Sci. 7, 421 (1969).

V I T A

Tzihong Chiueh was born in Taipei, Taiwan, on November 29,
1955, the son of King-Mu Chiueh and Yu-Jane Mu Chiueh.   He
entered Taiwan University in September 1974, majoring in
Physics.   In May 1978, he received the degree of Bachelor of
Science from the same university.   In September 1979, he en-
tered the University of California at Los Angeles, Califor-
nia, majoring in Physics, and received the degree of Master
of Science in May 1980 from UCLA.   In August 1982, he left
UCLA for Austin, Texas.   In January 1983, he entered The
University of Texas at Austin, majoring in Physics, and
joined the Institute for Fusion Studies since then.

Permanent Address: 9, Lane 47, Section 3, An-Ho Road
                     Shin-Dien City, Taiwan (ROC)

Martha Ann Zivley typing service

2707 HEMPHILL PARK • AUSTIN, TEXAS 78705 • AC 512 472-3210